ANALYSIS OF DEFORMATION MECHANISM OF PARTICULATE MATERIAL BASED ON THE PROBABILITY THEORY(Dissertation_全文)

AUTHOR(S):

Kitamura, Ryosuke

ANALYSIS OF DEFORMATION MECHANISM OF PARTICULATE MATERIAL BASED ON THE PROBABILITY THEORY

February, 1980

By

RYOSUKE KITAMURA

ANALYSIS OF DEFORMATION MECHANISM OF PARTICULATE MATERIAL BASED ON THE PROBABILITY THEORY

February, 1980

By

RYOSUKE KITAMURA

ACKNOWLEDGEMENTS

The author, firstly, wishes to express his deepest gratitude to Professors S. Murayama and K. Akai for their continuous guidances and encouragements, and their stimulating discussions throughout the present study. Grateful acknowledgements are made to Professors T. Shibata and H. Imamoto for their instructive suggestions. The author is also indebted to Associate Professor T. Adachi for his review of the manuscript and for his helpful suggestions concerning the experimental and theoretical studies.

The author would like to emphasize that this study has been promoted by many other peoples through the extensive discussions in daily academic activities. In this respect, he wishes to extend his gratitude to Associate Professors H.Ohta, H. Matsuoka, T. Sato, H. Sekiguchi, Dr. S. Ohmaki, Mr. T. Nakai and others for their constructive criticisms.

Finally, the author would like to express his heartleft thanks to his family for the daily research life.

SUMMARY

In this thesis a mechanical model of particulate material is proposed by using the probability theory. In modelling, the motions of particles under the deformation process are regarded as Markov process which is one of the most well-known stochastic processes. The coefficients in the basic equation of Markov process are determined by introducing the concepts of the potential barrier and the potential slip plane. These coefficients represent the mechanical properties of particulate material at the particle scale. The strains are defined for the particulate material and it is found that the discontinuous motions of particles at contact points play important roles. These discontinuous motions are considered to correspond to the dislocation under the plastic deformation of crystal material. Furthermore, the new modified triaxial apparatus is developed and the shearing tests of saturated sand are carried out under general stress conditions with various stress paths by using this apparatus. Finally, the numerical experiments are performed by using the mechanical model and the validity of this model is verified by comparing the results with ones obtained from the shearing tests and it is shown that the proposed medel can follow the various mechanical behaviours of particulate material by using several parameters whose physical meanings are apparent.

CONTENTS

CHAPTER 1 INTRODUCTION

1.1 General Description

Soil has been closely related to the human life since the day of antiquity in the civil engineering, for example, embankments for rivers and roads, foundations of structures, fill dams, tunnels and so on. Thus, it has been one of the most important objects for civil engineers to design and to construct these soil structures safely and economically, or to predict the deformations and failures of them, and to prevent the disasters caused by landslides, liquefactions of sands and settlements.

Recently the importance of the constitutive equations of soil has been realized with the rapid progress of the finite element method which has been brought by the development of electronic computer science. For two decades many researches have been carried out to establish the general constitutive equations all over the world in order to attain the above mentioned objects of civil engineering. These researches are largely divided into two categories by means of the adopted approaches. The first one is based on the continuum mechanics and applies the theories of elasticity and/or plasticity to analyse the mechanical behaviours of soil. The second approach adopts the standpoints that soil is composed of particles and voids among them, and the observable mechanical behaviours of soil are the summation of the relative motions of individual soil particles and voids. The former is called the macroscopic approach and the latter is named the microscopic one in this thesis.

Let's review these approaches in the following subsections.

1.1.1 Macroscopic approaches

The theories of elasticity and/or plasticity are applied in this approach where the plastic component in the total deformation is defined by the following principles;

(1) the yield condition (or energy equation) or the plastic potential function specifying the states of stress under which plastic flow occurs,

(2) the flow rule connecting the plastic strain increment tensor with the stress and stress increment tensors,

(3) the hardening rule specifying the modification of yield condition or plastic potential function in the course of plastic flow.

In this approach the first and world-famous model for soil has been established to represent both the consolidation and shearing processes of soil by Roscoe, Schofield, Burland and other researchers belonging to Cambridge University and this model is usually called the Cambridge model[1),2),3)].

The essential parts for the model are represented by the following equations.

Energy equation; $$\frac{p\dot{v}}{v} + q\dot{\epsilon} = M p \dot{\epsilon} \qquad (1.1)$$

v -ln p relation; $$v = \Gamma - \lambda \ln p \qquad (1.2)$$

where p ; spherical pressure,

q ; deviatoric stress,

v and $\dot{v}$; volumetric strain and strain increment,

$\dot{\epsilon}$; deviatoric strain increment,

M, Γ and λ ; model parameters.

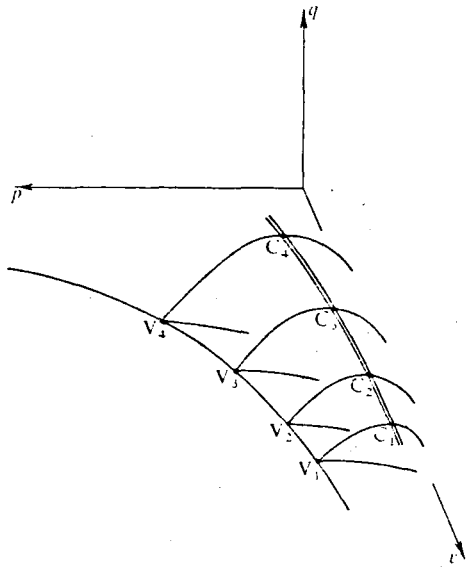

Fig.1.1 Upper half of state boundary surface (after Schofield and Wroth)

The constitutive relation is derived by using the state boundary surface, which is obtained from Eqs.(1.1) and (1.2), and the normality flow rule. Fig.1.1 shows the schematic view of state boundary surface in $v \sim p \sim q$ space.

The Cambridge model is the first one that can unifyingly represent both the consolidation and shearing processes of soil and extremely influences the subsequent researches[4),5),6)].

Furthermore, the constitutive equations are recently refined by Lade[7),8),9)], Prévost[10),11)], Pender[12),13)] and Mróz et al.[14)] in order to analyse the mechanical behaviours of soil by means of the finite element method. These modified constitutive equations by them are also derived by using the same three principles, but only modifying the yield condition and/or the plastic potential function and the hardening rule. The used yield conditions and/or the plastic potential functions by them are listed as follows.

Lade developed the constitutive equations for sands. He divided the plastic strains into two components, i.e., the plastic collapse strains and the plastic expansive strains as shown in Fig.1.2. For the plastic collapse strains the associated flow rule is used and for the plastic expansive strains the non-associated flow rule is adopted. Thus, the yield functions and the plastic potential functions for two plastic strain components are as follows.

For plastic collapse strains,

yield function (= plastic potential function);

$$f_c = g_c = I_1^2 - 2 I_2 \tag{1.3}$$

For plastic expansive strains

yield function; $$f_p = \left(I_1^3/I_3 - 27\right) \cdot \left(I_1/P_a\right)^m \tag{1.4}$$

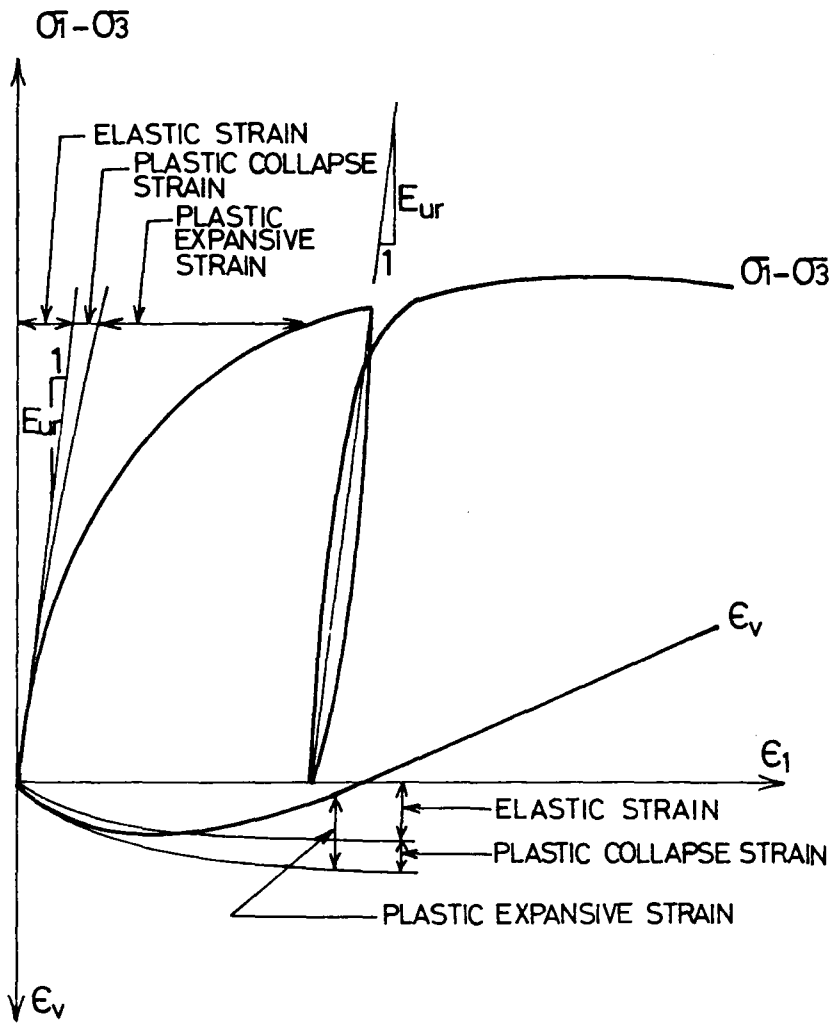

Fig.1.2 Schematic illustration of elastic, plastic collapse and plastic expansive strain components (after Lade)

plastic potential function;

$$g_p = I_1^3 - \left\{27 + \eta_2 \left(P_a / I_1\right)^m\right\} \cdot I_3 \qquad (1.5)$$

where I_1, I_2 and I_3 ; first, second and third effective stress invariants,

P_a ; atmospheric pressure,

m and η_2 ; model parameters.

Lade examines the validity of his constitutive equations by comparing them with the results obtained from the shearing tests under the triaxial compression and the general stress conditions.

Prévost's constitutive equations for undrained behaviours of saturated clays are given by combining the associated flow rule with the following yield condition.

$$\left\{\frac{3}{2}\left(s_{ij} - \alpha_{ij}^{(m)}\right)\left(s_{ij} - \alpha_{ij}^{(m)}\right)\right\}^{1/2} - k^{(m)} = 0 \qquad (1.6)$$

where s_{ij} ; deviatoric stress tensor,

$\alpha_{ij}^{(m)}$ and $k^{(m)}$; model parameters.

Prévost tries to obtain the stress-strain relations for the repeated loading conditions by using Eq.(1.6).

Pender derived the constitutive equations by adopting the non-associated flow rule with the following yield function and the plastic potential function, i.e.,

yield function; $$f = q - \eta_i p = 0 \qquad (1.7)$$

plastic potential function;

$$\frac{\partial g}{\partial p} = \left(p_0 / p_{cs} - 1\right) \cdot \left\{M\left(p / p_{cs}\right)\eta\right\} \qquad (1.8)$$

in which p ; mean principal effective stress,

q ; principal stress difference,

p_0 ; initial value of p ,

p_{cs} ; value of p for the point on the critical state line,

η ; stress ratio q/p ,

η_i ; stress ratio at a given stress ratio yield locus determined by the initial stress ratio,

M ; critical state friction parameter.

Pender applies his constitutive equations to the deformation behaviours of normally and overconsolidated soils with various stress paths.

Mróz et al. established the equations to explain the behaviours of normally and overconsolidated clays under the repeated loading and unloading processes by using the associated flow rule and two yield functions such as

boundary yield function;

$$\bar{F}(p, q, v^p, \Pi, d) = (p-c)^2 + \frac{(q-d)^2}{n^2} - a^2(v^p, \Pi) = 0 \quad (1.9)$$

inner yield function;

$$f_0 = (p-\alpha_p)^2 + \frac{(q-\alpha_q)^2}{n^2} - a_0^2(v^p) = 0 \quad (1.10)$$

where p ; mean effective principal stress,

q ; deviatoric stress,

a, c, d, n, Π, α_p and α_q ; model parameters,

v^p ; component of bulk density associated with plastic strain.

They also predict the stress paths and pore pressures under the repeated loading tests.

Concerning the hardening rule which represents the non-linear stress-strain relationships of soil, they determined the hardening

parameters based on their own considerations and experimental evidences.

1.1.2 Microscopic approaches

The microscopic approaches mean that the researches in which the constitutive equations of soil are derived based on the analysis of deformation mechanism at the soil particle scale.

Newland and Allely's work[15] is cited as the first one of these researches. They developed a theory to account for the difference between peak and residual stresses in term of the volume expansion of the mass during shear.

Subsequently Rowe[16),17)] derived the following stress-dilatancy equation based on the consideration of the frictional mechanism in an assembly of individual particles and the principle of the minimum energy ratio.

$$R = D \cdot K \tag{1.11}$$

where $R = \sigma_1'/\sigma_3'$; principal stress ratio,

$$D = \begin{cases} 1 - \dfrac{d\upsilon}{d\epsilon_1} & \text{for triaxial compression test,} \\ 1 - \dfrac{d\upsilon}{d\epsilon_3} & \text{for triaxial extension test,} \end{cases}$$

$K = \tan^2(45^\circ + \frac{1}{2}\phi_f)$,

$d\upsilon$; volumetric strain increment,

$d\epsilon_1$ and $d\epsilon_3$; maximum and minimum principal strain increments,

ϕ_f ; angle of friction in an assembly of particles.

Horne[18),19)] extended Rowe's stress-dilatancy theory and introduced the concept of so called mean projected solid path in

order both to measure the strain and to estimate the fabric anisotropy for an assembly of cohesionless particles. Similar approaches have been adopted by Oda[20], Matsuoka[21] and Tokue[22].

Based on statistical mechanics Murayama[23),24),25),26),27)] has established the constitutive equations of particulate material by means of analysing the particle motions on the plane of maximum mobilization. The plane of maximum mobilization in the conventional triaxial shearing test and the Mohr's stress circle at this stress state are illustrated in Fig.1.3. The plane of maximum mobilization is called $(\tau/\sigma)_{max}$ -plane.

For the elastic state the motions of particles are considered on $(\tau/\sigma)_{max}$ -plane based on the geometrical relations of particles as shown in Fig.1.4. The direction angle β_i of inter-particle force to $(\tau/\sigma)_{max}$ -plane and the contact angle $(\theta_i + \delta)$ are adopted as random variables. The joint normal distribution function of β_i and $(\theta_i + \delta)$ is introduced to obtain the probability of particles' sliding. Then, the following stress-strain relations are derived for the elastic state by using the change in geometrical relations of particles as shown in Fig.1.4.

$$\gamma_\beta = A \cdot \overline{W_e} \cdot Z \cdot \sqrt{1 + Z^2} \tag{1.12}$$

$$-d\epsilon_N = \tan \theta_s \cdot d\gamma_\beta \tag{1.13}$$

where γ_β ; shear strain on $(\tau/\sigma)_{max}$ -plane,

$d\epsilon_N$; normal strain increment on $(\tau/\sigma)_{max}$ -plane,

Z ; stress ratio $(\tau/\sigma)_{max}$,

A ; model parameter termed as the displacement factor,

$\overline{W_e}$; model parameter termed as the structural factor,

θ_s ; average value of θ_i in Fig.1.4.

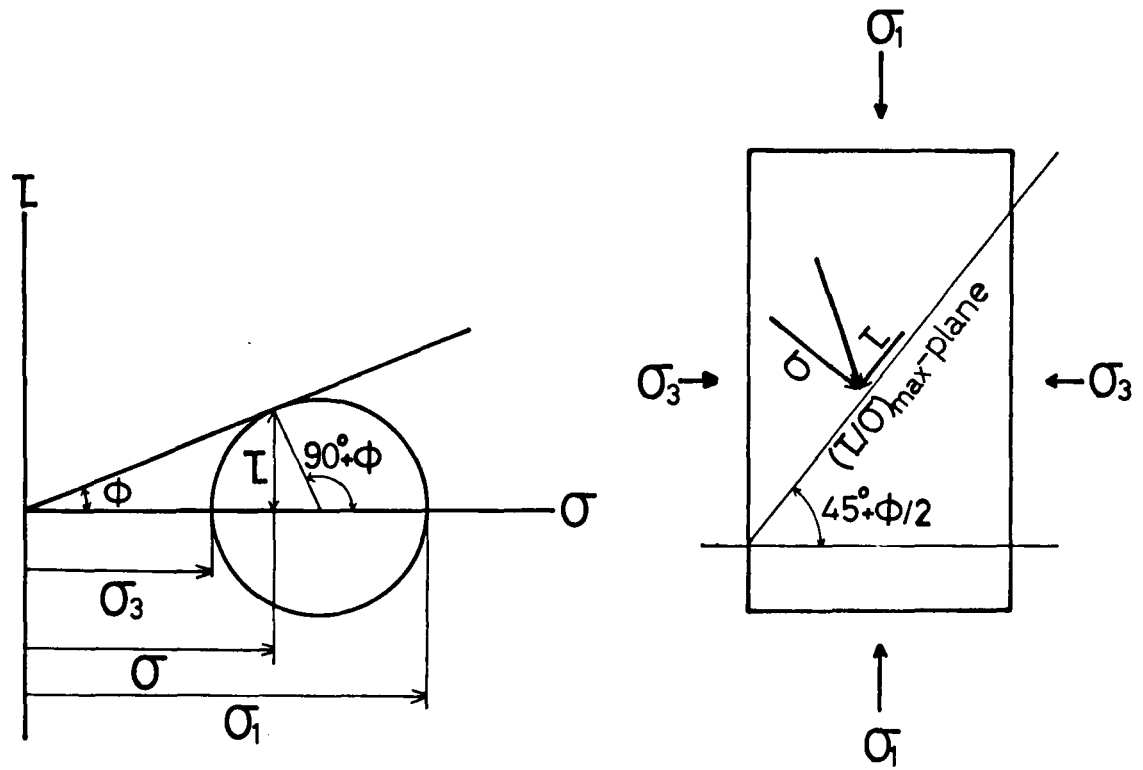

Fig.1.3 Plane of maximum mobilization where τ/σ is maximum (after Murayama)

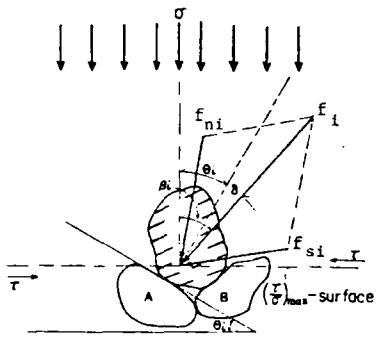

Fig.1.4 Geometrical relation of particles on $(\tau/\sigma)_{max}$ – surface (after Murayama)

For the plastic state two concepts of the activation and the potential barrier are introduced. By using these concepts, the particles are largely divided into two types by means of their mechanical properties, i.e., activated particles and non-activated particles. Furthermore, non-activated particles are divided into two groups, i.e., dislocated particles and non-dislocated particles. On the other hand, activated particles are also divided into two groups, i.e., the particles surrounded by non-dislocated particles and the particles surrounded by dislocated particles. Based on the considerations of the particle motions of these four types, the stress-strain relations are derived for the plastic state as follows.

$$\gamma^* = A \cdot W_e \cdot (1+\mu) \cdot S_w \cdot (Z - S_{el}) / (S_\infty - Z) \qquad (1.14)$$

where S_{el} ; stress ratio of elastic limit of the normal state sand,

S_∞ ; critical stress ratio which lies beyond the failure strength,

$S_w = S_\infty - S_{el}$,

μ ; constant coefficient of sand.

The similar considerations for the particle motions are also applied to the failure state, i.e., by using the four types of particles which possess the different mechanical properties, the stress ratio, the shear and the normal strains are obtained at the failure. Furthermore, the considerations for the particle motions are extended to the repeated loading and unloading processes. Then, the shear strains are derived for each loading or unloading process. A simple relations between the residual strains and the numbers of repeated cycles are also proposed.

Matsuoka[28),29),30)] derived the constitutive relations for cohesionless soil in the similar way.

Matsuoka and Nakai[31),32)] extended the mobilized plane to the three dimensional principal stress space and called the spatial mobilized plane or 'SMP'. They proposed the following two characteristic equations on the SMP based on the experimental results of sand.

$$\tau/\sigma_N = \lambda \cdot (-d\epsilon_N/d\gamma) + \mu \tag{1.15}$$

$$\tau/\sigma_N = \lambda \cdot (-\epsilon_N/\gamma) + \mu' \tag{1.16}$$

where τ/σ_N ; shear-normal stress ratio on the SMP,

ϵ_N , $d\epsilon_N$; normal strain and strain increment on the SMP,

γ , $d\gamma$; shear strain and strain increment on the SMP,

λ , μ and μ' ; soil parameters.

Eq.(1.15) shows the stress-dilatancy relation of soil on the SMP and is equivalent to Eq.(1.11) which is proposed by Rowe.
By solving the differential equations obtained from Eqs.(1.15) and (1.16), the stress-strain relations are derived on the SMP as follows.

$$\tau/\sigma_N = (\mu'-\mu) \cdot \ln(\gamma/\gamma_0) + \mu \tag{1.17}$$

$$\epsilon_N = \frac{\mu'-\mu}{\lambda} \cdot \gamma \cdot \{\ln(\gamma/\gamma_0) - 1\} \tag{1.18}$$

Mogami[33),34),35),36),37)] introduced the entropy which is used in statistical thermodynamics and information theory in order to estimate the distribution of voids in the particulate material and to analyse the deformation process including failure. Jowitt and Munro[38)] and Brown[39)] applied the principle of maximum entropy to

describe the most stable states and the mechanical properties of particulate materials. Marsal[40] used the statistical method in order to evaluate the frictional resistance in the particulate material.

Satake[41] introduced the graph theory to mathematically represent the deformation process of particulate material.

Combining the stress-dilatancy equation obtained by microscopic consideration with the flow rule in the theory of plasticity, the stress-strain relations were derived by Barden and Khayatt[42] and Tatsuoka[43].

Calladine[44] and Arthur et al.[45] applied the theory of plasticity to the local deformation mechanism of individual particles in soil.

De Josselin De Jong[46] applied the slip line concept in the theory of plasticity to the deformation of particulate material.

In this section the macroscopic and the microscopic researches have been reviewed and discussed. As the conclusion, Fig.1.5 is given to show the major approaches to derive the constitutive equations for soils as well as the foundamental theoretical background. It is clearly seen in Fig.1.5 that two basic equations (e.g. plastic potential function and flow rule) are at least required to derive the constitutive equations for soils, and the stress-dilatancy equation obtained in microscopic approach plays the equivalent role as the energy equation or plastic potential function. Statistics and probability theory are useful in the microscopic approach, but the procedures for the derivation of constitutive equations have not established yet although it has been clear that the contact angles of particles and the voids are the most essential state variables for the particulate material.

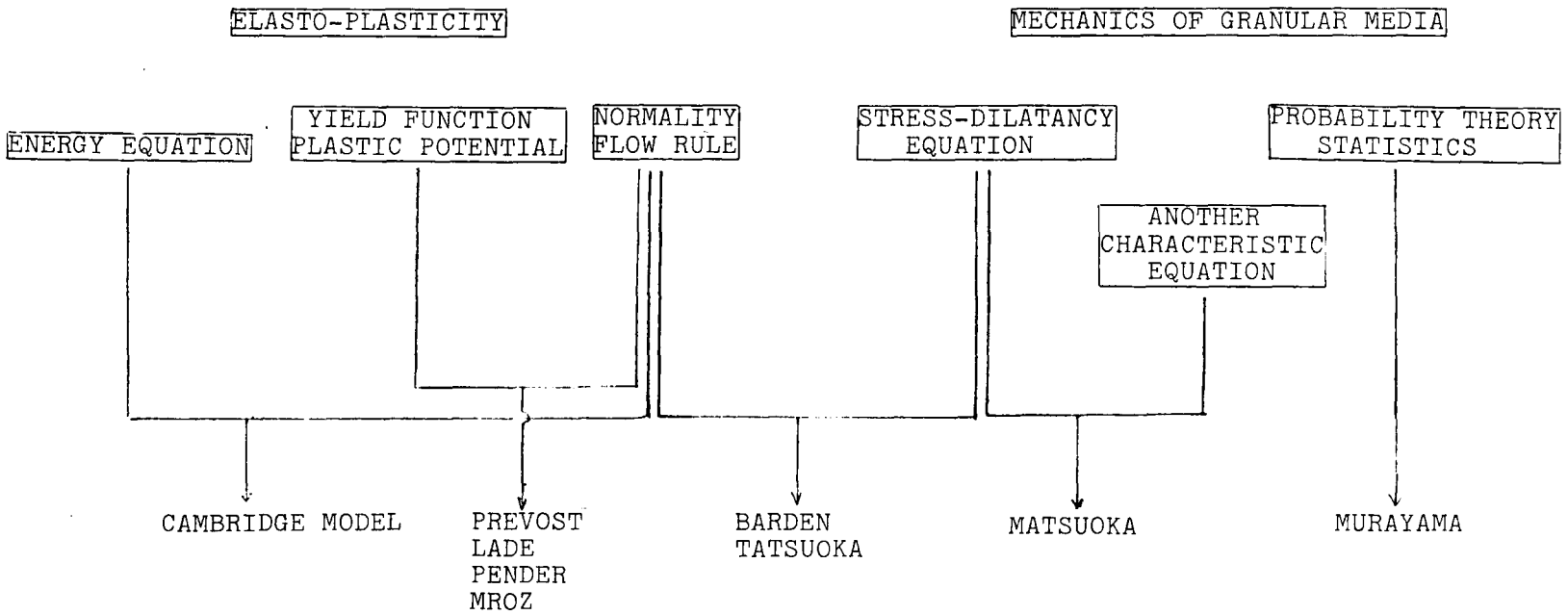

Fig.1.5 Approaches for constitutive equations

1.2 Scope of This Study

Various mechanical model for soil have been proposed in the previous researches as mentioned above, but the versatile constitutive equations cannot be found. Then, it seems to be imperative to provide the unified constitutive relation of soil reflecting exactly its various mechanical properties.

In this thesis the mechanical model of particulate material is proposed by applying the probability theory to analyse the motions of particles in the particulate material. Namely, the motion of particle under deformation process is assumed to be a Markov process. In this theoretical development the angle between the normal to tangential plane at a contact point of particle and the reference axis is taken as a random variable, since it is a major governing factor to represent the inner structure of particulate material.

Furthermore, the experiments with Toyoura sand under the general stress conditions including the stress reverse are performed by using a newly modified triaxial testing apparatus which can generate three different principal stresses. Finally, by using the proposed mechanical model the numerical experiments are carried out. The validity of proposed model is verified by comparing the results with the shearing test results for Toyoura sand.

In chapter 2, the Markov process is mathematically expressed and the basic equation is derived for the n-dimensional Markov process based on some mathematical assumptions.

In chapter 3, the Markov process is applied to the mechanical behaviours of particulate material. The necessity why the Markov process is applied to the motions of particles is explained at the particle scale. It is clearly shown that the coefficients A_i and

B_{ii} in the basic equation of Markov process play a very important role to represent the mechanical properties of particulate material. The validity of the model, therefore, depends on how to determine these coefficients. The concepts of the potential barrier and the potential slip plane are introduced in order to estimate quantitatively these coefficients with thorough considerations on the mechanical properties of particulate material at the particle scale.

In chapter 4, the definition of strain for the particulate material is given. It makes apparent that the strain can be determine by the distribution of contact angles at the contact points of particles and the discontinuous motions of particles which may correspond to the dislocation observed under the plastic deformation of crystal solid. Furthermore, it is shown that the discontinuous motions largely contribute to the deformation process of particulate material, and the method to quantitatively estimate the discontinuous motions is proposed based on the probabilistic considerations for the motions of particles.

In chapter 5, the true triaxial apparatus in the previous researches are reviewed and a modified triaxial apparatus is newly designed and made by the author. Error correction methods are discussed for this modified triaxial apparatus. Shearing tests with Toyoura sand under the general stress conditions including the stress reverse are carried out by the newly modified triaxial apparatus and the stress-strain relations obtained from these tests are shown. The angles of failure slip planes also investigated to verify the validity of the potential slip plane.

In chapter 6, the numerical experiments are carried out in order to evaluate the proposed mechanical model. The physical meanings of parameters in the model are discussed in detail. Finally, the stress-strain curves obtained by the proposed model

are compared with the shearing test results and it is shown that the proposed model can versatilely describe the mechanical behaviours of particulate material under the general stress conditions and under the repeated loading condition.

Reference for Chapter 1

1) Roscoe, K.H., Schofield, A.N. and Thurairajah, A.: Yielding of Clays in States Wetter than Critical, Géotechnique, Vol.13, No.2, 1963, pp.211-240.

2) Schofield, A.N. and Wroth, C.P.: Critical State Soil Mechanics, McGraw Hill, London, 1968.

3) Roscoe, K.H. and Burland, J.B.: On the Generalized Stress-Strain Behaviour of 'Wet' Clay, Engineering Plasticity, Cambridge University Press, 1968, pp.535-609.

4) Ohta, H.: Analysis of Deformation of Soils based on the Theory of Plasticity and its Application to Settlement of Embankment, Dr. Eng. Thesis, Kyoto University, 1971.

5) Adachi, T. and Okano, M.: A Constitutive Equation for Normally Consolidated Clay, Soils and Foundations, Vol.14, No.4, 1974, pp.55-63.

6) Karube, D.: Analysis of Mechanical Behaviour of Clay and its Application to Stability Analysis, Dr. Eng. Thesis, Kyoto University, 1974, (in Japanese).

7) Lade, P.V. and Duncan, J.M.: Elastoplastic Stress-Strain Theory for Cohesionless Soil, Proc. ASCE, Vol.101, No.GT10, 1975, pp.1037-1053.

8) Lade, P.V. and Duncan, J.M.: Stress-Path Dependent Behaviour of Cohesionless Soil, Proc. ASCE, Vol.102, No.GT1, 1976, pp.51-68.

9) Lade, P.V.: Prediction of Undrained Behaviour of Sand, Proc. ASCE, Vol.104, No.GT6, 1978, pp.721-735.

10) Prévost, J.-H.: Mathematical Modelling of Monotonic and Cyclic Undrained Clay Behaviour, International Journal for Numerical and Analytical Methods in Geomechanics, Vol.1, 1977, pp.195-216.

11) Prévost, J.-H.: Anisotropic Undrained Stress-Strain Behaviour of Clays, Proc. ASCE, Vol.104, No.GT8, 1978, pp.1075-1090.

12) Pender, M.J.: A Unified Model for Soil Stress-Strain Behaviour, Specialty Session 9, Proc. 9th Int. Conf. SMFE, 1977, pp.213-222.

13) Pender, M.J.: A Model for the Behaviour of Overconsolidated Soil, Géotechnique, Vol.28, No.1, 197[illegible], pp.1-25.

14) Mróz, Z., Norris, V.A. and Zienkiwicz, O.C.: Application of an Anisotropic Hardening Model in the Analysis of Elasto-Plastic Deformation of Soil, Géotechnique, Vol.29, No.1, 1979, pp.1-34.

15) Newland, P.L. and Allely, B.H.: Volume Change in Drained Triaxial Tests on Granular Materials, Géotechnique, Vol.7, No.1, 1957, pp.17-34.

16) Rowe, P.W.: The Stress-Dilatancy Relation for Static Equilibrium of an Assembly of Particles in Contact, Proc. Royal Soc., Vol.269, 1962, pp.500-527.

17) Rowe, P.W.: Theoretical Meaning and Observed Values of Deformation Parameters for Soil, Proc. Roscoe Memorial Symp., 1971, pp.143-194.

18) Horne, M.R.: The Behaviour of an Assembly of Rotund, Rigid, Cohesionless Particles, Part 1,2, Proc. Royal Soc.A, Vol.286, 1965, pp.62-97.

19) Horne, M.R.: The Behaviour of an Assembly of Rotund, Rigid, Cohesionless Particles, Part 3, Proc. Royal Soc.A, Vol.310, 1969, pp.21-34.

20) Oda, M.: A Mechanical and Statistical Model of Granular Materials, Soils and Foundations, Vol.14, No.1, 1974, pp.13-27.

21) Matsuoka, H.: Deformation Characteristics of Soil, Dr. Eng. Thesis, Kyoto University, 1973.

22) Tokue, T.: A Stress-Dilatancy Model of Granular Material under General Stress Condition, Soils and Foundations, Vol.19, No.1, 1979, pp.63-80.

23) Murayama, S.: A Theoretical Consideration on a Behaviour of Sand, Proc. IUTAM Symp. on Rheology and Soil Mech., Grenoble, 1964, pp.146-157, Springer-Verlag, 1966.

24) Murayama, S.: Constitutive Equations of Particulate Material in the Elastic State, Proc. Speialty Session 9, 9th Int. Conf. SMFE, 1977, pp.167-174.

25) Murayama, S.: Constitutive Equations of Particulate Material in the Plastic State, Proc. Specialty Session 9, 9th Int. Conf. SMFE, 1977, pp.175-182.

26) Murayama, S.: Constitutive Equations of Particulate Material in the Failure State, Proc. Specialty Session 9, 9th Int. Conf. SMFE, 1977, pp.183-190.

27) Murayama, S.: Effects of Deviatoric Stress History on the Constitutive Equations of Particulate Material, Proc. Specialty Session 9, 9th Int. Conf. SMFE, 1977, pp.191-199.

28) Matsuoka, H.: A Microscopic Study on Shear Mechanism of Granular Materials, Soils and Foundations, Vol.14, No.1, 1974, pp.29-43.

29) Matsuoka, H.: Stress-Strain Relationships of Sands based on the Mobilized Plane, Soils and Foundations, Vol.14, No.2, 1974, pp.47-61.

30) Matsuoka, H.: On the Significance of the Spatial Moblized Plane, Soils and Foundations, Vol.16, No.1, 1976, pp.91-100.

31) Matsuoka, H. and Nakai, T.: Stress-Deformation and Strength Characteristics of Soil under Three Different Principal Stresses, Proc. JSCE, No.232, 1974, pp.59-70.

32) Matsuoka, H. and Nakai, T.: Stress-Strain Relationship of Soil

Based on the "SMP", Proc. Specialty Session 9, 9th Int. Conf. SMFE, 1977, pp.153-162.

33) Mogami, T.: A Statistical Approach to the Mechanics of Granular Materials, Soils and Foundations, Vol.5, No.2, 1965, pp.26-36.

34) Mogami, T.: A Statistical Theory of Mechanics of Granular Materials, Jour. Faculty of Eng., Univ. of Tokyo, Ser.(B), Vol.28, No.2, 1965, pp.66-79.

35) Mogami, T.: Angle of Internal Friction and a Simple Transient Phenomenon of Granular Material, Trans. of JSCE, No.128, 1966, pp.53-62.

36) Mogami, T.: On the Deformation of Granular Material, Trans. of JSCE, No.129, 1966, pp.39-44.

37) Mogami, T.: Mechanics of Granular Material Composed of Particles of Various Size, Trans. of JSCE, No.137, 1967, pp.34-43.

38) Jowitt, P.W. and Munro, J.: The Influence of Void Distribution and Entropy on the Engineering Properties of Granular Media, Proc. Application of Statistics and Probability in Soil and Structural Engineering, DGEG2, Aachen, 1975, pp.365-385.

39) Brown, C.B.: The Use of Maximum Entropy in the Characterization of Granular Media, Proc. U.S.-Japan Seminar on Continuum-Mechanical and Statistical Approaches in the Mechanics of Granular Material, Sendai, 1978, pp.98-108.

40) Marsal, R.J.: A True Triaxial Apparatus to Test Rockfills, Proc. 8th Int. Conf. SMFE, Vol.1, 1973, pp.259-264.

41) Satake, M.: Constitution of Mechanics of Granular Materials through the Graph Theory, Proc. U.S.-Japan Seminar on Continuum-Mechanical and Statistical Approaches in the Mechaics of Granular Material, Sendai, 1978, pp.47-62.

42) Barden, L and Khayatt, A. J.: Incremental Strain Ratios and Strength of Sand in the Triaxial Test, Géotechnique, Vol.16,

No.4, 1966, pp.338-357.

43) Tatsuoka, F.: Stress-Dilatancy Relation of Anisotropic Sands in Three Dimensional Stress Condition, Soils and Foundations, Vol.16, No.2, 1976, pp.1-18.

44) Calladine, C.R.: A Microstructural View of the Mechanical Properties of Saturated Clay, Géotechnique, Vol.21, No.4, 1971, pp.391-415.

45) Arthur, J.R.F., Dunstan, T., Al-Ani, Q.A.J.L. and Assadi, A.: Plastic Deformation and Failure in Granular Media, Géotechnique, Vol.27, No.1, 1977, pp.53-74.

46) De Josselin De Jong, G.: Constitutive Relations for the Flow of a Granular Assembly in the Limit State of Stress, Proc. Specialty Session 9, 9th Int. Conf. SMFE, 1977, pp.87-95.

CHAPTER 2 MARKOV PROCESS

2.1 Introduction

In the classical mechanics the motions of bodies described by field equations. This means that the future motions are completely determined by the present state and are independent of the way how the present state has reached. On the other hand, in the probability theory the future is not uniquely determined, but we can only make the prediction with certain probability. The probability theory, therefore, plays an important and essential role when we understand and explain theoretically macroscopical phenomena based on the mechanical laws at the microscopical scale. For instance, the pressure gas can be derived from the collisions of randomly moving atoms.

The stochastic process, in which the future state can be probabilistically determined only by the present state, is called the Markov process. The Brownian motion of particles is a typical phenomenon of Markov process.

Before applying the Markov process to describe the mechanical behaviours of particulate materials, a brief mathematical explanation of Markov process is given in this chapter.

2.2 Markov Process[1),2),3)]

The Markov process is generally defined by the following equation.

$$P_n\{x(t_1), x(t_2), \cdots\cdots, x(t_{n-1}) | x(t_n)\} = P_2\{x(t_{n-1}) | x(t_n)\} \tag{2.1}$$

where t ; time

$X(t)$; stochastic process,

$x(t)$; specific value at time t in the stochastic process $X(t)$,

$P_n\{x(t_1), x(t_2), \cdots\cdots\cdots, x(t_{n-1}) | x(t_n)\}$; conditional probability of the relation $X(t_n)=x(t_n)$ on the hypothesis $X(t_1)=x(t_1)$, $X(t_2)=x(t_2)$, $\cdots\cdots$, $X(t_{n-1})=x(t_{n-1})$,

$P_2\{x(t_{n-1}) | x(t_n)\}$; conditional probability of the relation $X(t_n)=x(t_n)$ on the single hypothesis $X(t_{n-1})=x(t_{n-1})$.

Eq.(2.1) means that the conditional probability of the relation $X(t_n)=x(t_n)$ on the hypothesis $X(t_1)=x(t_1)$, $X(t_2)=x(t_2)$, $\cdots\cdots$, $X(t_{n-1})=x(t_{n-1})$ is identical with the conditional probability of $X(t_n)=x(t_n)$ on the single hypothesis $X(t_{n-1})=x(t_{n-1})$. In other words, this definition states that if the present state $x(t_{n-1})$ is given, no additional data concerning the past states of the system can alter the conditional probability of the future state $x(t_n)$.

Instead of the conditional probability $P_2\{x(t_{n-1}) | x(t_n)\}$ in Eq.(2.1), $P(x,y;t,s)$ which represents the conditional probability $X(s)=y$ on the hypothesis $X(t)=x$ will be used and called the transition probability in the following discussions. Then, the Markov process is rewritten as

$$P(x,y;t,s)=\int_{-\infty}^{\infty} P(x,z;t,u)P(z,y;u,s)\,dz \qquad (2.2)$$

where $t<u<s$.

Eq.(2.2) is called the Chapman-Kolmogorov equation.

In order to expand the mathematical discussions three assumptions for the transition probability $P(x,y;t,s)$ are required to

satisfied the regularity, i.e.,

Assumption 1: When s and y in $P(x, y; t, s)$ are given with $s - t \geq \epsilon\ (\epsilon > 0)$, $P(x, y; t, s)$ can be differentiated three times with respect to x and these partially differential coefficients are continuous and finite. On the other hand, $P(x, y; t, s)$ can be differentiated once with respect with s and $\frac{\partial}{\partial s} P(x, y; t, s)$ is continuous and finite.

Assumption 2: The following equations exist.

$$\lim_{\Delta \to 0} \frac{1}{\Delta} \int_{-\infty}^{\infty} (z - x) P(x, z; t, t+\Delta)\, dz = A(t, x) \tag{2.3}$$

$$\lim_{\Delta \to 0} \frac{1}{2\Delta} \int_{-\infty}^{\infty} (z - x)^2 P(x, z; t, t+\Delta)\, dz = B(t, x) \tag{2.4}$$

$$\lim_{\Delta \to 0} \frac{1}{\Delta} \int_{-\infty}^{\infty} |z - x|^3 P(x, z; t, t+\Delta)\, dz = 0 \tag{2.5}$$

Assumption 3: $R(y)$ is the function which is non-negative and always zero except within the closed interval $[\alpha, \beta]$. The derivations of the first and the second order, $R'(y)$ and $R''(y)$ exist and are continuous and finite.

From Assumptions 1 and 3, we have

$$\int_{\alpha}^{\beta} \frac{\partial}{\partial s} P(x, y; t, s) R(y)\, dy = \frac{\partial}{\partial s} \int_{\alpha}^{\beta} P(x, y; t, s) R(y)\, dy$$

$$= \lim_{\Delta \to 0} \frac{1}{\Delta} \int_{-\infty}^{\infty} \{P(x, y; t, s+\Delta) - P(x, y; t, s)\} R(y)\, dy$$

using Eq.(2.2) gives

$$= \lim_{\Delta \to 0} \frac{1}{\Delta} \left\{ \int_{-\infty}^{\infty} R(y)\, dy \int_{-\infty}^{\infty} P(x, z; t, s) P(z, y; s, s+\Delta)\, dz \right.$$

$$\left. - \int_{-\infty}^{\infty} P(x, y; t, s) R(y)\, dy \right\}$$

$$= \lim_{\Delta \to 0} \frac{1}{\Delta} \Big[\int_{-\infty}^{\infty} P(x, z; t, s) \int_{-\infty}^{\infty} P(z, y; s, s+\Delta) \Big\{ R(z) + R'(z)(y-z) + R''(z) \frac{(y-z)^2}{2!} + R'''(\xi) \frac{(y-z)^3}{3!} \Big\} dy\, dz - \int_{-\infty}^{\infty} P(x, z; t, s) R(z)\, dz \Big]$$

where $\xi = z + \theta(y-z)$, $0 < \theta < 1$,

using Eq.(2.2), and Assumptions 2 and 3 becomes

$$= \int_{\alpha}^{\beta} P(x, z; t, s) \Big\{ R'(z) A(z, s) + R''(z) B(z, s) \Big\} dz$$

and finally carrying out the integration of parts with $R(\alpha) = R(\beta) = R'(\alpha) = R'(\beta) = 0$, we obtain

$$= \int_{\alpha}^{\beta} \Big[-\frac{\partial}{\partial s} \Big\{ P(x, z; t, s) A(z, s) \Big\} + \frac{\partial^2}{\partial z^2} \Big\{ P(x, z; t, s) B(z, s) \Big\} \Big] R(z)\, dz$$

The above equation can be rewritten as follows.

$$\int_{\alpha}^{\beta} \Big[\frac{\partial}{\partial s} P(x, y; t, s) + \frac{\partial}{\partial y} \Big\{ A(y, s) P(x, y; t, s) \Big\} - \frac{\partial^2}{\partial y^2} \Big\{ B(y, s) P(x, y; t, s) \Big\} \Big] R(y)\, dy = 0 \quad (2.6)$$

As both the closed interval $[\alpha, \beta]$ and $R(y)$ are arbitrary, the terms of bracket in Eq.(2.6) is reduced to

$$\frac{\partial}{\partial s} P(x, y; t, s) = -\frac{\partial}{\partial y} \Big[A(y, s) P(x, y; t, s) \Big] + \frac{\partial^2}{\partial y^2} \Big[B(y, s) P(x, y; t, s) \Big] \quad (2.7)$$

Eq.(2.7) is called the Kormogorov's forward differential equation in the probability theory or the Fokker-Planck equation in the diffusion theory. The transition probability $P(x, y; t, s)$ for the random process $X(t)$ is obtained by solving Eq.(2.7) and then the change in the system as the Markov process can be

probabilistically determined.

Next, let's discuss the probability density function of $w(x,t)$ by using Eq.(2.7). The probability density function $w(x,t)$ satisfies the following equations.

$$w(x,t) \geqq 0 \quad , \int_{-\infty}^{\infty} w(x,t)\,dx = 1 \tag{2.8}$$

Then, from Eqs.(2.2) and (2.8) we have

$$\int_{-\infty}^{\infty} w(x,t)\,P(x,y;t,s)\,dx = w(y,s) \tag{2.9}$$

$$w(y,s) \geqq 0 \quad , \int_{-\infty}^{\infty} w(y,s)\,dy = 1 \tag{2.10}$$

Differentiating Eq.(2.9) with respect to s gives

$$\frac{\partial}{\partial s} w(y,s) = \frac{\partial}{\partial s}\left\{\int_{-\infty}^{\infty} w(x,t)\,P(x,y;t,s)\right\}$$

$$= \int_{-\infty}^{\infty} w(x,t)\,\frac{\partial}{\partial s} P(x,y;t,s)\,dx$$

using Eq.(2.7),

$$= \int_{-\infty}^{\infty} w(x,t)\left[-\frac{\partial}{\partial y}\left\{A(y,s)P(x,y;t,s)\right\} + \frac{\partial^2}{\partial y^2}\left\{B(y,s)\,P(x,y;t,s)\right\}\right] dx$$

$$= -\frac{\partial}{\partial y}\left[A(y,s)\,w(y,s)\right] + \frac{\partial^2}{\partial y^2}\left[B(y,s)\,w(y,s)\right]$$

Rewriting the above equation, we finally obtain

$$\frac{\partial}{\partial s} w(y,s) = -\frac{\partial}{\partial y}\left[A(y,s)\,w(y,s)\right] + \frac{\partial^2}{\partial y^2}\left[B(y,s)\,w(y,s)\right] \tag{2.11}$$

Eq.(2.7) or Eq.(2.11) is the basic equation of Markov process.

Let's extend the above discussions for the one dimensional Markov process to the n-dimensional Markov process. In the case that a point $\xi = (x_1, x_2, \cdots\cdots, x_n)$ in the n-dimensional space moves stochastically, the transition probability of the point $\eta = (y_1, y_2, \cdots\cdots, y_n)$ at time s which was the point ξ at time t can be written by $P(\xi, \eta; t, s)$ in the similar way. Then, the Kolmogorov's forward differential equation in the n-dimensional Markov process becomes as follows.

$$\frac{\partial}{\partial s}P(\xi, \eta; t, s) = -\sum_{i=1}^{n} \frac{\partial}{\partial y_i}\left[A_i(\eta, s)P(\xi, \eta; t, s)\right] + \sum_{i,j=1}^{n} \frac{\partial^2}{\partial y_i \partial y_j}\left[B_{ij}(\eta, s)P(\xi, \eta; t, s)\right] \quad (2.12)$$

Furthermore, the probability density function $w(x, t)$ which represents the motions of $x(t)$ in the n-dimensional Markov process is defined as follows.

$$\frac{\partial}{\partial s}w(\eta, s) = -\sum_{i=1}^{n} \frac{\partial}{\partial y_i}\left[A_i(\eta, s)w(\eta, s)\right] + \sum_{i,j=1}^{n} \frac{\partial^2}{\partial y_i \partial y_j}\left[B_{ij}(\eta, s)w(\eta, s)\right] \quad (2.13)$$

where

$$A_i(\eta, s) = \lim_{\Delta \to 0} \frac{1}{\Delta} \int_{-\infty}^{\infty} \cdots \int_{-\infty}^{\infty} (z_i - y_i) P(\eta, \zeta; s, s+\Delta)\, dz_1 dz_2 \cdots dz_n \quad (2.14)$$

$$B_{ij}(\eta, s) = \lim_{\Delta \to 0} \frac{1}{\Delta} \int_{-\infty}^{\infty} \cdots \int_{-\infty}^{\infty} (z_i - y_i)(z_j - y_j) P(\eta, \zeta; s, s+\Delta)\, dz_1 dz_2 \cdots dz_n \quad (2.15)$$

$\zeta(z_1, z_2, \cdots\cdots, z_n)$; a point in the n-dimensional space at time $s+\Delta$.

In consequence, the n-dimensional Markov process is mathematically governed by Eq.(2.12) or Eq.(2.13) and the change in the system as the n-dimensional Markov process can be completely described by solving Eq.(2.12) or Eq.(2.13). In the following discussions Eq.(2.12) or Eq.(2.13) is called the basic equation of Markov

process.

2.3 Conclusions

In this chapter the mathematical explanation of Markov process is carried out based on the probability theory. The mathematical treatment of Markov process should strictly be done by using the measurement theory, but is omitted in this discussion because it is extremely complicated and is not much necessary in the following chapters.

Throughout this chapter, the following conclusions are obtained.

(1) The Markov process is defined by Eq.(2.1). This equation means that $X(t_n)=x(t_n)$ at time t_n depends on only $X(t_{n-1}) = x(t_{n-1})$ at time t_{n-1} and is independent of $X(t)$ at times $t_1, t_2, \cdots\cdots\cdots, t_{n-2}$ in the stochastic process $X(t)$.

(2) Based on three mathematical assumptions, the basic equation, Eq.(2.7), of one-dimensional Markov process is derived from the Chapman-Kolmogorov equation. This basic equation is called the Kolmogorov's forward differential equation or the Fokker-Planck equation.

(3) The basic equation, Eq.(2.12), for the n-dimensional Markov process is extended from Eq.(2.7). The probability density function $w(x, t)$ in the n-dimensional Markov process is given by Eq.(2.13). Namely, the n-dimensional Markov process is mathematically expressed by Eq.(2.12) or Eq.(2.13).

References for Chapter 2

1) Feller, W.: An Introduction to Probability Theory and its Applications, John Wiley & Sons, Inc., 1957.

2) Gnedenko, B.V.: Theory of Probability, Chelsea, New York, 1969.

3) Yoshida, K.: Introduction of Pysical Mathematics (Butsuri-Sugaku Gairon), Sangyo-Tosho, 1974, (in Japanese).

CHAPTER 3 APPLICATION OF MARKOV PROCESS TO MECHANICAL BEHAVIOURS OF PARTICULATE MATERIAL

3.1 Introduction

Many researches concerning the mechanical behaviours of particulate materials have been carried out based on microscopic approaches as shown in section 1.1. In most of these researches, the motions of particles are uniquely determined since they use the frictional law with the constant frictional angle. However, the actual motions of particles are not unique but random because of the irregularities of particles in both shape and size, and the complicated fabric of particulate material. Thus, it is reasonable that the probability theory is applied in order to analyse the mechanical behaviours of particulate material at the particle scale.

The first attempt that applied the Markov process to the deformation processes of particulate materials has been carried out by Litwiniszyn[1),2),3)]. In order to solve the subsidence problem of particulate material he adopted the random walk model of particle which is the simplest case of Markov process. Fig.3.1 shows a system of cage by which his considerations were done. The probability $P(x, z)$ of a void occurring in the cage with the coordinate (x, z) can be given as the following equation, assuming that the probabilities of a migration of a particle from the cage B to the cage A and from the cage C to the cage A are equal.

$$P(x, z+\rho) = \frac{1}{2} P(x-a, z) + \frac{1}{2} P(x+a, z) \qquad (3.1)$$

Taking $a \to 0$ and $\rho \to 0$ in Eq.(3.1), we derive

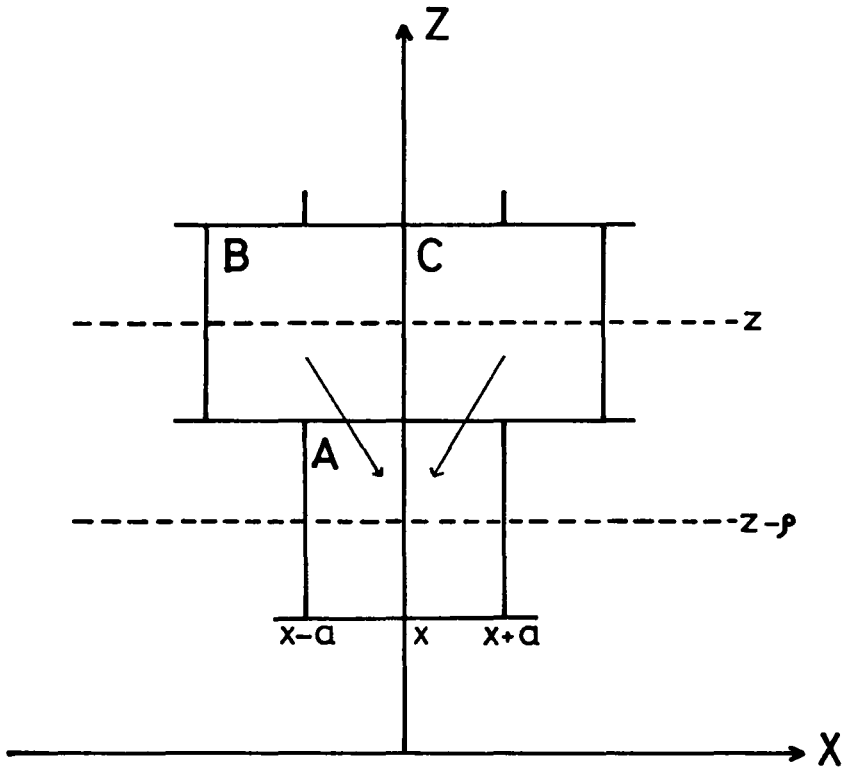

Fig.3.1 System of cage (after Litwiniszyn)

$$\frac{\partial}{\partial z} P(x,z) = B \frac{\partial^2}{\partial x^2} P(x,z) \tag{3.2}$$

where

$$B = \lim_{a \to 0,\, \delta \to 0} \frac{a^2}{2\delta} \tag{3.3}$$

Putting $n = 1$, $A_1 = 0$ and $B_{11} = B$ in Eq.(2.12), Eq.(2.12) becomes equal to Eq.(3.3)

Sweet and Bogdanoff[4),5)] used the same approach as Litwiniszyn to predict the subsidence of particulate material. The model proposed by them treated only the settlement and did not take account of the relation between the stress and the displacement.

Brahma[6)] tried to investigate the two-dimensional creep behaviours of particulate material from probabilistic consideration and derived the following equation.

$$\frac{\partial \bar{F}}{\partial t} = \beta_1 \frac{\partial \bar{F}}{\partial X} + \beta_2 \frac{\partial \bar{F}}{\partial Y} + D_1 \frac{\partial^2 \bar{F}}{\partial X^2} + D_2 \frac{\partial^2 \bar{F}}{\partial Y^2} \tag{3.4}$$

where $F(X, Y, t)$; probability of occupying a position with ordinates (X, Y) at time t ,

β_1 and β_2 ; quantities depending on the mean values of displacements with respect to X- axis and Y- axis respectively,

D_1 and D_2 ; quantities depending on the variances of displacements of rods with respect to X- axis and Y- axis.

Putting $n = 2$, $A_1 = \beta_1$, $A_2 = \beta_2$, $B_{11} = D_1$ and $B_{22} = D$ in Eq.(2.13), Eq.(2.13) becomes equal to Eq.(3.4). Furthermore, he performed creep tests on samples composed of steel rods and examined the validity of Eq.(3.4) by means of taking photographs and measuring the displacement of rods on these photographs. From the comparison of test results with calculated values which are obtained by using

Eq.(3.4), he concluded that the two-dimensional creep behaviours of particulate material regarded as the Markov process.

Goldstein et al.[7] tried to apply Eq.(2.12) to the rheological behaviours of clays.

In these attempts it is apparent that the mechanical behaviours of particulate material as the Markov process are governed by Eq.(2.12) or Eq.(2.13) in the deformation process. When the mechanical behaviours of particulate material are considered as the Markov process, it is also known how important to choose which physical quantities as the random variables. In these researches, however, the shear deformation processes of particulate material have not been treated yet, and then complete stress-strain relations have never been attained.

In the following sections a mechanical model of particulate material will be proposed by extending their application

3.2 Random Variable

A random variable is mathematically defined by using the measurement theory, but in this section we do not give the strict definition and define it as a variable which takes various values by chance.

Fig.3.2 shows the geometrical relation between two adjacent particles in a particulate material. The deformation of particulate material is considered to be the summation of the relative motion of two particles. Let's denote by a_{ji} the probability that the upper particle in Fig.3.2 moves to the right or the left. Namely, a_{ji} is the probability that a random variable changes from the state i to the state j . If the state at every contact points of particles are represented by n discontinuous states, the change in the states caused by an external force is expressed

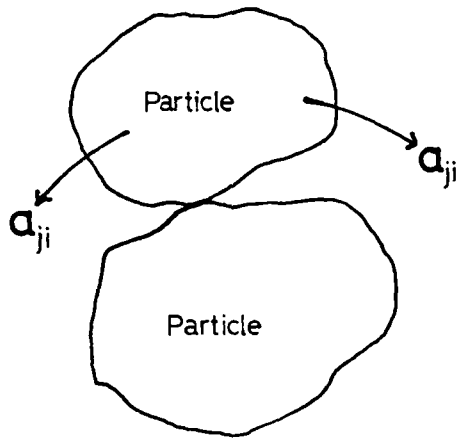

Fig.3.2 Relative motion
of two particles

by the following transition probability matrix $[\underset{\sim}{a}]$.

$$[\underset{\sim}{a}] = \begin{pmatrix} a_{11} & a_{12} & \cdots\cdots & a_{1n} \\ a_{21} & a_{22} & \cdots\cdots & a_{2n} \\ \cdots & \cdots & \cdots & \cdots \\ \cdots & \cdots & \cdots & \cdots \\ a_{n1} & a_{n2} & \cdots\cdots & a_{nn} \end{pmatrix} \tag{3.5}$$

where $\sum_{j=1}^{n} a_{ji} = 1$.

If the external forces are also divided into discontinuous steps (for example, loading or unloading process under stress controlled triaxial test), the transition probability matrix $[\underset{\sim}{a}]_{1\to m}$ from the first step to the m-th step becomes as follows.

$$[\underset{\sim}{a}]_{1\to m} = \prod_{k=1}^{m-1} [\underset{\sim}{a}]_{m-k} \tag{3.6}$$

where $[\underset{\sim}{a}]_k$; transition probability matrix which represents the change in state in the particulate material due to the change in external force from the k-th step to the (k+1)-th step.

On the other hand, putting $\Delta t = (s-t)/m$ in Eq.(2.2), the following equation is derived.

$$P(x, y; t, s) = \int_{-\infty}^{\infty} \cdots \int_{-\infty}^{\infty} P(x, z_1; t, t+\Delta t) \cdot P(z_1, z_2; t+\Delta t, t+2\Delta t) \cdots\cdots\cdots P(z_{m-1}, y; s-\Delta t, s)\, dz_1 dz_2 \cdots\cdots dz_{m-1} \tag{3.7}$$

Though Eq.(3.6) is a discontinuous equation, it is essentially equal to Eq.(3.7) which defines the continuous Markov process. Thus, it is shown that the motions of particles in Fig.3.2 are considered to be the Markov process.

The usefulness for the mechanical model of particulate material based on the Markov process mainly depends on the choice of

random variable as a state variable. Thus, the random variable will be chosen so as to be the best representation of the state of the particulate material at the particle scale after the following consideration.

If all physical quantities which contribute to the deformation processes of particulate material are known, the deformation processes regarded as the Markov process are theoretically described by solving the basic equation of the n-dimensional Markov process, i.e., Eq.(2.12) or Eq.(2.13). However, it is impossible to list up all the quantities because the deformation mechanisms have not been made clear at the particle scale.

In microstructural continuum theories porosity has been used as a physical quantity which represents the state in the particulate material. On the other hand, it has been pointed out that the contact angle of particles which represents the fabric of particulate material is a profound important state variable during the deformation processes by Rowe[8], Murayama[9] and Horne[10),11]. The experimental researches performed by Oda[12),13], Murayama and Matsuoka[14], Matsuoka[15] and Borowicka[16] have verified the importance of the contact angle. From these results the contact angle of particles which is considered to be the most contributed quantity to the deformation of particulate material is adopted as a random variable in this study. This means that the motions of particles under the deformation process are replaced by the change in the contact angle of particles. In the proposed model a particle is assumed to be rigid and not to be crushed. Then, the deformation of particulate material is only caused by the rearrangement of the particle positions.

A set of particles in the particulate material is depicted in Fig.3.3. The direction of orthogonal three principal stresses

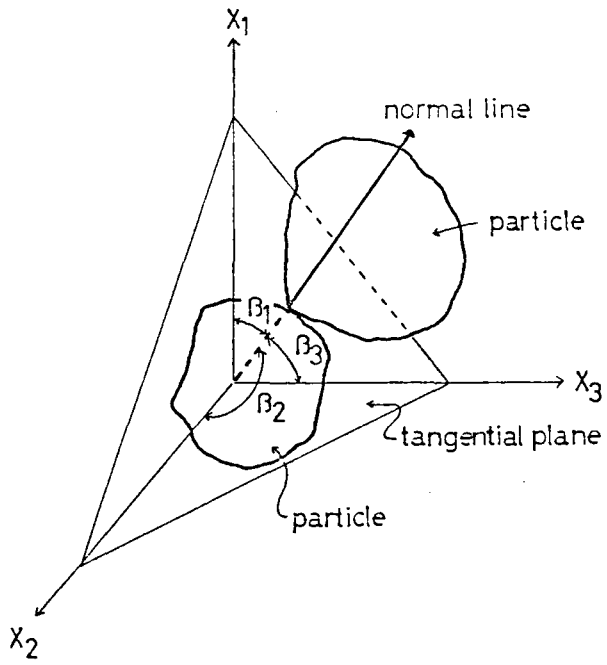

Fig.3.3 Two adjacent particles and reference frame

are shown as the reference axes. The angles between the normal to tangential plane at the contact point of adjacent particles and the reference axes are represented by β_1 , β_2 and β_3 respectively. The direction of normal to tangential plane is prescribed by two angles of them. Then, the angles β_1 and β_2 are adopted as random variables in the proposed model. The angle β_1 ranges between zero and $\pi/2$, and the angle β_2 between zero and 2π because all the normals to tangential planes are prescribed in these ranges. In the following discussions a pair of β_1 and β_2 is called a contact angle of particles and is denoted by η .

3.3 Basic Equation of Markov Process

Let try to apply the basic equation of Markov process to the mechanical model of particulate material in this section.

As the angles β_1 and β_2 defined in the previous section are probabilistically independent each other, B_{ij} $(i \neq j)$ in Eq.(2.15) which corresponds to the covariance of β_1 and β_2 is reduced to zero. Thus, the basic equation of Markov process, Eq.(2.13), is rewritten as follows.

$$\frac{\partial}{\partial s} w(\eta, s) = -\sum_{i=1}^{2} \frac{\partial}{\partial \beta_i} [A_i(\eta, s)\, w(\eta, s)] + \sum_{i=1}^{2} \frac{\partial^2}{\partial \beta_i^2} [B_{ii}(\eta, s)\, w(\eta, s)] \tag{3.8}$$

where

$$A_i(\eta, s) = \lim_{\Delta \to 0} \frac{1}{\Delta} \int_0^{2\pi} \int_0^{\pi/2} (\beta_{i, s+\Delta} - \beta_{i, s}) P(\eta_s, \eta_{s+\Delta})\, d\beta_1\, d\beta_2 \tag{3.9}$$

$$B_{ii}(\eta, s) = \lim_{\Delta \to 0} \frac{1}{2\Delta} \int_0^{2\pi} \int_0^{\pi/2} (\beta_{i, s+\Delta} - \beta_{i, s})^2 P(\eta_s, \eta_{s+\Delta})\, d\beta_1\, d\beta_2 \tag{3.10}$$

$\eta(\beta_1, \beta_2)$; contact angle of particles,

$w(\eta, s)$; probability density function of contact angle at s ,

$P(\eta_s, \eta_{s+\Delta})$; transition probability of contact angle which represents the change in angle from η_s at s to $\eta_{s+\Delta}$ at $s+\Delta$.

The variable s in Eq.(3.8) usually represents time in the Markov process, but must not be physical time as far as the variable s can evaluate the change of state for the particulate material. Then, the stress or the stress ratio may be used as a state variable in the case when the mechanical behaviours do not depend on time such as the shearing processes of sands. In the proposed model the stress ratio is adopted as s in Eq.(3.8) for the shearing processes of particulate material. Therefore, the coefficients A_i and B_{ii} defined by Eqs.(3.9) and (3.10) correspond respectively to the mean value and the variance with respect to the change in contact angles when the stress ratio varies from s to $s+\Delta$. It is found that A_i and B_{ii} are the important coefficients which represent the mechanical properties of particulate material at the contact points. Namely, the validity of the proposed model depends on the way to determine the coefficients.

3.4 Method to Determine the Coefficients A_i and B_{ii}

In the previous section it has been clear that the rational method to determine the statistical quantities A_i and B_{ii} influences the validity of the model based on the Markov process as well as the choice of random variables. In this section the concepts of the potential barrier and the potential slip plane will be introduced in order to determine the coefficients A_i and B_{ii} .

3.4.1 Potential barrier

Fig.3.4 illustrates typical figures which are often used to explain the behaviours of elastic, viscous and visco-elastic bodies

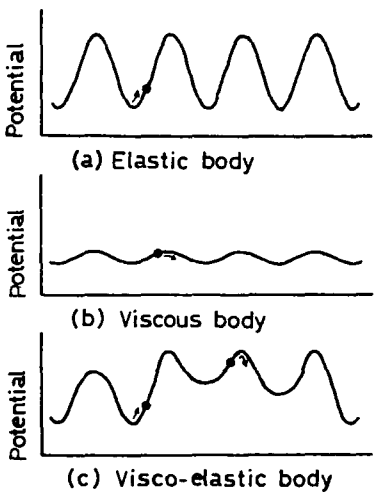

Fig.3.4 Concept of potential barrier

at the micro-structural scale[17]. In the elastic body the potential barrier is so high that the atoms composing the elastic body cannot surmount it as shown in Fig.3.4(a). Thus, the body exibits elastic behaviour. In the viscous body, however, the potential barrier is low as shown in Fig.3.4(b), the atoms composing the body can easily surmount it and the body exhibits viscous flow. Furthermore, in the vosco-elastic body the height of the potential barrier is random as shown in Fig.3.4(c). This is a micro-structural explanation of the visco-elastic behaviour.

In the proposed model the similar micro-structural concept stated above is assumed to be applied to a potential barrier for the change in contact angle at a contact point. That is to say, in the application of the potential barrier to the mechanical model the following are assumed; a recoverable change in contact angle occurs at the contact point where the activation energy cannot surmount the potential barrier; an irrecoverable change in contact angle takes place at the contact point where the activation energy can surmount the potential barrier; and the height of potential barrier at each contact point depends on the direction of change in contact angle. Based on these considerations the potential barrier extends to the three dimensional space for particulate material. Fig.3.5 shows a potential barrier of deformed bell shape in the three dimensional space. The deformed bell shaped potential barrier is related to the concept of the potential slip plane. The detail explanations for this remain to be done later.

In order to determine the coefficients A_i and B_{ii}, it is necessary to make clear inter-relation between microscopic quantities and macroscopic quantities. It is assumed that the direction of change in a contact angle agrees with the direction of the

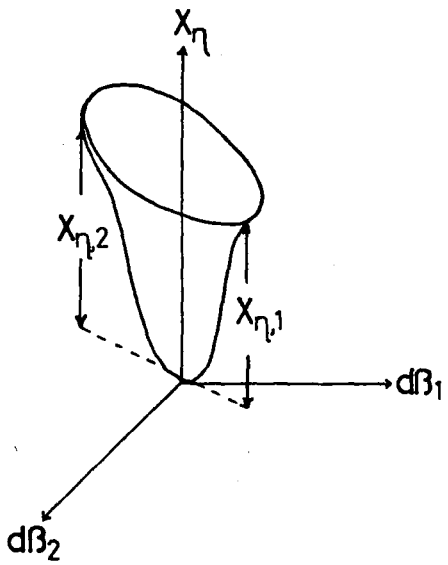

Fig.3.5 Potential barrier at contact point

minimum or the maximum height of the deformed bell as shown in Fig. 3.5. The minimum and the maximum heights of the potential barrier at the contact angle η are denoted by $x_{\eta,1}$ and $x_{\eta,2}$ respectively. Furthermore, the total number of contact points in the particulate material is denoted by N_c, the number of contact points with the contact angle η is denoted by n_η, the number of contact points where the activation energy can surmount the potential barriers $x_{\eta,1}$ and $x_{\eta,2}$ in x_η are denoted by $n_{\eta,1}$ and $n_{\eta,2}$ respectively, and the number of contact points where the activation energy cannot surmount the potential barrier is denoted by $n_{\eta,0}$. Then, the following equations are derived.

$$\sum_{\beta_1=0}^{\pi/2}\sum_{\beta_2=0}^{2\pi}(n_{\eta,1}+n_{\eta,2}+n_{\eta,0}) = \sum_{\beta_1=0}^{\pi/2}\sum_{\beta_2=0}^{2\pi} n_\eta = N_c \tag{3.11}$$

$$\sum_{\beta_1=0}^{\pi/2}\sum_{\beta_2=0}^{2\pi}(n_{\eta,1}\cdot x_{\eta,1}+n_{\eta,2}\cdot x_{\eta,2}+n_{\eta,0}\frac{x_{\eta,1}+x_{\eta,2}}{2R_\eta}) = \Delta\overline{W} \tag{3.12}$$

$$N_c\cdot w(\eta,s)\,d\beta_1\cdot d\beta_2 = n_\eta \tag{3.13}$$

where N_c ; total number of contact points in the particulate material,

$\Delta\overline{W}$; work done into the particulate material by the change of external force,

R_η ; coefficient expressing the amount of activation energy at the contact points where the recoverable change in contact angles occurs and macroscopically corresponding to the ratio of elastic strain component to total strain.

In Eq.(3.12) the left hand side represents the internal energy of the body and the right hand side is the work done by the external agency. Namely, Eq.(3.12) corresponds to the first law of thermodynamics or the energy balance equation.

For later convenience, let us denote the ratio $x_{\eta,1}/x_{\eta,2}$ and $n_{\eta,2}/n_{\eta,1}$ by $R_{p,\eta}$ and $R_{n,\eta}$ respectively, i.e.,

$$x_{\eta,1}/x_{\eta,2} = R_{p,\eta} \tag{3.14}$$

$$n_{\eta,2}/n_{\eta,1} = R_{n,\eta} \tag{3.15}$$

For the case of the activation energy surmounting the minimum potential barrier at each contact angle, the probability density function of the contact angles is assumed to be same in form as the probability density function of the contact angles in the whole particulate material. Then, the following equation is given.

$$n_{\eta,1} = N_{c,1} \cdot w(\eta, s)\, d\beta_1 \cdot d\beta_2 \tag{3.16}$$

where $N_{c,1}$; total number of contact points where the activation energy can surmount the minimum potential barrier at each contact angle.

By using Eqs.(3.11), (3.12), (3.14), (3.15) and (3.16), we solve them with respect to $N_{c,1}$ and have the following equation (see Appendix 3.1).

$$N_{c,1} = \frac{\Delta W - \sum_{\beta_1=0}^{\pi/2} \sum_{\beta_2=0}^{2\pi} \left(\frac{R_{p,\eta}+1}{2R_\eta \cdot R_{p,\eta}} \cdot x_{\eta,1} \cdot n_\eta \right)}{\sum_{\beta_1=0}^{\pi/2} \sum_{\beta_2=0}^{2\pi} \left[x_{\eta,1} \cdot w(\eta,s)\, d\beta_1 \cdot d\beta_2 \cdot \left\{ \left(1+\frac{R_{n,\eta}}{R_{p,\eta}}\right) - \left(1+\frac{1}{R_{p,\eta}}\right)(1+R_{n,\eta})/2R_\eta \right\} \right]} \tag{3.17}$$

The right hand side of Eq.(3.17) includes the six quantities, $x_{\eta,1}$, n_η , $w(\eta,s)$, $R_{p,\eta}$, $R_{n,\eta}$ and R_η which represent the mechanical properties of particulate material at the particle scale. When these quantities are given, $n_{\eta,1}$ is expressed in

terms of the quantities by substituting Eq.(3.17) into Eq.(3.16) and $n_{\eta,2}$ is then obtained by using Eq.(3.15). Furthermore, $n_{\eta,0}$ is determined from Eqs.(3.11) and (3.13). The details about physical meanings of the six quantities will be explained from the microscopic view point later.

3.4.2 Potential slip plane

when the stress ratio change from the peak to the residual value in a triaxial shearing test with particulate material, slip planes are usually observed on the surface of a relative dense sample. This macroscopically observed phenomenon of the formation of slip planes is considered to be the convergence of the local slip plane, which develop randomly at the numerous contact points in the shearing process. The potential slip planes used in this study finally coincide with the macroscopically observed slip planes when the stress ratio reaches to the residual value in the shearing process. It is impossible to uniquely determine the motions of particles under deformation process due to the randomness of particles in both shape and size, the complicated fabric and the restraint of adjacent particles. Thus, it is necessary to introduce the probabilistic consideration in order to establish the relation between the local slip planes and the potential slip plane.

The direction of local slip plane at a contact point should coincide with that of the potential slip plane, but in reality the direction of local slip plane may not coincide with the direction of the potential slip plane due to the restraint by adjacent particles. It is supposed, therefore, that the probabilistic variation of directions of local slip planes tends to coincide with the direction of the potential slip plane. The relation between

the potential slip plane and local slip planes is shown in Fig.3.6. Fig.3.6(a) illustrates a conventional triaxial specimen under the shearing test in which a potential slip plane and numerous local slip planes are shown. Fig.3.6(b) shows the relation between one of the numerous local slip planes in the specimen and the potential slip plane. The term 'probabilistic' means that the probability of the tendency of local slip planes to be parallel with the potential slip plane is larger than that to move to the reverse direction as shown in Fig.3.6(b). Namely, the directions of local slip planes with the minimum potential barrier tend towards that of the potenial slip plane. On the othe hand, the maximum potential barrier corresponds to opposite behaviours. This tendency for the motions of particles under shearing process is called the concept of the potential slip plane in this study. In Fig.3.5 $\chi_{\eta,1}$ is the height of the potential barrier at contact points with contact angle η when local slip planes tend towards the potential slip plane. $\chi_{\eta,2}$ is that for the case of the opposite behaviours. Generally, $\chi_{\eta,1}$ and $\chi_{\eta,2}$ take different values, and then the potential barrier shown in Fig.3.5 has a distorted bell shape.

The potential slip plane has already been considered by Murayama[18),19)], Matsuoka and Nakai[20)] and Satake[21)]. Murayama for the first time paid attention to the plane where the stress ratio τ/σ is the maximum in the triaxila test specimen as shown in Fig.3.7. He gave the meaning of this plane along which the mobilization of particles due to the deviatoric stress is most violent, and named it the plane of maximum mobilization. Matsuoka and Nakai extended the $(\tau/\sigma)_{max}$ - plane proposed by Murayama to the three dimensional space as shown in Fig.3.8 and called the spatial mobilized plane (SMP). They defined that on the average soil particles are most mobilized along the SMP in the three dimen-

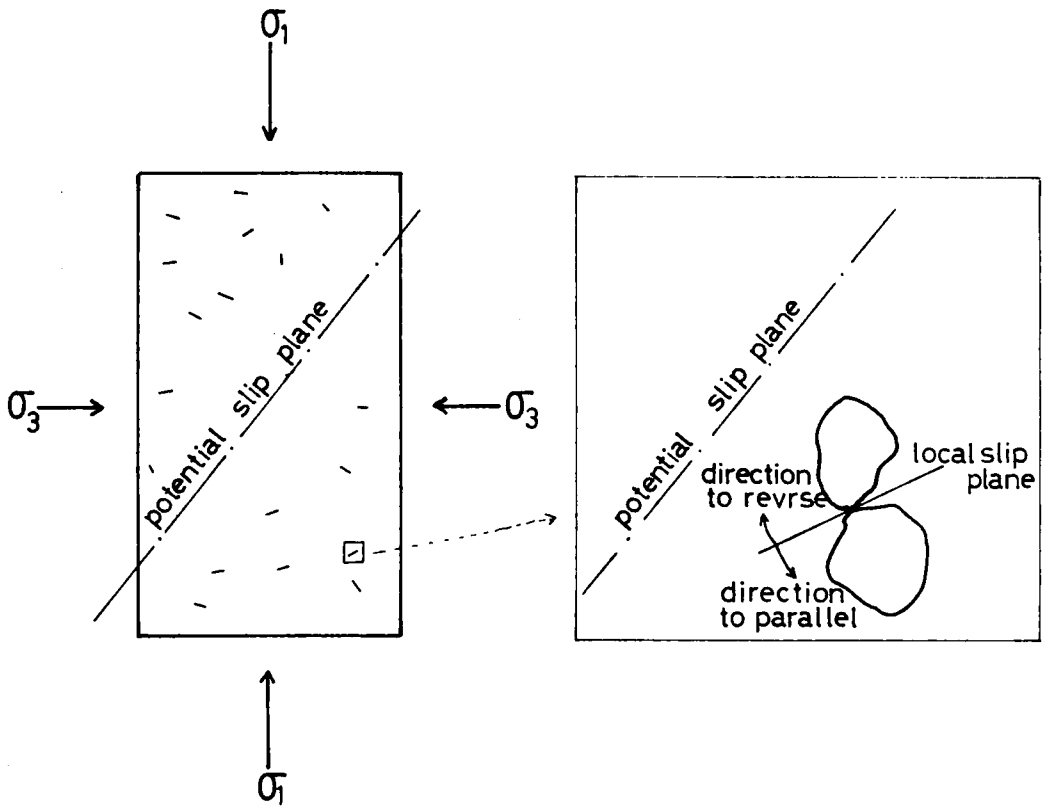

(a) (b)

Fig.3.6 Relation between potential slip plane and local slip planes

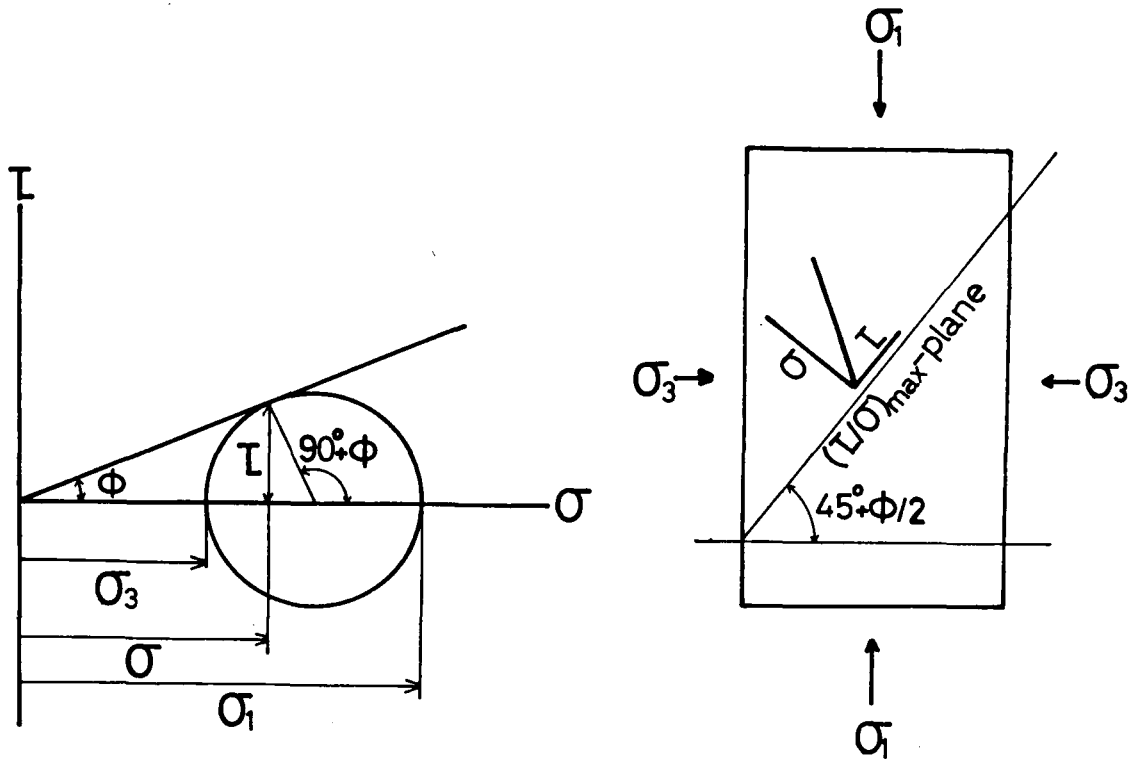

Fig.3.7 Plane of maximum mobilization (after Murayama)

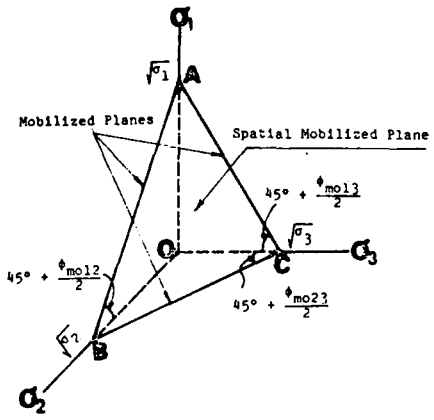

Fig.3.8 Spatial mobilized plane in three dimensional stress space (after Matsuoka and Nakai)

sional stress space. The shear-normal stress ratio τ/σ_N on the SMP and the direction of the normal to the SMP are derived from Fig.3.8 as follows.

$$\frac{\tau}{\sigma_N} = \sqrt{\frac{I_1 I_2 - 9 I_3}{9 I_3}} \tag{3.18}$$

$$\cos\phi_{mo,i} = \sqrt{\frac{I_3}{\sigma_i I_2}} \qquad (i = 1, 2, 3) \tag{3.19}$$

where I_1, I_2 and I_3 ; first, second and third effective invariants,

$\phi_{mo,i}$; angle between the normal to the SMP and the reference axis X_i .

When von Mises' yield criterion is applied, the octahedral plane in the three dimensional stress space may be regarded as the potential slip plane. Satake stated that the octahedral plane is an average slip plane in the reference frame when local slips in a material are assumed to occur uniformly in all directions.

In this study the SMP defined by Eq.(3.19) is adopted as the potential slip plane because it can well represent the mechanical properties of particulate material in the three dimensional stress space.

3.4.3 Derivation of the coefficients A_i and B_{ii}

Let us define the amount of change in contact angle η by $\delta\eta$ during the deformation process. Furthermore, we assume that the contact angle can only change either in the direction of the minimum or in the direction of the maximum height of the potential barrier. When the activation energy at a contact point can surmount the minimum or the maximum height of the potential barrier, we denote $\delta\eta = \delta\eta_{,1,i}$ or $\delta\eta = \delta\eta_{,2,i}$ respectively. If the activation energy at a contact point cannot surmount the potential barrier,

δ_η is expressed as $\delta_{\eta,0,i}$, $(i=1,2)$. Once δ_η is given, the coefficients A_i and B_{ii} defined by Eqs.(2.14) and (2.15) are re-written in the following form.

$$A_i(\eta,s)=\frac{1}{n_\eta}\left(n_{\eta,1}\cdot\overline{\delta_{\eta,1,i}}+n_{\eta,2}\cdot\overline{\delta_{\eta,2,i}}+n_{\eta,0}\cdot\overline{\delta_{\eta,0,i}}\right) \tag{3.20}$$

$$B_{ii}(\eta,s)=\frac{1}{2n_\eta}\left(n_{\eta,1}\cdot\overline{\delta^2_{\eta,1,i}}+n_{\eta,2}\cdot\overline{\delta^2_{\eta,2,i}}+n_{\eta,0}\cdot\overline{\delta^2_{\eta,0,i}}\right) \tag{3.21}$$

where $\overline{\delta_{\eta,k,i}}$; mean value of $\delta_{\eta,k,i}$, $(k=0,1,2)$,

$\overline{\delta^2_{\eta,k,i}}$; variance of $\delta^2_{\eta,k,i}$, $(k=0,1,2)$.

3.5 Quantities in the Coefficients A_i and B_{ii}

In order to completely determine the coefficients A_i and B_{ii} in Eqs.(3.20) and (3.21), eight quantities N_c , $x_{\eta,1}$, $x_{\eta,2}$, R_η , $R_{p,\eta}$, $R_{n,\eta}$, $\overline{\delta_{\eta,k,i}}$ and $\overline{\delta^2_{\eta,k,i}}$ remain to be discussed. Let us investigate these quantities in this section.

3.5.1 Total number of contact points, N_c

The factors which represent the properties due to the number of contact points and particle size are given by the following relations.

$$N_c=\frac{C_a}{2}\cdot N_p \tag{3.22}$$

$$N_p=\frac{V}{1+e}\cdot\frac{1}{\overline{v}} \tag{3.23}$$

where N_c ; total number of contact points in the particulate material,

C_a ; average number of contact points per particle (coordination number),

N_p ; total number of particles in the particulate material,

e ; void ratio of particulate material,

V ; volume of particulate material,

$\bar{v}$; average volume of particle.

By using Eqs.(3.22) and (3.23), the total number of contact points N_c is written as follows.

$$N_c = \frac{C_a}{2} \cdot \frac{V}{1+e} \cdot \frac{1}{\bar{v}} \tag{3.24}$$

V and e are measured for a given specimen and $\bar{v}$ is calculated from the grain size distribution. C_a is experimentally investigated by Marsal[22], Field[23], Ingles[24], Harr[25], Oda[26] and O'cornnor[27]. Then, they proposed empirical equations relating the average number of contact points per particle to void ratio and/or shape and volume of particle. In the numerical experiments which will be performed in chapter 6 by using the mechanical model proposed in chapter 3 and 4, C_a is determined by Field's empirical equation, i.e.,

$$C_a = \frac{12}{1+e} \tag{3.25}$$

3.5.2 Heights of the potential barrier, $x_{\eta,1}$ and $x_{\eta,2}$

First of all, let us consider the minimum height of the potential barrier $x_{\eta,1}$ depicted in Fig.3.5. The potential is the physical quantity whose dimension is [force] x [length] as well as the energy. In order to determine $x_{\eta,1}$, it is necessary to know the force $\underset{\sim}{I}$ which cause the change in contact angle at each contact point and the amount of change in contact angle δ. Here, a method to obtain $x_{\eta,1}$ will be described by using the inter-particle force $\underset{\sim}{F}$ at each contact point, the frictional coefficient μ between particles, and the displacement of contact points due to the change in contact angle.

When the relative sliding due to the external force takes place along the contact planes as shown in Fig.3.9, the frictional force $\underset{\sim}{R}$ generates and is given by the relation

$$|\underset{\sim}{R}| = |\underset{\sim}{F}| \cdot \sin\theta = \mu' \cdot |\underset{\sim}{F}| \cdot \cos\theta \tag{3.26}$$

where μ' ; coefficient of static friction,

θ ; angle between the direction of external force and the vertical as shown in Fig.3.9.

Thus, the sliding condition is given by the following inequality.

$$|\underset{\sim}{F}| \cdot \sin\theta \geqq \mu' \cdot |\underset{\sim}{F}| \cdot \cos\theta \tag{3.27}$$

The relation between the normal to tangential plane and the direction of inter-particle force at a contact point of particle in the particulate material is shown in Fig.3.10. The angle between the normal to tangential plane and the inter-particle force is denoted by θ . The angles between the inter-particle force and the reference axes are given as α_1 , α_2 and α_3 . Even if the whole particulate material satisfies the sliding condition Eq.(3.27), it cannot directly be used as the sliding condition at each contact point. When the global sliding condition is satisfied, some contact points may not move and on the other hand some contact points may move even when the global sliding condition is not satisfied due to the restraints of adjacent particles.

Referring to Fig.3.10, $|\underset{\sim}{T}|$ is given as follows,

for $0 \leqq \theta \leqq \tan^{-1}\mu$, $|\underset{\sim}{T}| = \mu \cdot |\underset{\sim}{F}| \cdot \cos\theta$ (3.28)

for $\tan^{-1}\mu < \theta \leqq \pi/2$, $|\underset{\sim}{T}| = |\underset{\sim}{F}| \cdot \sin\theta$ (3.29)

where μ ; coefficient of friction between particles.

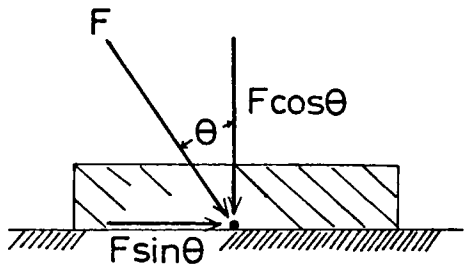

Fig.3.9 Friction between plates

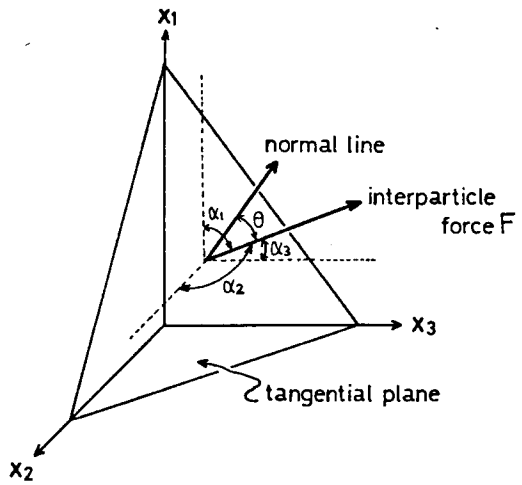

Fig.3.10 Relation between normal of tangential plane and interparticle force

Here, we assume that the principal stresses σ_1 , σ_2 and σ_3 are taken in the direction of the reference axes X_1 , X_2 and X_3 . Then, the angle θ in Fig.3.10 is given as

$$\cos\theta = \sum_{i=1}^{3} \cos\alpha_i \cdot \cos\beta_i$$

$$= \frac{1}{\sqrt{\sigma_1^2+\sigma_2^2+\sigma_3^2}} \cdot (\sigma_1 \cdot \cos\beta_1 + \sigma_2 \cdot \cos\beta_2 + \sigma_3 \cdot \cos\beta_3) \qquad (3.30)$$

As it is almost impossible to measure the inter-particle forces during the deformation process at every contact points in the particulate material, the statistical treatment are adopted in order to obtain $|\underset{\sim}{F}|$ by Marsal[22], Oda[28], Konishi[29] and Brown[30]. But the perfect procedure by which the inter-particle forces at every contact points can be accurately estimated has not established yet. Thus, in this study the inter-particle force is determined by the simplest arithmetical mean as the first approximation as follows.

$$|\underset{\sim}{F}| = \frac{[\text{ resultant force per unit area }]}{[\text{ number of contact points per unit area }]}$$

$$= \sqrt{\sigma_1^2+\sigma_2^2+\sigma_3^2} \Big/ \left\{ \frac{N_c}{h/D} \cdot \frac{1}{A} \right\}$$

$$= A \cdot \sqrt{\sigma_1^2+\sigma_2^2+\sigma_3^2} \cdot \frac{h}{N_c \cdot \overline{D}} \qquad (3.31)$$

where A ; cross sectional area in the particulate material,

h ; height of particulate material,

$\overline{D}$; mean diameter of particles,

Next, let us consider the amount of change in contact angle δ.

When the contact angle changes from $\eta=(\beta_1, \beta_2, \beta_3)$ to $\eta'(\beta_1', \beta_2', \beta_3')$ due to the change in the stress, the absolute value of change in contact angle δ_η is derived as follows.

$$\delta_\eta = |\eta - \eta'|$$

$$= \left| \cos^{-1}\left(\cos\beta_1 \cdot \cos\beta_1' + \cos\beta_2 \cdot \cos\beta_2' + \cos\beta_3 \cdot \cos\beta_3' \right) \right| \tag{3.32}$$

Denoting the mean value of δ_η by $\overline{\delta_\eta}$, the following equation is derived from Eq.(3.32).

$$\overline{\delta_\eta} = \int_{-\infty}^{\infty} \left| \cos^{-1}\left(\cos\beta_1 \cdot \cos\beta_1' + \cos\beta_2 \cdot \cos\beta_2' + \cos\beta_3 \cdot \cos\beta_3' \right) \right| \cdot P(\eta, \eta')\, d\eta' \tag{3.33}$$

where $P(\eta, \eta')$; transition probability of change in contact angle from η to η' .

By using Eqs.(3.28), (3.29), (3.31) and (3.33), the minimum height of the potential barrier $x_{\eta,1}$ is expressed as follows,

for $0 \leq \theta \leq \tan^{-1}\mu$

$$x_{\eta,1} = |\underset{\sim}{I}| \cdot \overline{\delta_\eta} \cdot \overline{D}/2$$

$$= \mu \cdot A \cdot \overline{\delta_\eta} \cdot \sqrt{\sigma_1^2 + \sigma_2^2 + \sigma_3^2} \cdot \frac{h}{2N_c} \cdot \cos\theta \tag{3.34}$$

for $\tan^{-1}\mu < \theta \leq \pi/2$

$$x_{\eta,1} = |\underset{\sim}{I}| \cdot \overline{\delta_\eta} \cdot D/2$$

$$= A \cdot \overline{\delta_\eta} \cdot \sqrt{\sigma_1^2 + \sigma_2^2 + \sigma_3^2} \cdot \frac{h}{2N_c} \cdot \sin\theta \tag{3.35}$$

Meanwhile the coefficients of inter-particle friction on the various materials have been measured by Horn and Deere[31], Procter and Barton[32] and Nascimento[33]. From these measurements it has been found that the coefficients of inter-particle friction are not constant but depend on various factors on the surfaces of

materials, for example, the presence of fluid, the micro-topology and chemical conditions of surfaces. Thus, Procter and Barton concluded that 'single contact' behaviour is generally inapplicable to the shearing of a mass of particles of quartz, feldspar or glass ballotini, even when identical conditions appear to prevail.

On the other hand, Matsuoka and Nakai[20] derived the following stress-dilatancy equation on the SMP.

$$\tau/\sigma_N = \lambda\,(-d\epsilon_N/d\gamma) + \mu \tag{3.36}$$

where τ/σ_N ; shear-normal stress ratio on the SMP,

$d\epsilon_N$, $d\gamma$; vertical and shear strain increments on the SMP.

Furthermore, they experimentally verified that λ and μ in Eq.(3.36) are constant and independent of void ratios and stress paths in the shearing tests as far as the materials are same. They also gave the physical meaning that μ equals the coefficient of inter-particle friction because the stress ratio τ/σ_N is equal to the coefficient of friction in the particulate material when the vertical strain increment $d\epsilon_N$ is zero on the SMP.

In this study μ in Eq.(3.36) is adopted as the coefficient of friction in the particulate material and is used in calculating the height of the potential barrier.

3.5.3 Ratios $R_{p,\eta}$ and $R_{n,\eta}$ in Eqs.(3.14) and (3.15)

First, let us consider $R_{p,\eta}$ which represents the ratio of the minimum height to the maximum height of the potential barrier as shown in Eq.(3.14). For later convenience, the angle β_2 between the reference axis X_2 and the normal to tangential plane at the contact point is ranged from zero to $\pi/2$.

Referring to Fig.3.3, the probability of change in contact

angle is supposed to be equal in all directions at the contact points where β_1 or β_2 is zero or $\pi/2$. This means that the height of the potential barrier is same in all directions of change in contact angle and the bell shape in Fig.3.5 becomes symmetric. Then, the ratio $R_{p,\eta}$ is equal to unit at the contact points where the contact angle β_1 or β_2 is zero or $\pi/2$.

At all the contact points where the tangential plane is parallel to the potential slip plane which is identified with the SMP, the direction of change in contact angle is considered to be the same as the direction of change in potential slip plane. This means that the change in contact angle occurs in one specified direction. Namely, at these contact points the maximum height of the potential barrier may be considered as infinite and then the ratio $R_{p,\eta}$ becomes zero.

Thus, the ratio $R_{p,\eta}$ is generally a function of contact angle η . $R_{p,\eta}$ has the specified values at the specified contact angles such as $R_{p,\eta}=1$ when the tangential planes are perpendicular or parallel to X_1- axis and $R_{p,\eta}=0$ when it coincides with the potential slip plane. The simplest form of this function is a linear function which is satistied at both specified values in $R_{p,\eta}$. Fig.3.11 illustrates the relationship between $R_{p,\eta}$ and η . $\phi_{mo,i}$ in Fig.3.11 represents the angle between the normal to the SMP and the reference axis X_i . As shown in Fig.3.11, $R_{p,\eta}$ can be shown by four planes which are named Plane(1), Plane (2), Plane(3) and Plane(4). The relations between $R_{p,\eta}$ and η on these planes are expressed by the following equations,

for Plane(1)

$$R_{p,\eta} = \frac{\beta_2 - \phi_{mo,2}}{\pi/2 - \phi_{mo,2}} \tag{3.37}$$

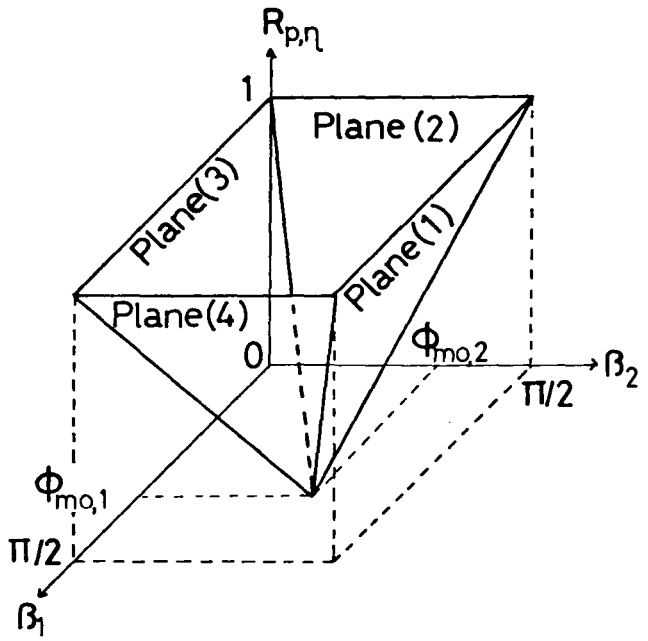

Fig.3.11 Relation between $R_{p,\eta}$ and η

for Plane(2)

$$R_{p,\eta} = \frac{\phi_{mo,1} - \beta_1}{\phi_{mo,1}} \tag{3.38}$$

for Plane(3)

$$R_{p,\eta} = \frac{\phi_{mo,2} - \beta_2}{\phi_{mo,2}} \tag{3.39}$$

for Plane(4)

$$R_{p,\eta} = \frac{\beta_1 - \phi_{mo,1}}{\pi/2 - \phi_{mo,1}} \tag{3.40}$$

The numbers, $n_{\eta,1}$ and $n_{\eta,2}$, of contact points where the activation energy can surmount the potential barrier are considered to be inversely propotional to the height of the potential barrier. Thus, the ratio, $R_{n,\eta}$, of the numbers of contact points is linearly proportional to the ratio, $R_{p,\eta}$, of the heights of the potential barriers. At the contact points where either β_1 or β_2 is zero or $\pi/2$, the numbers of contact points, $n_{\eta,1}$ and $n_{\eta,2}$ are both same because the heights of the potential barriers, $x_{\eta,1}$ and $x_{\eta,2}$ are equal. At the contact points where the tangential planes are parallel to the SMP, $R_{n,\eta}$ becomes zero because the height of the potential barrier is infinite. In this study the ratio, $R_{n,\eta}$ is assumed to be equal to the ratio, $R_{p,\eta}$, as the first approximation.

3.5.4 R_η in Eq.(3.12)

The coefficient R_η expresses the ratio of the amount of the activation energy at a contact point to the height of the potential barrier as shown in Eq.(3.12). Thus, R_η is always less than unit and relates to the recoverable change in contact angle. As the numbers, $n_{\eta,1}$ and $n_{\eta,2}$, of contact points where the activation energy can surmount the potential barriers are zero in such a case,

Eq.(3.12) is rewritten as follows.

$$\sum_{\beta_1=0}^{\pi/2}\sum_{\beta_2=0}^{2\pi}\left\{n_\eta\left(x_{\eta,1}+x_{\eta,2}\right)/2R_\eta\right\}=\Delta W_e \tag{3.41}$$

where ΔW_e ; elastic component of work transferred into the particulata material and contributing to the recoverable change in contact angle.

If it is assumed that R_η is independent of the contact angle η , the following equation is derived.

$$R_\eta=\frac{\sum_{\beta_1=0}^{\pi/2}\sum_{\beta_2=0}^{2\pi}\left\{n_\eta\left(x_{\eta,1}+x_{\eta,2}\right)\right\}}{2\cdot\Delta W_e} \tag{3.42}$$

3.5.5 $\overline{\delta_{\eta,k,i}}$ and $\overline{\delta^2_{\eta,k,i}}$ in Eqs.(3.20) and (3.21)

The distribution function $f_{\eta,i}(\delta)$ which is a function of δ with respect to β_i at the contact angle η is introduced to obtain $\overline{\delta_{\eta,k,i}}$ and $\overline{\delta^2_{\eta,k,i}}$ which are the mean value and the variance of change in contact angle respectively. In the proposed model the distribution function $f_{\eta,i}(\delta)$ is determined from the following considerations.

In the shearing process the potential slip plane changes with the change in the stress ratio τ/σ_N on the SMP. Furthermore, it has assumed in 3.4.2 that the probability of the change of tangential planes in the direction of the potential plane is larger than that of the reverse change in tangential planes. Thus, as the first approximate function satisfying above conditions, the distribution function $f_{\eta,i}(\delta)$ is assumed to be independent of η and to be a normal distribution function whose mean value and standard deviation are both equal to the amount of change in the potential slip plane as follows.

for $0 \leqq \beta_i \leqq \phi_{mo,i}$

$$f_{\eta,i}(\delta) = \frac{1}{\Delta\phi_{mo,i}\sqrt{2\pi}} \exp\left\{-\frac{(\delta-\Delta\phi_{mo,i})^2}{2(\Delta\phi_{mo,i})^2}\right\} \tag{3.43}$$

for $\phi_{mo,i} < \beta_i \leqq \pi/2$

$$f_{\eta,i}(\delta) = \frac{1}{\Delta\phi_{mo,i}\sqrt{2\pi}} \exp\left\{-\frac{(\delta+\Delta\phi_{mo,i})^2}{2(\Delta\phi_{mo,i})^2}\right\} \tag{3.44}$$

where $\phi_{mo,i}$; see Eq.(3.19) or Fig.3.11,

$\Delta\phi_{mo,i}$; change in $\phi_{mo,i}$ due to the change in the SMP.

Denoting the angles which represent the minimum amount of change in contact angles where the activation energy surmount the minimum and the maximum potential barriers by $\delta_{1,i}$ and $\delta_{2,i}$ respectively, $\overline{\delta}_{\eta,k,i}$ and $\overline{\delta^2}_{\eta,k,i}$, which are the mean values of $\delta_{\eta,k,i}$ and $\delta^2_{\eta,k,i}$, are derived as follows.

for $0 \leqq \beta_i \leqq \phi_{maxi}$, $(i = 1, 2)$

$$\overline{\delta}_{\eta,0,i} = \int_{\delta_{2,i}}^{\delta_{1,i}} \delta f_{\eta,i}(\delta)\, d\delta \tag{3.45}$$

$$\overline{\delta}_{\eta,1,i} = \int_{\delta_{1,i}}^{\infty} \delta f_{\eta,i}(\delta)\, d\delta \tag{3.46}$$

$$\overline{\delta}_{\eta,2,i} = \int_{-\infty}^{\delta_{2,i}} \delta f_{\eta,i}(\delta)\, d\delta \tag{3.47}$$

$$\overline{\delta^2}_{\eta,0,i} = \int_{\delta_{2,i}}^{\delta_{1,i}} \delta^2 f_{\eta,i}(\delta)\, d\delta \tag{3.48}$$

$$\overline{\delta^2}_{\eta,1,i} = \int_{\delta_{1,i}}^{\infty} \delta^2 f_{\eta,i}(\delta)\, d\delta \tag{3.49}$$

$$\overline{\delta^2}_{\eta,2,i} = \int_{-\infty}^{\delta_{2,i}} \delta^2 f_{\eta,i}(\delta)\, d\delta \tag{3.50}$$

where

$$\delta_{1,i} = \frac{3}{2}\Delta\phi_{mo,i} \quad , \quad \delta_{2,i} = \frac{1}{2}\Delta\phi_{mo,i} \tag{3.51}$$

for $\phi_{mo,i} < \beta_i \leqq \pi/2$, $(i = 1, 2)$

$$\delta_{\eta,0,i} = \int_{\delta_{1,i}}^{\delta_{2,i}} \delta f_{\eta,i}(\delta)\, d\delta \tag{3.52}$$

$$\delta_{\eta,1,i} = \int_{-\infty}^{\delta_{1,i}} \delta f_{\eta,i}(\delta)\, d\delta \tag{3.53}$$

$$\delta_{\eta,2,i} = \int_{\delta_{2,i}}^{\infty} \delta f_{\eta,i}(\delta)\, d\delta \tag{3.54}$$

$$\delta^2_{\eta,0,i} = \int_{\delta_{1,i}}^{\delta_{2,i}} \delta^2 f_{\eta,i}(\delta)\, d\delta \tag{3.55}$$

$$\delta^2_{\eta,1,i} = \int_{-\infty}^{\delta_{1,i}} \delta^2 f_{\eta,i}(\delta)\, d\delta \tag{3.56}$$

$$\delta^2_{\eta,2,i} = \int_{\delta_{2,i}}^{\infty} \delta^2 f_{\eta,i}(\delta)\, d\delta \tag{3.57}$$

where

$$\delta_{1,i} = -\frac{3}{2}\Delta\phi_{mo,i} \quad , \quad \delta_{2,i} = -\frac{1}{2}\Delta\phi_{mo,i} \tag{3.58}$$

As shown in Eqs.(3.51) and (3.58) it is assumed that the recoverable motions of contact angles occur at the contact points where the absolute values of change in contact angle fall within $\frac{1}{2}\Delta\phi_{mo,i}$. Furthermore, from the distribution function defined in Eqs.(3.43) and (3.44) the absolute value of $\overline{\delta_\eta}$ defined in Eq.(3.33) is rewritten as follows.

$$\delta_\eta = |\Delta\phi_{mo}| = \left| \cos^{-1}\left\{ \sum_{i=1}^{3} \cos\phi_{mo,i} \cdot \cos(\phi_{mo,i} + \Delta\phi_{mo,i}) \right\} \right| \tag{3.59}$$

3.6 Conclusions

In the present chapter an approach has been described about the application of Markov process to the mechanical behaviours of particulate material during the shearing process. From the investigation of particle motions in the particulate materials it is shown that the deformation process of particulate material is re-

garded as the Markov process. In order to determine the coefficients in the basic equation of Markov process the concepts of the potential barrier and the potential slip plane are introduced based on the investigations of the mechanism for the deformation of particulate material at the particle scale. It is impossible to directly measure those several quantities introduced to estimate the coefficients in the basic equation of Markov process. Thus, the validity of these quantities will be indirectly verified by carrying out the triaxial tests with various stress paths and the numerical experiments using the proposed model in the later chapters.

The main conclusions obtained in this chapter may be summarized as follows.

(1) The contact angle between particles at a contact point is an important state variable which can express the deformation of particulate material at the particle scale. In this study the contact angle is adopted as a random variable and the mechanical model is formed for particulate materials based on the Markov process.

(2) The Markov process is applied to the deformation process of particulate material and the basic equation is derived. The coefficients in the basic equation of Markov process reflect the mechanical characteristics of particulate material at the particle scale. Thus, the validity of the mechanical model depends on the rational derivation of these coefficients. In this study the numbers of contact points and the changes in contact angles during the deformation process are used in order to define thses coefficients.

(3) The concepts of the potential barrier and the potential slip plane are introduced in order to determine the coefficients

in the basic equation of Markov process. The concept of the potential barrier is applied at contact points of particles to consider recoverable (elastic) motions or irrecoverable (plastic) motions of particles. The concept of the potential slip plane is used to discuss the probabilistic motions of particles in the shearing process. In this study the SMP proposed by Matsuoka and Nakai is used as the potential slip plane. Thus, it is found that these concepts are very useful when the deformation mechanism of particulate material is studied at the particle scale based on the statistics and/or the probability theory.

(4) In quantitative estimation of the coefficients in the basic equation of Markov process, those several quantities reflecting the mechanical characteristics of particulate material are introduced and determined based on the informations and probabilistic considerations available about the motions of particles during the shearing process. The total number of contact points is obtained by void ratio, grain size distribution curve, mean volume of particles and number of contact points per particle. The height of potential barriers are derived by inter-particle forces at contact points, frictional coefficient for particulate material and probabilistic relations between the local slip planes and the potential slip plane. R_η in Eq.(3.12) is obtained by the elastic component of work done into the particulate material. Ratios $R_{p,\eta}$ and $R_{n,\eta}$ in Eqs.(3.14) and (3.15) are determined by analysing the probabilistic motions of particles based on the concept of the potential slip plane. In determining the change in contact angles the normal distribution function is used where the mean and the standard deviation values are equal to the

change in the potential slip plane.

References for Chapter 3

1) Litwiniszyn, J.: Application of the Equation of Stochastic Pro-Processes to Spatial Problem of Mechanics of Some Typers of Bodies. Bull. de l'Acad. Polon. Sci., Vol.4, No.2, 1956, pp. 91-95.

2) Litwiniszyn, J.: The Model of a Random Walk of Particles Adopt Adopted to Researches on Problems of Mechanics of Loose Media, Bull. de l'Acad. Polon. Sci. Tech., Vol.11, No.10, 1963, pp. 61-70.

3) Litwiniszyn, J.: The Model of a Random Walk of Particles Adopted to Researches on Problems of Mechanics of Loose Media 2, Bull. de l'Acad. Polon. Sci. Tech., Vol.12, No.5, 1964, pp. 281-286.

4) Sweet, A.L. and Bogdanoff, J.L.: Stochastic Model for Predicting Subsidence, Proc. ASCE, Vol.91, No.EM2, 1965, pp.21-45.

5) Sweet, A.L. and Bogdanoff, J.L.: Validity of a Stochastic Model for Prediction Subsidence, Proc.ASCE, Vol.91, No.EM6, 1965, PP.111-128.

6) Brahma, C.H.: Analysis of Granular Soil Deformation as a Stochastic Process, Ph. D. Thesis of Ohio Univ., 1969.

7) Goldstein, M.N., Misumsky, V.A. and Lapidus, L.S.: The Theory of Probability and Statistics in Relation to the Rheology of Soil, Proc. 5th Int. Conf. SMFE. Vol.1, 1961, PP.123-126.

8) see ref. 16) in Chapter 1.

9) see ref. 23) in Chapter 1.

10) see ref. 18) in Chapter 1.

11) see ref. 19) in Chapter 1.

12) Oda, M.: Initial Fabric and their Relations to Mechanical Properties of Granular Material, Soils and Foundations, Vol.12, No.1, 1972, pp.17-36.

13) Oda, M.: The Mechanism of Fabric Changes during Compressional Deformation of Sand, Soils and Foundations, Vol.12, No.2, 1972, pp.1-18.

14) Murayama, S. and Matsuoka, H.: A Microscopic Consideration on the Shearing Behaviour of Granular Materials Using the Two-Dimensional Model, Annuals, Disaster Prevention Research Institute, Kyoto Univ., No.13B, 1970, pp.505-523, (in Japanese).

15) see ref. 28) in Chapter 1.

16) Borowicka, H.: Rearrangement of Grains by Shear Tests with Sand, Proc. 8th Int. Conf. SMFE, Vol.1, Part 1, 1973, pp.71-77.

17) Mukaibo, T. et al.: Structure and Properties of Material 1, Kiso-Kogaku, Vol.13, Iwanami, 1968, (in Japanese).

18) see ref. 24) in chapter 1.

19) see ref. 25) in Chapter 1.

20) see ref. 31) in Chapter 1.

21) Satake, M.: Yield Criteria and their Statistical Consideration, Annual Meeting of JSCE, Part 1, 1974, pp.1-3, (in Japanese).

22) Marsal, R.J.: Contact Force in Soils and Rockfill Materials, Proc. 2nd Panam. Conf. SMFE, 1963, pp.68-98.

23) Field, W.G.: Towards the Statistical Deformation of a Granular Mass, Proc. 4th A. and N.Z. Conf. SMFE, 1963, pp.143-148.

24) Ingles, O.G.: Discussion of "Towards the Statistical Definition of a Granular Mass", by Field, W.G., Proc. 4th A. and N.Z. Conf. SMFE,1963, p.314.

25) Harr, M.E.: Mechanics of Particulate Media - A Probabilistic Approach, McGraw-Hill Book Co. Inc., New York, 1977, p.28.

26) Oda, M.: Co-ordination Number and its Relation to Shear Strenght of Granular Material, Soils and Foundations, Vol.17, No.2, 1977, pp.29-42.

27) O'Cornnor, K.M., Krizek, R.J. and Atmatzidis, D.K.: Micro-Characteristics of Chemically Stabilized Granular Material, Proc. ASCE, Vol.105, No.GT7, 1978, pp.939-952.

28) see ref. 20) in Chapter 1.

29) Konishi, J.: A Relation between the Microscopic Fabrics of Particulate Material and Stress, Annual Meeting of JSCE, Part 3, 1977, pp.84-85, (in Japanese).

30) see ref. 35) in Chapter 1.

31) Horn, H.M. and Deere, D.V.: Frictional Characteristics of Minerals, Geotechnique, Vol.12, No.4, 1962, pp.319-334.

32) Procter, D.C. and Barton, R.R.: Measurement of the Angle of Interparticle Friction, Géotechnique, Vol.24, No.4, 1974, pp.581-604.

33) Nacimento, U.: Goniometer for Determining Interparticle Friction, Proc. 9th Int. Conf. SMFE, Vol.1, 1977, pp.229-233.

Appendix 3.1

Eqs.(3.11), (3.12), (3.14), (3.15) and (3.16) are again given below.

$$n_{\eta,1} + n_{\eta,2} + n_{\eta,0} = n_\eta \tag{3.11}$$

$$\sum_{\beta_1=0}^{\pi/2} \sum_{\beta_2=0}^{2\pi} \left(n_{\eta,1} \cdot x_{\eta,1} + n_{\eta,2} \cdot x_{\eta,2} + n_{\eta,0} \cdot \frac{x_{\eta,1} + x_{\eta,2}}{2R_\eta} \right) = \Delta W \tag{3.12}$$

$$x_{\eta,1} / x_{\eta,2} = R_{p,\eta} \tag{3.14}$$

$$n_{\eta,2} / n_{\eta,1} = R_{n,\eta} \tag{3.15}$$

$$n_{\eta,1} = N_{c,1} \cdot W(\eta, s) \cdot d\beta_1 \cdot d\beta_2 \tag{3.16}$$

Eliminating $x_{\eta,2}$ and $n_{\eta,2}$ in these simultaneous equations, Eqs. (3.11) and (3.12) are rewritten as follows.

$$n_{\eta,0} = n_\eta - n_{\eta,1} \left(1 + R_{n,\eta} \right) \tag{3.11'}$$

$$\sum_{\beta_1=0}^{\pi/2} \sum_{\beta_2=0}^{2\pi} \left\{ n_{\eta,1} \cdot x_{\eta,1} + \frac{R_{n,\eta}}{R_{p,\eta}} \cdot x_{\eta,1} \cdot n_{\eta,1} + n_{\eta,0} \cdot \frac{\left(1 + \frac{1}{R_{p,\eta}}\right) \cdot x_{\eta,1}}{2R_\eta} \right\} = \Delta W \tag{3.12'}$$

Furthermore, by the elimination of $n_{\eta,0}$ and $n_{\eta,1}$ in Eqs.(3.11'), (3.12') and (3.16), the following equation is derived.

$$N_{c,1} \cdot \sum_{\beta_1=0}^{\pi/2} \sum_{\beta_2=0}^{2\pi} \left[x_{\eta,1} \cdot W(\eta, s) d\beta_1 \cdot d\beta_2 \left\{ \left(1 + \frac{R_{n,\eta}}{R_{p,\eta}}\right) - \left(1 + \frac{1}{R_{p,\eta}}\right) \left(1 + R_{n,\eta}\right) / 2R_\eta \right\} \right.$$

$$= \Delta W - \sum_{\beta_1=0}^{\pi/2} \sum_{\beta_2=0}^{2\pi} \left\{ \frac{1}{2R_\eta} \left(1 + \frac{1}{R_{p,\eta}}\right) \cdot x_{\eta,1} \cdot n_\eta \right\}$$

Thus, $N_{c,1}$ is obtained as follows.

$$N_{c,1} = \frac{\Delta W - \sum_{\beta_1=0}^{\pi/2} \sum_{\beta_2=0}^{2\pi} \left\{ \frac{R_{p,\eta} + 1}{2R_\eta \cdot R_{p,\eta}} \cdot x_{\eta,1} \cdot n_\eta \right\}}{\sum_{\beta_1=0}^{\pi/2} \sum_{\beta_2=0}^{2\pi} \left[x_{\eta,1} \cdot w(\eta, s)\, d\beta_1 \cdot d\beta_2 \left\{ \left(1 + \frac{R_{n,\eta}}{R_{p,\eta}}\right) - \left(1 + \frac{1}{R_{p,\eta}}\right)\left(1 + R_{n,\eta}\right)/2R_\eta \right\} \right]}$$

CHAPTER 4 DEFINITION OF STRAIN FOR PARTICULATE MATERIAL

4.1 Introduction

In the formation of continuum mechanics the deformation of a solid body is described by a continuous mathematical model whose geometrical points are identified with the place of the material particles of the body. When such a continuous body changes its configuration under some physical action, we imposed the assumption that the change is continuous. Thus, in continuous mechanics all the informations about the deformation of the body can be mathematically expressed by the strain tensors.

On the other hand, in the particulate materials such as sands composed of particles and voids among them whose shapes and sizes are irregular, the motions of particles include the slip, rolling, and discontinuous motions of particles under deformation process. Consequently, it is inapplicable to use the definition of strain in the continuum mechanics. Especially, when we analyse the deformation mechanism of particulate material at the particle scale and derive its constitutive equations, it is essential to define the strain of particulate material based on the exact motions of particles. From this view point, some researches tried to define the strain for particulate material. For instance, Murayama[1] paid attention to the plane of maximum mobilization and derived the strain by summing up the relative motion of two adjacent particles on this plane. Horne[2] introduced the original concept called the mean projected solid paths in order to express the structural anisotropy of particulate material and derived the strain by using this concept. Matsuoka[3] and Oda[4] defined the strain of particulate material in the similar way to Horne's research. The results

of these researches show that to average the relative motions of adjacent particles in some way is promising when the strain of particulate material is defined. In this chapter, based on the results of these previous researches, the strain of particulate material is intended to be derived from the probabilistic and the statistical considerations of the motions of particles, i.e., the probability density function of contact angles and the quantities which can estimate the discontinuous motions of particles are used in the definition of strain.

4.2 Definition of Strain[5)]

Fig.4.1 depicts a unit element of particulate material which plays the important role on the following considerations. The unit element is the rectangular prism which contains numerous particles composing of particulate material. In Fig.4.1 the reference frame is fixed so that the vertical direction is X_1- axis and the two horizontal directions are X_2- and X_3- axes. Let us denote the length of the side of unit element in the direction X_i-axis at the stress ratio S by L_{S,x_i} . When the stress ratio changes from $S-\Delta S$ to S and the length of the side $L_{S-\Delta S,x_i}$ changes to L_{S,x_i} , the strain ϵ_{S,x_i} in the direction of X_i-axis at the stress ratio S is defined as follows.

$$\epsilon_{S,x_i} = \frac{L_{S,x_i} - L_{S-\Delta S,x_i}}{L_{S-\Delta S,x_i}} \tag{4.1}$$

Fig.4.2 shows a path which passes through the centroids of particles from one side to the opposite side of a unit element. Let us denote the number of particles contained in the path by N_{S,x_i} . The j-th and (j+1)-th particles in the path are shown in Fig.4.3. Denoting the projected length between the centroids of adjacent particles in the direction of X_i- axis by $l_{S,x_i,j}$ as shown in

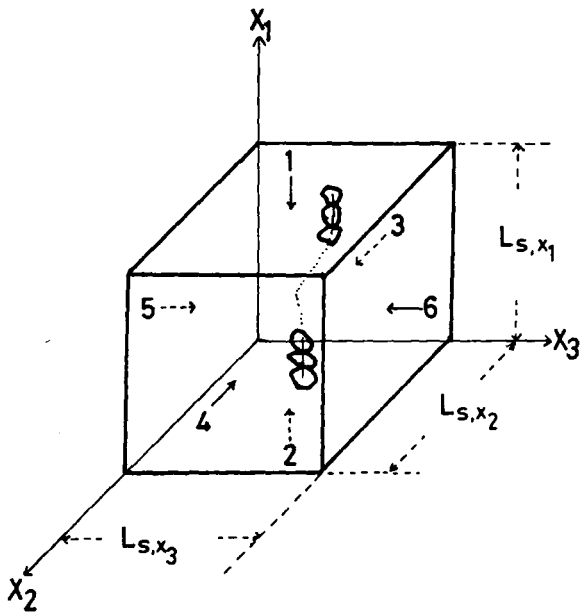

Fig.4.1 Unit element of particulate material

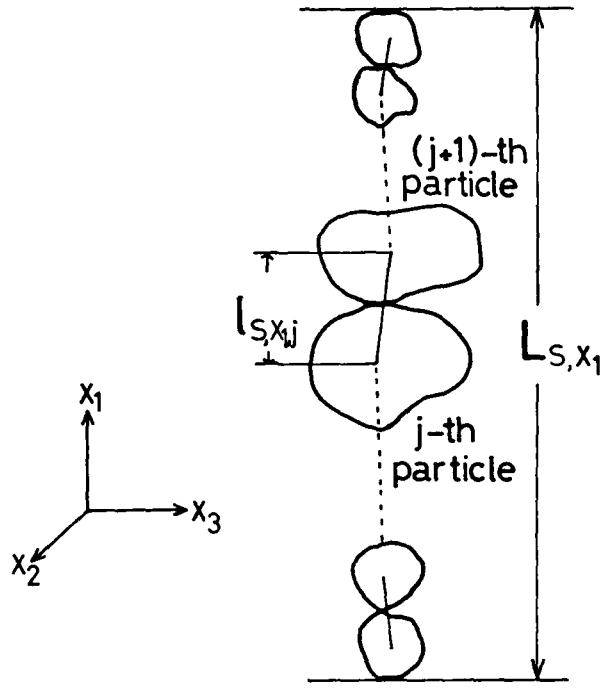

Fig.4.2 Path through centroids of particles

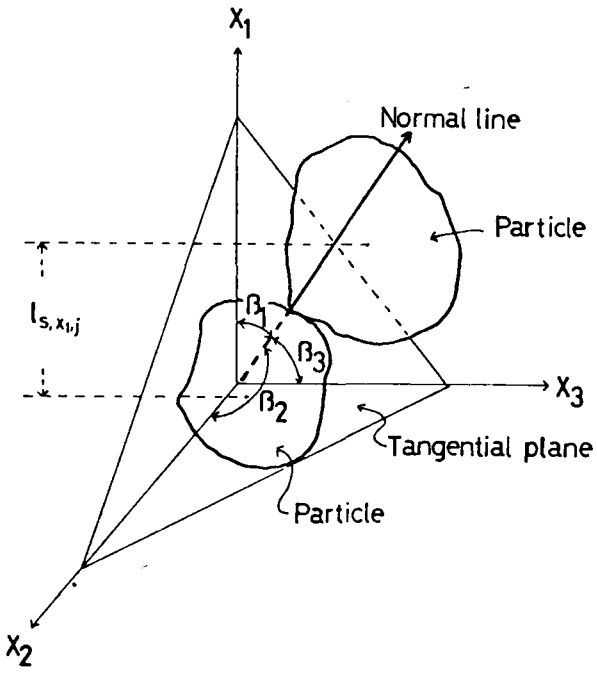

Fig.4.3 j-th and (j+1)-th particles in the path

Fig.4.3, the following relation between L_{s,x_i} and $\ell_{s,x_i,j}$ is derived because the lengths of the sides are much larger than the diameters of particles.

$$L_{s,x_i} = \sum_{j=1}^{N_{s,x_i}} \ell_{s,x_i,j} \tag{4.2}$$

Substitution of Eq.(4.2) into Eq.(4.1) leads to the following equation.

$$\epsilon_{s,x_i} = \frac{\sum_{j=1}^{N_{s,x_i}} \ell_{s,x_i,j} - \sum_{j=1}^{N_{s-\Delta s,x_i}} \ell_{s-\Delta s,x_i,j}}{\sum_{j=1}^{N_{s-\Delta s,x_i}} \ell_{s-\Delta s,x_i,j}} \tag{4.3}$$

Dividing both the denominator and the numerator in the right hand side of Eq.(4.3) by $N_{s-\Delta s,x_i}$, the following equation is derived.

$$\epsilon_{s,x_i} = \frac{1/N_{s-\Delta s,x_i} \sum_{j=1}^{N_{s,x_i}} \ell_{s,x_i,j} - 1/N_{s-\Delta s,x_i} \sum_{j=1}^{N_{s-\Delta s,x_i}} \ell_{s-\Delta s,x_i,j}}{1/N_{s-\Delta s,x_i} \sum_{j=1}^{N_{s-\Delta s,x_i}} \ell_{s-\Delta s,x_i,j}}$$

$$= \frac{N_{s,x_i}/N_{s-\Delta s,x_i}\, E[\ell_{s,x_i,j}] - E[\ell_{s-\Delta s,x_i,j}]}{E[\ell_{s-\Delta s,x_i,j}]} \tag{4.4}$$

where $E[\ell_{s,x_i,j}]$; mean value of $\ell_{s,x_i,j}$ along the path as shown in Fig.4.2.

Denoting the mean value of $\ell_{s,x_i,j}$ along the numerous possible paths by $M[\ell_{s,x_i,j}]$, the following relation should hold as far as the fabric of particulate material in the direction of X_i- axis is stochastically uniform.

$$E[\ell_{s,x_i,j}] = M[\ell_{s,x_i,j}] \tag{4.5}$$

Meanwhile, if it is stochastically assumed that a line connecting

the centroids of adjacent particles along the path is identified with the normal to tangential plane at the contact points, $M[l_{s,x_i,j}]$ can be expressed by using the probability density function $w(\eta, s)$ and $g(D)$ which respectively represent the distributions of contact angle and grain size as follows.

$$M[l_{s,x_i,j}] = \int_0^\infty \int_0^{2\pi} \int_0^{\pi/2} D \cos\beta_i \cdot g(D)\, w(\eta, s)\, d\beta_1\, d\beta_2\, dD$$

$$= D \int_0^{2\pi} \int_0^{\pi/2} \cos\beta_i \cdot w(\eta, s)\, d\beta_1\, d\beta_2 \qquad (4.6)$$

where D ; mean diameter of particles in the particulate material.

Substituting Eqs.(4.5) and (4.6) into Eq.(4.4), the strain ϵ_{s,x_i} is given by

$$\epsilon_{s,x_i} = \frac{N_{s,x_i}/N_{s-\Delta s,x_i} \int_0^{2\pi} \int_0^{\pi/2} \cos\beta_i \cdot w(\eta,s)\, d\beta_1 \cdot d\beta_2 - \int_0^{2\pi} \int_0^{\pi/2} \cos\beta_i \cdot w(\eta, s-\Delta s)\, d\beta_1 \cdot d\beta_2}{\int_0^{2\pi} \int_0^{\pi/2} \cos\beta_i \cdot w(\eta, s-\Delta s)\, d\beta_1 \cdot d\beta_2} \qquad (4.7)$$

It is found from Eq.(4.7) that the strain in the direction of X_i-axis due to the change in the stress ratio from $s-\Delta s$ to s can be expressed in terms of $N_{s,x_i}/N_{s-\Delta s,x_i}$ and $w(\eta, s)$.

Let's consider the physical meanings of $N_{s,x_i}/N_{s-\Delta s,x_i}$ in the remaining part of this section.

For the case that $N_{s,x_i}/N_{s-\Delta s,x_i}$ is not unit, the number of particles contained in the path in Fig.4.2 changes with the change in the stress ratio from $s-\Delta s$ to s , i.e., it may be considered that some particles along the path part from $(N_{s,x_i}/N_{s-\Delta s,x_i} < 1)$ or newly join to the path $(N_{s,x_i}/N_{s-\Delta s,x_i} > 1)$ and consequently

the contact points disappear or appear along the path. In the following discussions these discontiouous motions are called the disappearance for $N_{s,x_i}/N_{s-\Delta s,x_i} < 1$ and the appearance for $N_{s,x_i}/N_{s-\Delta s,x_i} > 1$ respectively. Ohmaki[6] has already pointed out these discontinuous motions of particles at the contact points by carrying out the two dimensional model tests with washers. It is considered that these discontinuous motions correspond to the dislocation which can be microscopically observed in the crystal solid under the process of the plastic deformation.

Let's introduce the probability function $P_d(\beta_1)$ of β_1 in order to estimate $N_{s,x_i}/N_{s-\Delta s,x_i}$ quantitatively. Here, $P_d(\beta_1)$ represents the ratio of the number of points where the discontinuous motion of the disappearance occurs to the number of points where the activation energy surmounts the potential barrier at the contact angle $\eta=(\beta_1,\beta_2)$. Denoting these numbers by $(n_{\eta,1}+n_{\eta,2})_d$ and $(n_{\eta,1}+n_{\eta,2})$, $P_d(\beta_1)$ is shown as follows.

$$P_d(\beta_1)=\frac{(n_{\eta,1}+n_{\eta,2})_d}{(n_{\eta,1}+n_{\eta,2})} \tag{4.8}$$

As the direction of X_1- axis is agree with the direction of the maximum principal stress, it may be assumed that at all the contact points where the normals to tangential planes are parallel with the direction of X_1- axis, i.e., at $\beta_1=0$, the discontinuous motions do not occur and then $P_d(0)=0$. On the other hand, at all the contact points where the normals are perpendicular to the direction of X_1- axis, i.e., at $\beta_1=\pi/2$, the discontinuous motions occur and then $P_d(\pi/2)=1$. In the proposed model $P_d(\beta_1)$ is assumed to be the following form so as to satisfy the above extreme cases.

For the case that the direction of X_1- axis is agree with the

maximum principal stress,

$$P_d(\beta_1) = \frac{(n_{\eta,1} + n_{\eta,2})_d}{(n_{\eta,1} + n_{\eta,2})} = \left(\frac{2}{\pi}\beta_1\right)^{\lambda} \tag{4.9}$$

where λ ; parameter depending on the stress state, void ratio, fabric of particulate material and so on.

When the direction of the maximum principal stress is perpendicular to the direction of X_1-axis, it may be assumed as follows. At all the contact points where the normals to tangential planes are also perpendicular to the direction of X_1-axis, i.e., $\beta_1 = \pi/2$, the discontinuous motions do not occur and then $P_d(\pi/2) = 0$. On the other hand, at all the contact points where the normals to tangential planes are perpendicular to the direction of X_2-axis, i.e., $\beta_1 = 0$, the discontinuous motions occur and then $P_d(0) = 1$. Thus, the following equation is similarly assumed as Eq.(4.9).

For the case that the direction of X_2-axis is perpendicular to the maximum principal stress,

$$P_d(\beta_1) = \left\{\frac{2}{\pi}\left(\frac{\pi}{2} - \beta_1\right)\right\}^{\lambda} \tag{4.10}$$

Using the discussions in chapter 3 and Eq.(4.8), the following equation for the disappearance is derived.

$$\begin{aligned} N_{s,x_i}/N_{s-\Delta s,x_i} &= 1 - \frac{N_{s,x_i} - N_{s-\Delta s,x_i}}{N_{s-\Delta s,x_i}} \\ &= 1 - \frac{\sum_{\beta_1=0}^{\pi/2}\sum_{\beta_2=0}^{2\pi}\left\{(n_{\eta,1} + n_{\eta,2})\right\}}{\sum_{\beta_1=0}^{\pi/2}\sum_{\beta_2=0}^{2\pi} n_\eta} \\ &= 1 - \frac{1}{N_c}\sum_{\beta_1=0}^{\pi/2}\sum_{\beta_2=0}^{2\pi}\left\{P_d(\beta_1)(n_{\eta,1} + n_{\eta,2})\right\} \end{aligned} \tag{4.11}$$

Furthermore, denoting the ratio of the appearance probability of

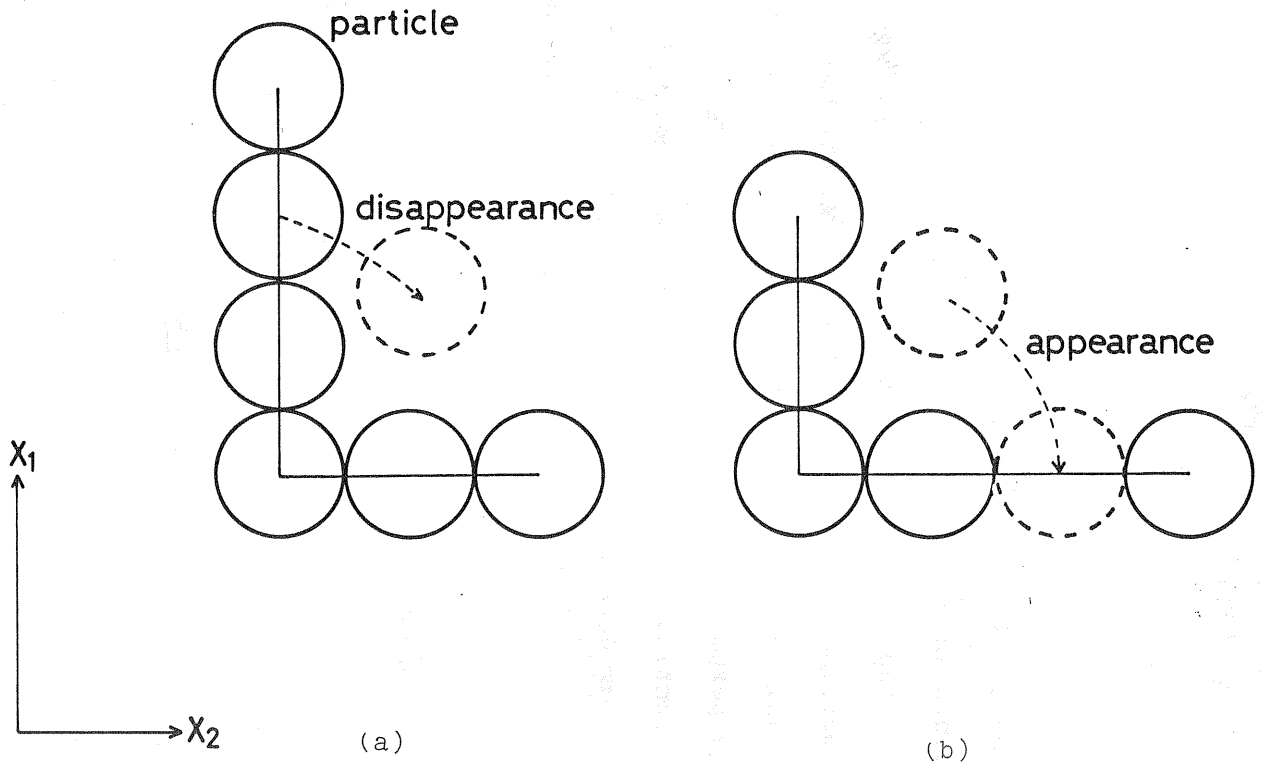

Fig.4.4 Discontinuous motions of disappearance and appearance

contact points along the path to the disappearance probability of contact points by K , the equation for the appearance can be written as follows.

$$N_{s,x_i}/N_{s-\Delta s,x_i} = 1 + \frac{1}{N_c}\sum_{\beta_1=0}^{\pi/2}\sum_{\beta_2=0}^{2\pi}\left\{K P_d(\beta_1)(n_{\eta,1}+n_{\eta,2})\right\} \qquad (4.12)$$

where K ; parameter depending on the stress state, void ratio, fabric of particulate material and so on.

The discontinuous motions of the disappearance and the appearance are schematically shown in Fig.4.4. Fig.4.4 shows particles and paths in the orthogonal directions. The motion of the disappearance is shown in Fig.4.4(a), i.e., a particle drops into a void and disappear in the path of X_1-direction. The motion of appearance is shown in Fig.4.4(b), i.e., the particle which has disappeared in the path of X_1- direction appears in the path of X_2-direction. Thus, the parameter K defined in Eq.(4.12) is considered to correspond to the Poisson's ratio in the continuum mechanics.

4.3 Conclusions

The present chapter has dealt with the definition of strain for the particulate material based on the motions of particles. The strain of particulate material has been defined by using the probability density function of contact angles and the discontinuous motions of particles which are called the disappearance and the appearance of contact points, i.e., the strain of particulate material has derived by $w(\eta,s)$ and $N_{s,x_i}/N_{s-\Delta s,x_i}$ as shown in Eq.(4.7).

The results obtained in the present chapter may be summarized as follows.

(1) In the particulate material the deformation can be expressed

by two kinds of particle motions, i.e., the continuous motion of change in contact angles and the discontinuous motion of particles.

(2) The continuous motion of change in contact angles is estimated by the probability density function which is obtained in chapter 3.

(3) The discontinuous motions are called the disappearance and the appearance. These motions at the contact points are considered to correspond to the dislocation of crystal solid and are estimated the parameters λ and κ which reflect the mechanical properties of particulate material, i.e., void ratio, distribution of particle size, stress ratio, fabric of particulate material and so on.

(4) It is found that the discontinuous motions at the contact points of particles play profoundly important role as well as the continuous motion in the deformation process of particulate material composed of particles whose shapes and sizes are

Reference for Chapter 4

1) see ref. 23) in Chapter 1.

2) see ref. 18) in Chapter 1.

3) Matsuoka, H.: The Stress-Strain Relation of Soils under Shearing Derived from a Microscopic Consideration, Annuals, Disaster Prevention Research Institute, Kyoto Univ., No.15B, 1972, pp.499-511, (in Japanese).

4) see ref. 20) in Chapter 1.

5) Kitamura, R.: Definition of Strain on the Particulate Material, Proc. Annual Meeting of Kansai Br. JSCE, 1978, 3-5, (in Japanese).

6) Ohmaki, S.: Two-Dimensional Deformation of Particulate Material, Proc. Annual Meeting of JSSMFE, 1974, pp.199-202, (in Japanese).

CHAPTER 5 EXPERIMENTAL RESULTS OBTAINED BY MODIFIED TRIAXIAL APPARATUS

5.1 Introduction

A mechanical model of particulate material based on Markov process has been proposed in chapters 3 and 4. What the model can describe are not the real but the projected figure of it and therefore, we are anxious to obtain the sophisticated model. It is orthodox procedure for the establishment of model to verify the validity of the model and to modify the model according to the results obtained by the experments with real particulate materials. This orthodox procedure is taken in this thesis. In this chapter the drained shearing tests with Toyoura sand are carried out along the various stress paths by using a newly modified triaxial apparatus which can generate three different principal stresses in the specimen. The validity of proposed model is verified by examining the stress-strain relations of Toyoura sand and the slip planes of specimen which can be observed after failure.

First of all, the true triaxial apparatus which were used by other researchers are reviewed and classified in terms of loading system. The merits and demerits of these apparatus are briefly described. The samples used in this investigation and test procedures is explained. Then, we discuss the accuracy and compensation of errors induced by the newly triaxial testing apparatus. Finally, experimental results is solely examined.

5.2 New Triaxial Apparatus[1)]

5.2.1 True triaxial apparatus in the previous researches

The conventional triaxial apparatus have been widely used in

the laboratory tests to investigate the deformation and the strength characteristics of soils, and determine the soil parameters since the operation of this apparatus is relatively simple and supplies the data with the good accuracy as an element test. But the stress state in the specimen are limited to be axi-symmetrical and consequently two principal stresses are always same in the horizontal direction. On the other hand, in the real ground the amounts and the directions of principal stresses change place to place. Therefore, it has been realized that the soil tests under three different principal stress states must be carried out in the laboratory in order to elucidate the mechanical properties of soil subjected to these stress states. The apparatus which can generate three different principal stress state have been developed all over the world. In this study these apparatus are called the true triaxial apparatus.

Let's review these apparatus, classify them by means of loading system and briefly describe the merits and the demerits of them. The true triaxial apparatus are largely divided into three groups by means of the method of generating stresses in the specimen.

The triaxial apparatus for hollow cylindrical specimen belong to the first group. The apparatus in this group generate three different principal stresses by applying the different pressures on the inside and outside of hollow cylindrical specimen, and further giving the axial and torsional forces on the ends of specimen. These apparatus are called the hollow cylindrical apparatus in the following description.

The second group includes the apparatus which have an additional loading equipment to the conventional triaxial apparatus

and generate three different principal stresses in the vertical and two horizontal directions of cubic or rectangular prism specimen. The apparatus in this group are called the modified triaxial apparatus in the following description. This group is further divided into two subgroups by means of the loading system, i.e., one is equipped with the flexible rubber bags filled with liquid and the other is equipped with the rigid plates such as steel plates for the additional loading system.

The apparatus in the third group are usually called the box type triaxial apparatus. In these apparatus three different principal stresses are generated in the specimen by applying the forces on planes of cubic or rectangular prism specimen. This group is also divided into two subgroups by means of the loading system equipped with the flexible rubber bags or the rigid plates which transmit the loading forces into the specimen.

The classification of the true triaxial apparatus above explained is illustrated in Fig.5.1. The authors who performed the experiments by using these apparatus are also given and further the literatures for the references are listed up in Table 5.1.

The specimen in the hollow cylindrical testings can experience larger strains than the conventional triaxial apparatus. Thus, the apparatus in the first group are beneficial to the experimental researches for the residual strength, the critical void ratio and so on. Furthermore, as these apparatus can be easily given the alternating torsional forces on the ends of specimen, they are recently used in dynamic soil tests. However, comparing them with the conventional triaxial apparatus, the stresses and strains induced in the specimen tend to be non-uniform.

In the second or third group the specimens being in contact

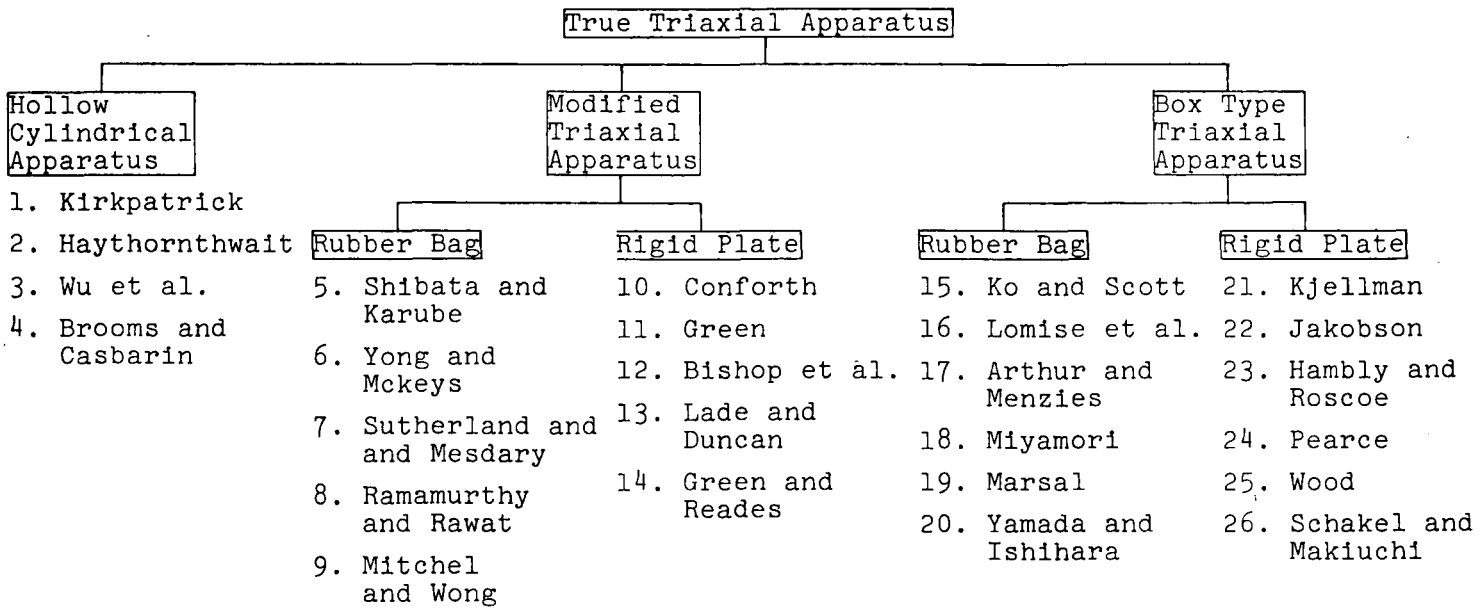

Fig.5.1 Classification of true triaxial apparatus

Table 5.1 References in Fig.5.1

No.	Literature
1	Proc.4th Int. Conf.SMFE, Vol.1, 1957, pp.172-178
2	Proc.ASCE, Vol.86, No.SM5, 1960, pp.35-62
3	Proc.ASCE, Vol.89. No.SM1, 1963, pp.145-181
4	Proc.6th Int. Conf.SMFE, Vol.1, 1965, pp.179-183
5	Proc.6th Int. Conf.SMFE, Vol.1, 1965, pp.359-363
6	Proc.3rd Panam. Conf.SMFE, Vol.1, 1967, pp.131-143
7	Proc.7th Int.Conf.SMFE, Vol.1, 1969, pp.391-399
8	Proc.8th Int.Conf.SMFE, Vol.1, 1973, pp.339-342
9	Canadian Geotech. J., Vol.10,1973, pp.520-527
10	Geotechnique, Vol.14, No.2, 1964, pp.143-167
11	Proc.Roscoe Memorial Symp., Cambridge,1971, pp.285-323
12	Proc.8th Int. Conf.SMFE, Vol.1, 1973, pp.57-64
13	Proc.ASCE, Vol.99, No.SM10, 1973, pp.793-812
14	Geotechnique, Vol.25, No.2, 1975, pp.333-356
15	Geotechnique, Vol.17, No.1, 1967, pp.40-57
16	Proc.7th Int. Conf.SMFE, Vol.1, 1969, pp.257-265
17	Geotechnique, Vol.22, No.1, 1972, pp.115-128
18	Proc.JSCE, No.255, 1976, pp.81-91
19	Proc.8th Int. Conf.SMFE, Vol.1, 1973,pp.259-264
20	Soils and Foundations, Vol.18, No.2, 1979, pp.79-94
21	Proc.1st Int. Conf.SMFE, Vol.2, 1936, pp.16-20
22	Proc.4th Int. Conf.SMFE, Vol.1, 1957, pp.167-171
23	Proc.7th Int. Conf.SMFE, Vol.2, 1969, pp.173-181
24	Proc.Roscoe Memorial Symp., Cambridge,1971, pp.330-339
25	Geotechnique, Vol.25, No.4, 1975, pp.783-797
26	Proc.9th Int. Conf.SMFE, Vol.1, 1977, pp.295-300

with the flexible rubber bags are subjected to the uniform forces because the pressure in liquid is isotropic and uniform. However, as the rubber bag is flexible, the deformation occurring in the specimen tends to be non-uniform and the expansion of the rubber bag under high pressure often causes some troubles at the corners of the specimen. Furthermore, as the deformations of specimen in the directions of three principal strains are measured by the change in volume of the rubber bags, it may be considered that the penetration of rubber bags into the specimen such as coarse sand causes some errors for measurement of strains.

On the other hand, as contrasted with the flexible rubber bags, the rigid plates generate the uniform deformation in the specimen. But, because of difficulty to accurately measure the contact area between the loading rigid plates and the specimen, some errors take place in the calculation of stresses. In all the apparatus except the ones in the third group, two different types of loading method are used to apply the stresses on the specimens, i.e., the liquid pressure in the chamber or in the flexible rubber bags, and the rigid plates. Such a difference of the boundary conditions is supposed to give some influences to the mechanical behaviours of specimen in these apparatus. The considerations about these influences remain to be a future research. In the present stage it may be concluded not to be able to judge which apparatus in Fig.5.1 is superior to others because every apparatus have both the merits and the demerits as mentioned above. Finally, it may be fairly difficult to develop the more accurate true triaxial apparatus than the conventional testing device because additional quantities must be measured with respect to stress and strain.

5.2.2 Modified triaxial apparatus

The modified triaxial apparatus is designed and constructed for the purpose of studying the mechanical behaviours of particulate material under general three dimensional stress conditions. This apparatus having rigid loading plates for additional loading direction belongs to the second group in Fig.5.1. The schematic diagram of this modified triaxial apparatus including the pressure system is illustrated in Fig.5.2 and its whole view is given in Photo 5.1. The pressure applied system is similar to the conventional triaxial apparatus by means of the air pressure controlled method which has been developed by Akai et al.[2]. The loadings in the three orthogonal directions of a cubic specimen are applied by controlling of air pressures. The controlling of air pressures is done by using air pressure regulators (see (7) in Fig.5.2). The vertical loading (X_1- axis) is applied to the specimen through the bellofram cylinder (see (1) in Fig.5.2) mounted on the loading frame (see (2) in Fig.5.2). The loading in one of the horizontal directions (X_2- axis) is transmitted through the bellofram cylinder set up in the triaxial chamber (see (4) in Fig.5.2) and the loading in another horizontal direction (X_3- axis) is applied by chamber water pressure. The vertical force is measured by a proving ring (see (3) in Fig.5.2).

The detail cross sections of modified triaxial apparatus for a cubic specimen with 10 x 10 x 10 cm are shown in Fig.5.3. The central axis of triaxial chamber does not coincide with the one of specimen as shown in Fig.5.3(a) ao that the horizontal loading system shown in Photo 5.2 might be set in the triaxial chamber. The chamber (see (2) in Fig.5.3) is made of acrylic resins whose dimension is 26 cm and 30 cm in inner and outer diameters respec-

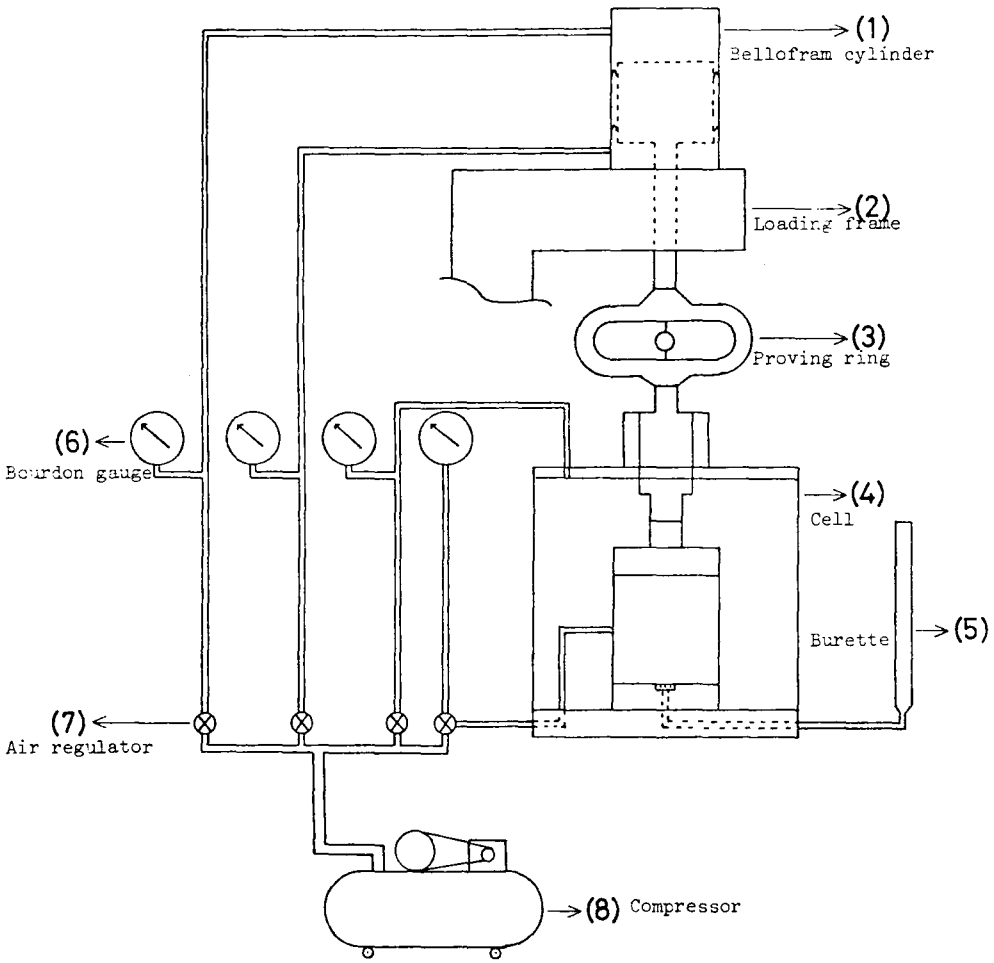

Fig.5.2 Schematic diagram of modified triaxial apparatus

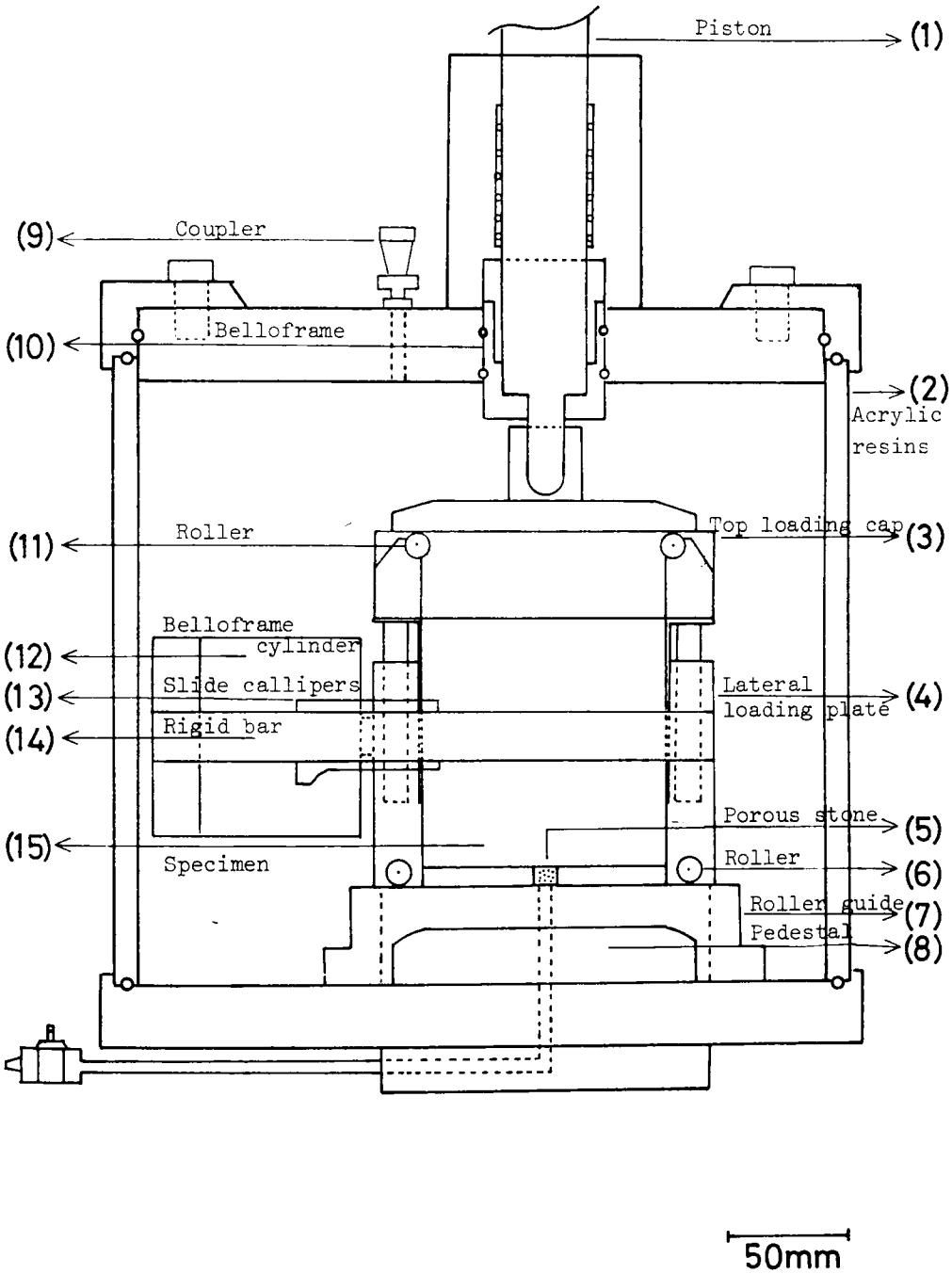

Fig.5.3(a) Front view of modified triaxial cell

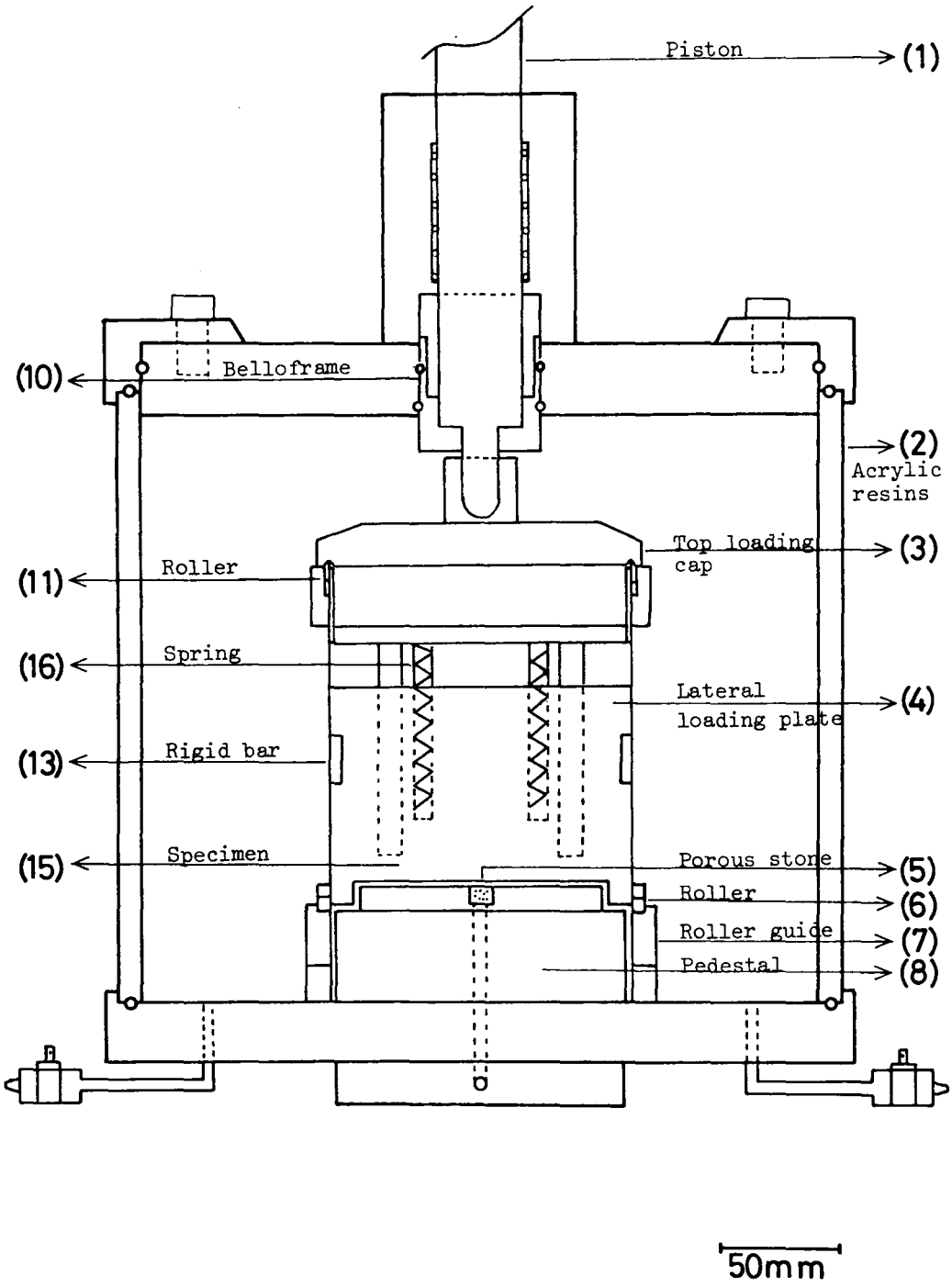

Fig.5.3(b) Side view of modified triaxial cell

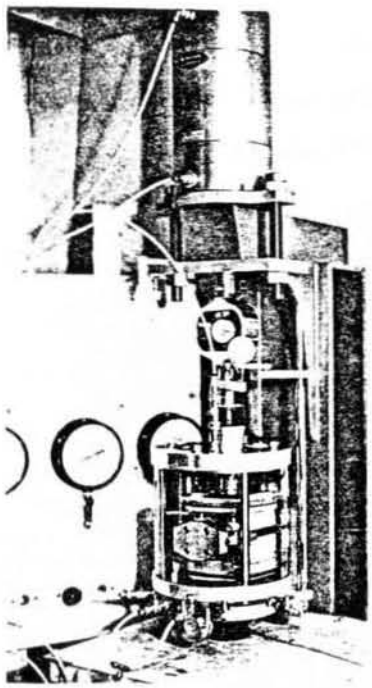

Photo 5.1 Whole view of modified triaxial apparatus

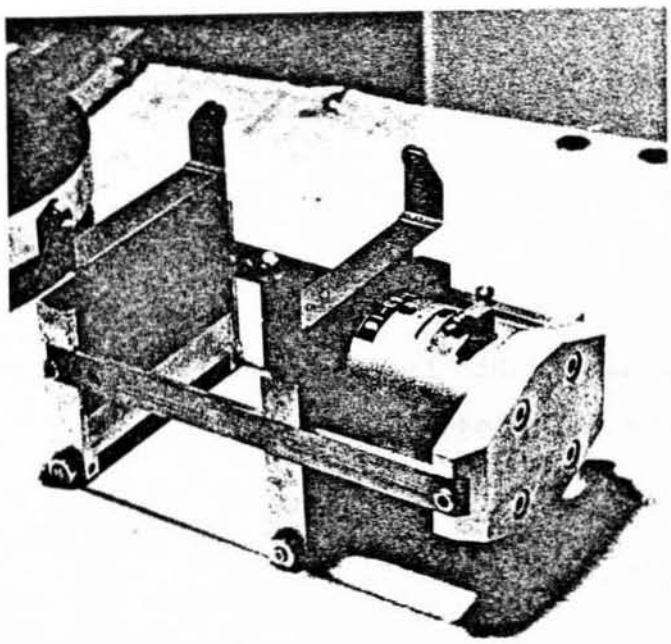

Photo 5.2 Horizontal loading system

tively and 25 cm in height.

The horizontal loading system consists of two inter-connected rigid plates (see (4) in Fig.5.3) which sit opposite each other. One of the rigid plates is proviede with a bellofram cylinder (see (12) in Fig.5.3) which applies the horizontal load. Each plate is composed of two sliding sections connected by springs (see (16) in Fig.5.3). Each plate possesses four little rollers (see (6) and (11) in Fig.5.3) to guarantee for smooth horizontal movement of the rigid plates under the condition of contact between the plates and the cap or the pedestal. This loading system is similar to the one that has been developed by Lade and Duncan[3] in principle.

The vertical deformation is measured with the dial gauge which can be read to 1/100 mm. The horizontal deformation is measured with the slide calipers (see (13) in Fig.5.3) which is mounted on the inter-connected rigid bar (see (14) in Fig.5.3) and can be read to 2/100 mm. The volumetric change in the specimen is measured with the burette which can be read to 0.05 cc. The pedestal (see (8) in Fig.5.3) is provided with the porous stone (see (5) in Fig. 5.3) which is set in the center of pedestal and has 1 cm in diameter, and the drainage line which is connected to the burette.

Finally, by exchanging the cap and pedestal, the conventional axi-symmetrical triaxial tests can be performed with the cylindrical specimens, whose dimensions have 5 cm or 10 cm in diameter and 10 cm in height.

5.3 Material and Testing Procedures

All the tests to be shown in the present chapter have been carried out on Toyoura sand whose mean diameter of particles is 0.2 mm, uniformity coefficient is 1.6 and specific gravity is 2.65.

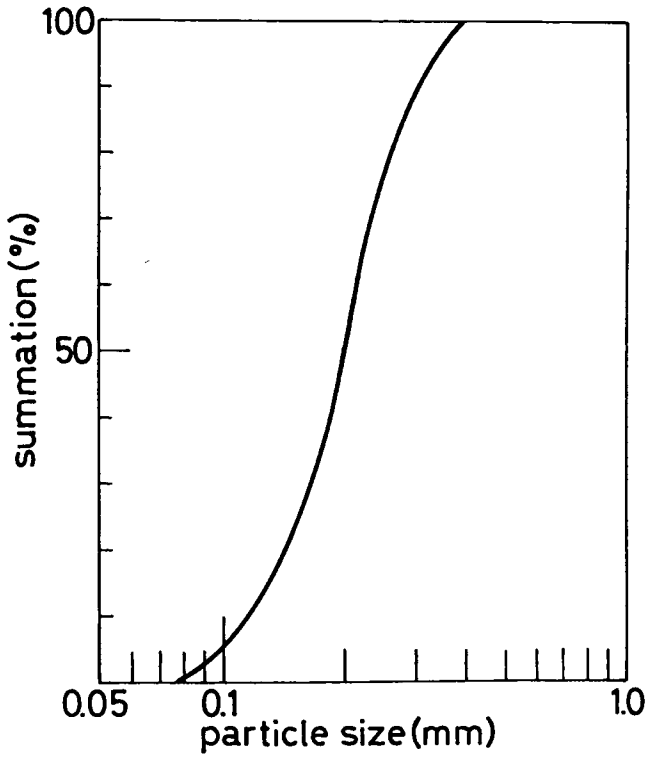

Fig.5.4 Grain size accumulation curve of Toyoura sand

The grain size accumulation curve of Toyoura sand is shown in Fig. 5.4. The material is boiled more than one hour in order to deair. Specimens are prepared by pouring saturated sand into mould. The initial void ratio is prescribed by the number of tamping with a rod, i.e., the dense specimens are prepared by dividing the specimen into three layers and tamping each layer about 15 times by the rod whose diameter is 1 cm. On the other hand, loose specimens are prepared by the following way, i.e., a specimen is divided into two layers and sand is poured into the mould filled with water and lightly tamped 4 times on each layer.

After sealing the specimen by O-rings, the suction with 0.005 kg/cm^2 is imposed on the specimen in order to stand by itself when the mould is dissolved. Then the size of specimen is measured by the slide calipers and the horizontal loading system is set on the rails. Photo 5.3 shows this phase of preparation. The preparation of triaxial tests is finished by putting on the acrylic resins cell and filling the triaxial chamber with water. This step is shown in Photo 5.4. After specimens are consolidated under the isotropic pressures, the shearing tests are conducted. The initial void ratios of specimens after the isotropic consolidation in the experiments are listed up in Table 5.2 with stress conditions of tests.

All the tests are performed under the drained condition. For the tests under the constant confining pressures the strain-controlled method is adopted with the vertical strain rate of 0.05 %/min. In these cases we use cylindrical specimens whose dimensions are 10 cm in diameter and 10 cm in height. The stress-controlled method is adopted for the other tests with various stress paths including the stress reverse under the constant mean effective principal stress.

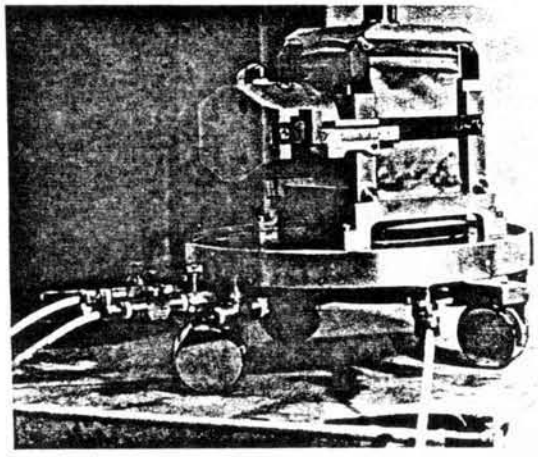

Photo 5.3 Phase of preparation of horizontal loading system

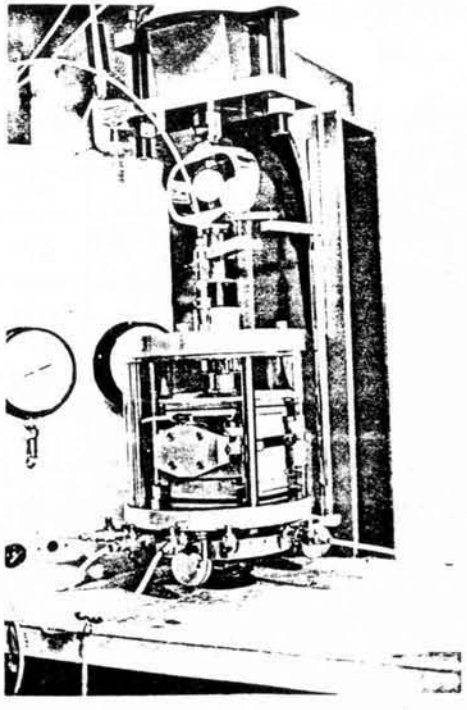

Photo 5.4 Phase of apparatus under isotropic consolidation

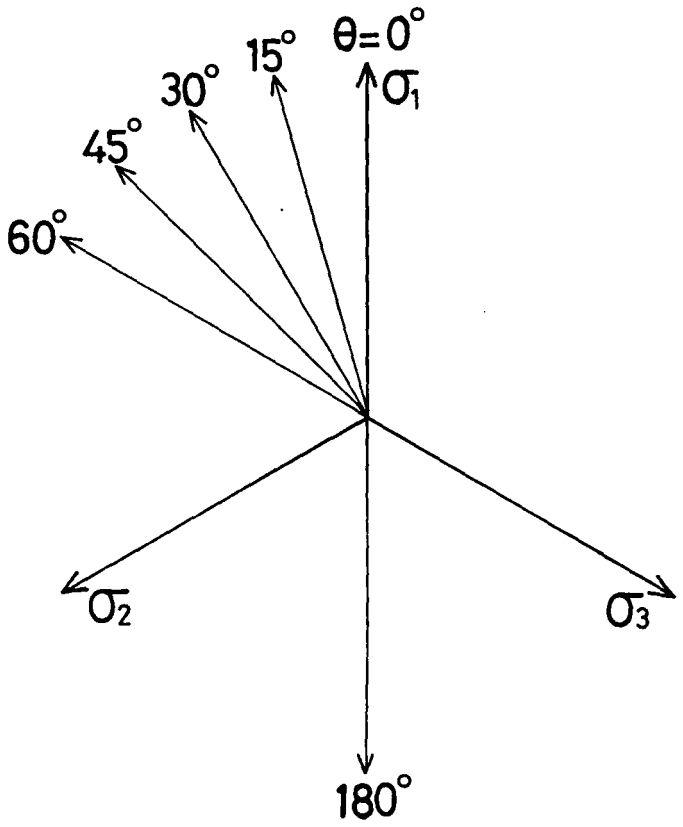

Fig.5.5 Stress paths on π-plane

Table 5.2

(a) Tests under constant confining pressures

σ_3(kg/cm^2)	e_o	Remarks
2.0	0.713	monotonous
3.0	0.720	
4.0	0.713	
3.0	0.645	one-way repeated
4.0	0.671	

(b) Tests under constant mean effective principal stress

θ°	e_o	Remaks
0	0.656	medium dense, monotonous
15	0.664	
30	0.653	
45	0.701	
60	0.705	
180	0.692	
0	0.801	loose, monotonous
180	0.812	
0→180	0.689	two-way repeated
180→0	0.694	

The stress-controlled tests are performed such that the difference between the maximum and the minimum principal stresses is increased or decreased by 0.1 kg/cm^2 in every loading or unloading stages and the next stage is commenced after the vertical strain rate decreases less than 0.005%/min at the present stage. The monotonous loading tests under the constant mean effective principal stress are performed along the stress paths as shown in Fig.5.5 which illustrates the radial stress paths on the octahedral plane (π- plane) in three effective principal stress space. The radial stress paths with $\theta = 0°$ and $\theta = 180°$ in Fig.5.5 correspond to the conventional triaxial compression and extension tests respectively.

In the following description, let's denote the vertical principal stress and strain by σ_1 and ϵ_1, one of horizontal principal stress and strain in the direction loaded by the bellofram cylinder by σ_2 and ϵ_2, and the other horizontal principal stress and strain by σ_3 and ϵ_3 in order that the subscripts are coincided with the reference axes in Fig.4.1. Thus, the conventional triaxial extension test σ_2 and σ_3 are the maximum principal stress and σ_1 is the minimum principal stress.

The repeated loading tests are carried out under the constant confinig pressure and the constant mean effective principal stress. In the cases of constant confining pressures, the strain-controlled tests are conducted under the repeated loading only in compression side. On the other hand, two types of stress-controlled tests are performed by applying the repeated loading in both sides of compression and extension. One of them is started towards the compression side, the other towards the extension side. For later convenience the loading and the unloading processes in these repeated tests are divided and named as shown in Fig.5.6.

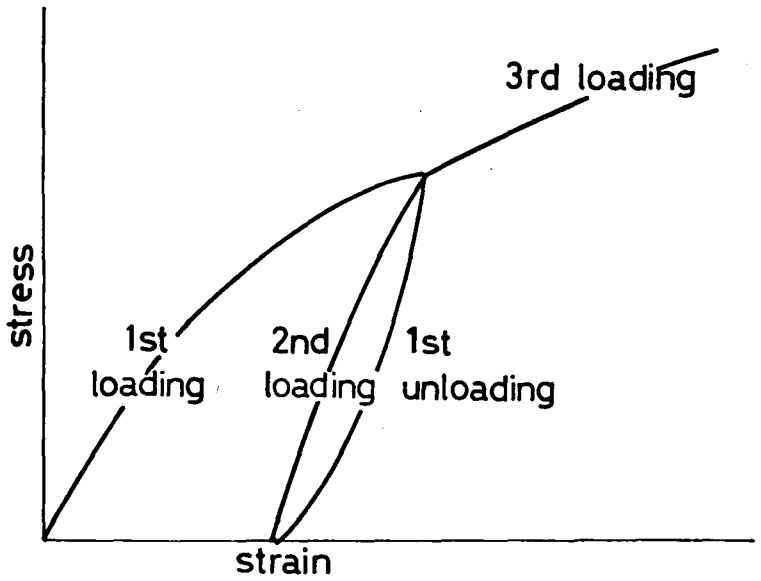

Fig.5.6(a) Loading and unloading processes in the one-way repeated loading test

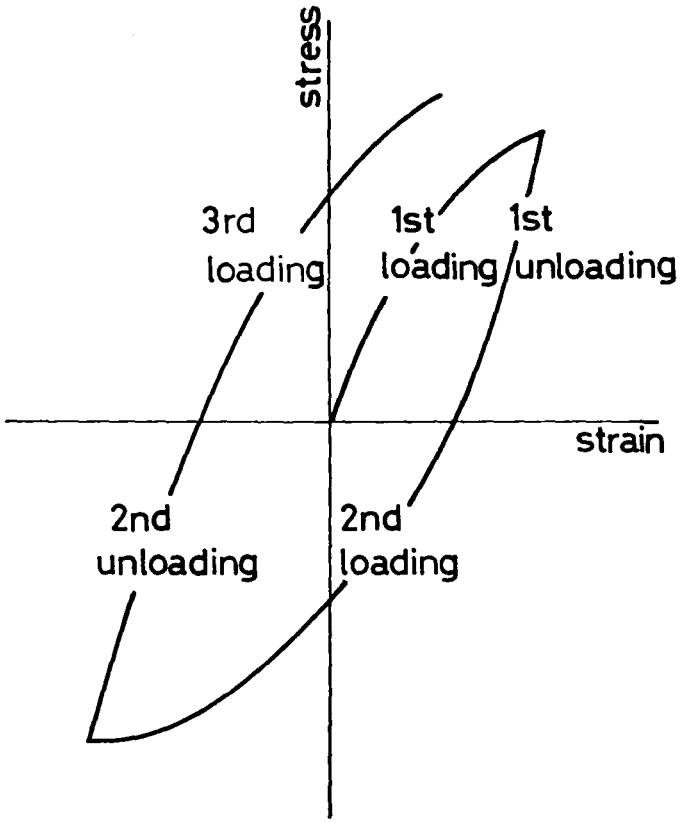

Fig.5.6(b) Loading and unloading processes in the two-way repeated loading test

5.4 Error Corrections for the Modified Triaxial Apparatus

The main errors caused in the conventional triaxial tests are mentioned as follows.

1) The non-uniformity of stress and strain distribution in the specimen due to the end restraint effects between specimen and cap or pedestal.
2) The errors of vertical force due to the friction between the rod and its guide.
3) The penetration of rubber membrane to the specimen due to the change in the chamber pressure.
4) The restraint of deformation in the horizontal direction due to the tensile force of rubber membrane.

For the tests conducted by using the modified triaxial apparatus, additional errors must be taken into account due to the horizontal loading system. In this section, let's review the corrections for these errors which have been elaborately established by previous experimental researches and give the explanations for these corrections in the usage of the modified triaxial apparatus.

Concerning the non-uniform stress and deformation in the specimen, Rowe and Barden[4] carried out the experimental research to clarify the end restraint effects of specimen. They performed the triaxial compression tests in which two kinds of triaxial compression tests were used. The one was for specimen of 4 inches in diameter and 4 inches in height, and with the friction reducer by thin rubber sheets placed between the specimen and the end plates. The other was for specimen of 4 inches in diameter and 8 inches in height without the friction reducer. Comparing these test results, they clarified that the more uniformed stress and deformation were

obtained in the former test than the latter based on the observation of the deformation and the slip surfaces in the specimen. Barden and McDermott[5] extended the above experimental research to the shearing tests under other stress conditions, i.e., plane strain and triaxial extension tests, and obtained the same results.

Aiming at the research of strenght and dilatancy characteristics of cohesionless soil, Bishop and Green[6] carried out the triaxial compression tests for different friction reducing methods and specimens with various ratios of height to diameter. From the test results they concluded that the end effects were of little significance for the specimen which has a height to diameter ratio of 2 to 1 or more and has a height to diameter ratio of 1 to 1 with two thin greased membranes.

Lee[7] has recently reviewed the previous papers concerning the end restraint effects, and Lee and Vernese[8] have pointed out the significance of the end restraint effects for cyclic loading tests of sand under undrained condition.

Arthur and Dalili[9] investigated the lubrication properties of rubber surfaces coated with various grease by using the modified shear box.

For our tests by using the modified triaxial apparatus, two lubricated thin rubber sheets are used between the ends of specimen and the loading plates. It is found that the end restraint effects are sufficiently reduced in our experiments from the facts that several slip planes are observed after failure. Therefore, it can be assumed that the specimen keeps to be uniform in geometry during the deformation process.

Concerning the friction between rod and its guide, some reducing techniques are devised, for example, the so-called forced

lubrication method was adopted in the air pressure controlled triaxial apparatus[2] and in N.G.I. type triaxial apparatus the frictionis reduced by ontinuously circulating the lubrication oil. For the newly modified triaxial apparatus the silicon grease is interposed between rod and O-ring set in its guide in order to reduce the rod friction.

Concerning the membrane misfit due to its penetration to the specimen, the experimental researches have been carried out by Moroto[10], Raju and Sadasivan[11], Kiekbusch and Schuppener[12], and Lade and Hernandez[13]. The correction method for this error in volume change is also standarized by JSSMFE[14] in which the volumetric changes are measured for the cylindrical specimen with the rods of different diameters under various confining pressures and the membrane misfit is known by extrapolating the volumetric changes for the specimen with the rod having the same diameter of specimen. In the experiments the correction of membrane penetration is performed in accordance with JSSMFE correction method by using the relation between the membrane penetration and pressure as shown in Fig.5.7. According to Fig.5.7, errors for volumetric strain is approximately 0.3% near the failure. Kiekbusch and Schuppener's experimental results showed that errors for volumetric strain due to the membrane penetration are approximately 0.03% near the failure. Lade and Hernandez described that the membrane penetration is negligible for soil with mean particle size below 0.1 mm - 0.2 mm.

Concerning the errors due to the tensile force of rubber membrane, experimental and theoretical works have been carried out by Henkel and Gilbert[15], Chandler[16], La Rochelle[17] and recently by Pachakis[18]. Based on the previous researches, this error can be

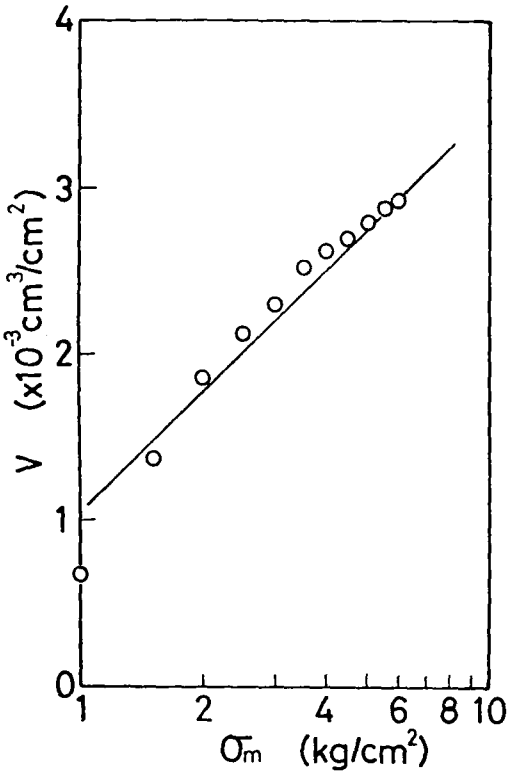

Fig.5.7 Relation between membrane penetration and pressure

neglected in our experiments since the failures take place at less than 5% vertical strain and we use a thin rubber membrane of 0.2 mm.

When using the modified triaxial apparatus, we must consider additional errors due to the horizontal loading system.

Let's discuss the errors caused by the horizontal loading system in the directions of X_1- and X_2-axes, and how to correct them. The prescribed stress σ_2 in the direction of X_2-axis is applied by the following way. The relation between the input air pressure and the output total force of bellofram cylinder in horizontal loading system is previously calibrated. It is necessary to know the contact area between the rigid plate and the specimen inorder to apply the prescribed stress in the direction of X_2-axis on the specimen. It is extremely difficult to measure the exact contact area between the rigid plate and specimen because the corners of cubic specimen do not form perfectly a right angle as shown in Fig.5.8. Thus, the initial untouched lengths are measured at the lower end of specimen when the specimen is placed on the pedestal. The contact area between the rigid plate and the specimen is assumed to be determined by using the values subtracted the initial untouched length from the current side lengths of specimen. It is also required to take account of the errors in the vertical force due to the springs installed between two sliding parts of rigid plates and both the frictions between two overlapped parts of rigid plates as well as between the specimen and the rigid plates. The frictional resistance between the overlapped parts of rigid plates are reduced by coating silicon grease. The lubricated thin rubber sheets are also provided between the specimen and the rigid plates as well as the upper and the lower ends of specimen.

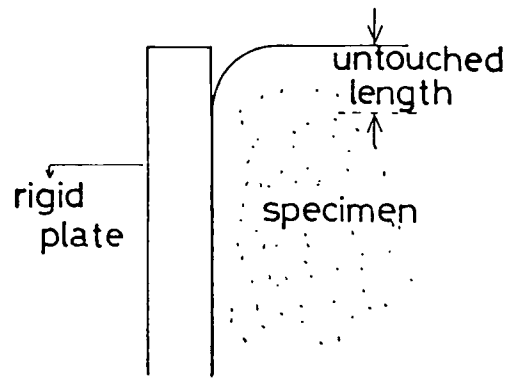

Fig.5.8 Corner of cubic specimen and rigid plate

The vertical force is corrected by giving considerations to the friction between rod and O-ring, and to the resistance of springs and the overlapped portion of rigid plates in the following way. The horizontal system without specimen is set up in the triaxial chamber. The vertical forces for the correction are measured by giving the vertical displacement under several confining pressures which range from 0 kg/cm^2 to 4 kg/cm^2, since confining pressure especially effects on the friction between rod and O-ring. The validity of these corrections for the stresses σ_1 and σ_2 are verified by conducting an axi-symmetrical triaxial compression test with the horizontal loading system under the constant mean effective stress condition, $\sigma_m = 2$ kg/cm^2. In this test the displacements in the directions of X_1- and X_2- axes, the volumetric change in specimen are measured. Fig.5.9 shows the obtained stress-strain relation between the principal strains ϵ_1 and ϵ_2, and the stress ratio σ_1/σ_3. When infinitesimal strain conditions can be assumed, the following strain relation is satisfied,

$$\epsilon_1 + \epsilon_2 + \epsilon_3 = \epsilon_v \qquad (5.1)$$

Therefore, the strain ϵ_3 can be obtained by using Eq.(5.1) and the measured strains ϵ_v, ϵ_1 and ϵ_2. The calculated strain is also given in Fig.5.9. As the fabric of sand specimen is supposed to be isotropic in the horizontal directions, the strains in the horizontal directions, ϵ_2 and ϵ_3, should be theoretically same under the axi-symmetrical stress state. From Fig.5.9 it is found that the measured strain ϵ_2 and the calculated strain ϵ_3 are almost same and then the correction method adopted here is satisfactory. This correction method is used in shearing tests

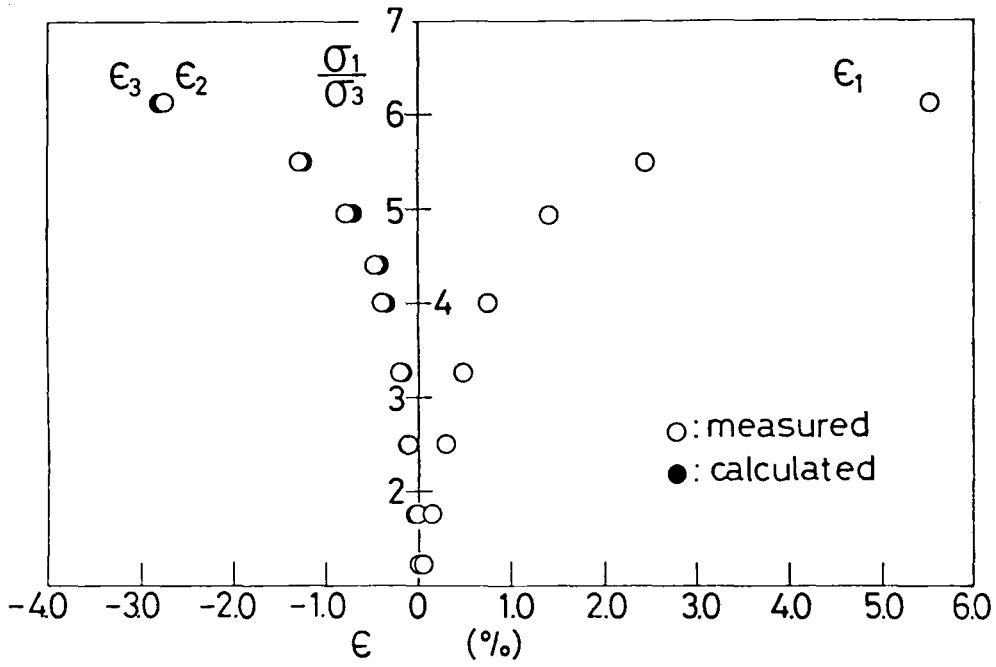

Fig.5.9 Measured and calculated strains under axi-symmetric stress state

for general three dimensional stress conditions along the stress paths of $\theta = 15°$, $30°$, $45°$ and $60°$ shown in Fig.5.5.

5.5 Experimental Results

In the experiments the shearing tests with Toyoura sand are carried out under various stress conditions after isotropic consolidation. Three monotonous and two repeated loading conventional triaxial compression tests for medium dense specimens are carried out under the constant confining pressures as shown in Table 5.2 (a). The stress-strain relations between the principal strains ϵ_1 and ϵ_3 , and the stress ratio σ_1/σ_3 are illustrated in Fig. 5.10(a)-(e).

Six monotonous and two repeated loading tests with medium dense specimens, and two monotonous loading tests with loose specimens are performed under the constant mean effective principal stress, σ_m = 2 kg/cm^2, as shown in Table 5.2(b). The stress-strain relations obtained by six monotonous loading tests are shown in Figs. 5.11(a)-(f). It is easily seen that the stress paths effect on the stress-strain relation. From Figs.5.11(b) and (c) the stress path for plain strain condition is supposed to exist in the range between $\theta = 15°$ and $30°$. The shearing test for $\theta = 60°$ corresponds to the extension test for which both the stresses σ_1 and σ_2 in the directions of X_1- and X_2- axes are the maximum principal stress. Then the strains ϵ_1 and ϵ_2 must be equal, if the fabric of sand is isotropic on the plane including X_1- and X_2- axes. It is found, however, the difference between strains ϵ_1 and ϵ_2 from Fig.5.11(e). This fact means the anisotropic fabric of sand specimen on the plane including X_1- axis.

For loose specimens Figs.5.12(a)-(b) show the test results of conventional triaxial compression ($\theta = 0°$) and conventional exten-

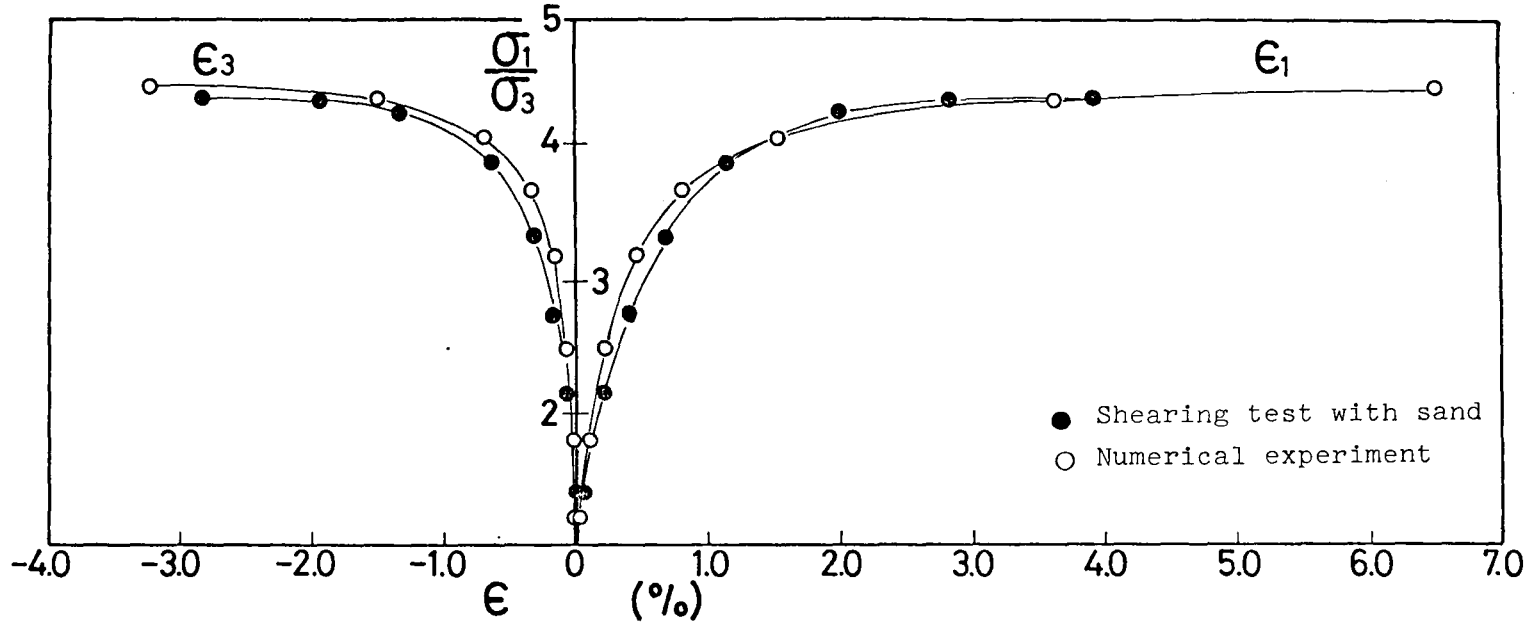

Fig.5.10(a) Stress-strain relations obtained by shearing test and numerical experiment under constant confining pressure, $\sigma_3 = 2 kg/cm^2$

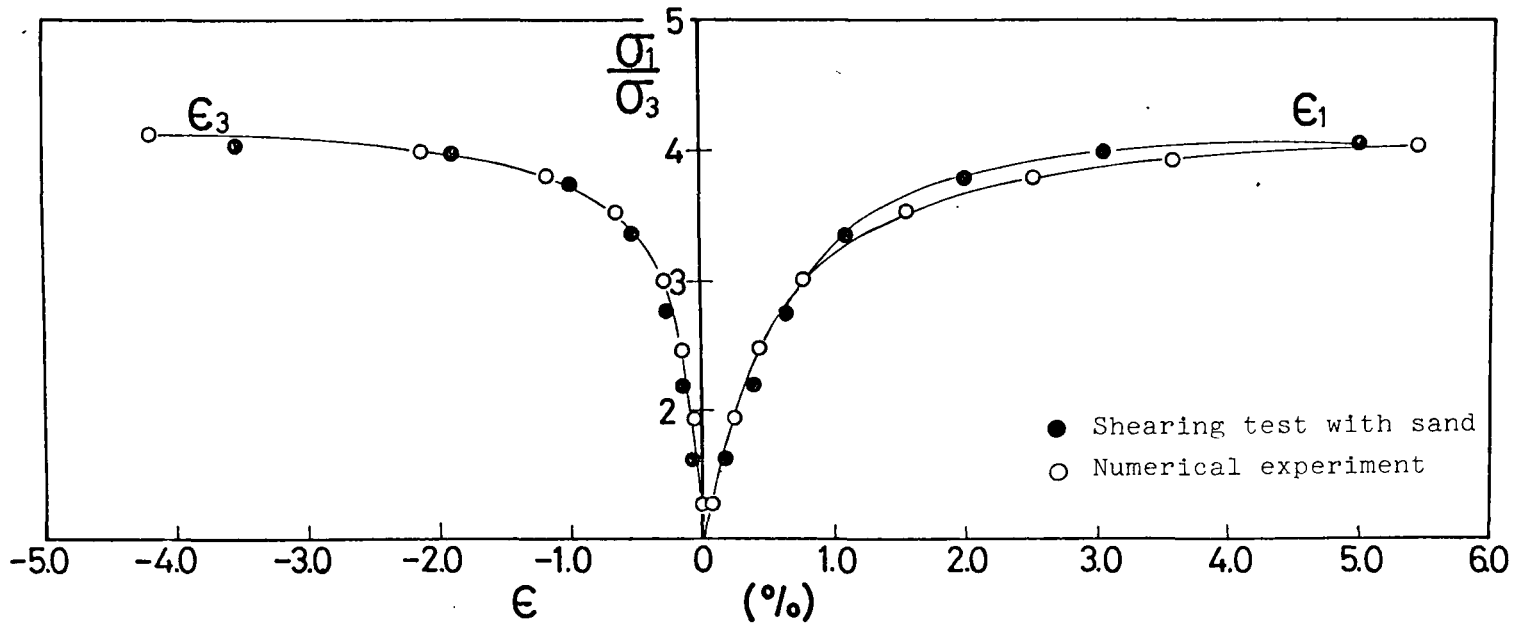

Fig.5.10(b) Stress-strain relations obtained by shearing test and numerical experiment under constant confining pressure, σ_3=3kg/cm^2

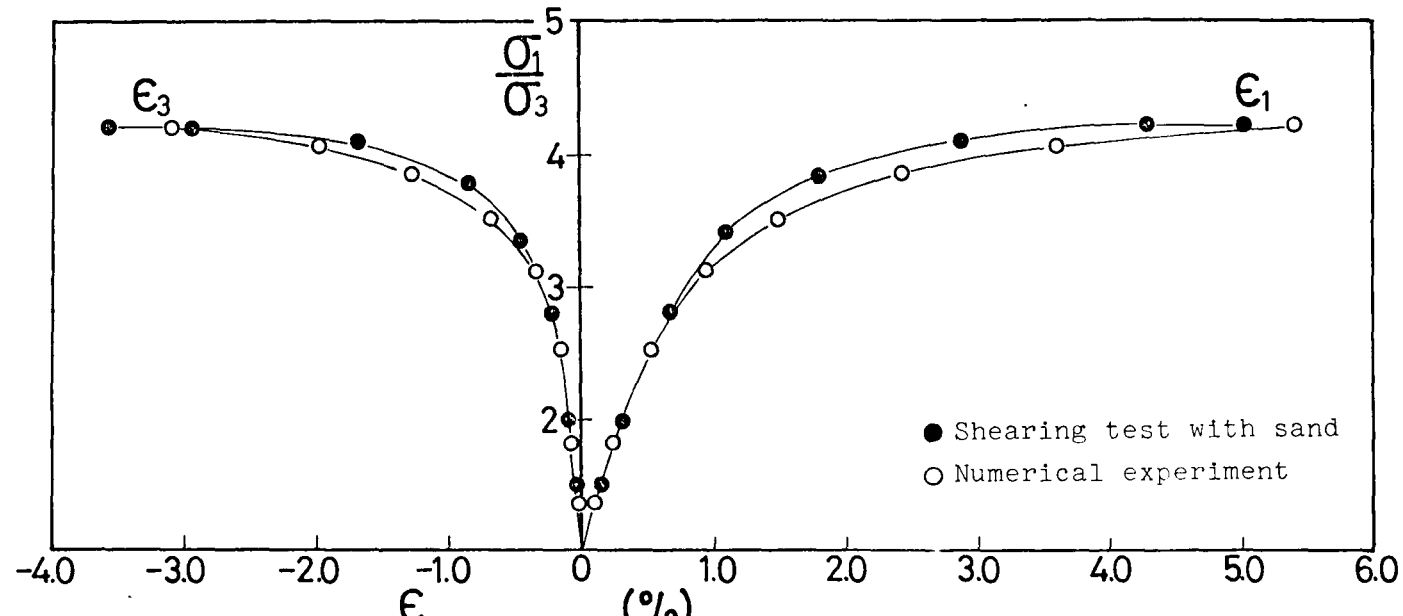

Fig.5.10(c) Stress-strain relations obtained by shearing test and numerical experiment under constant confining pressure, σ_3=4kg/cm^2

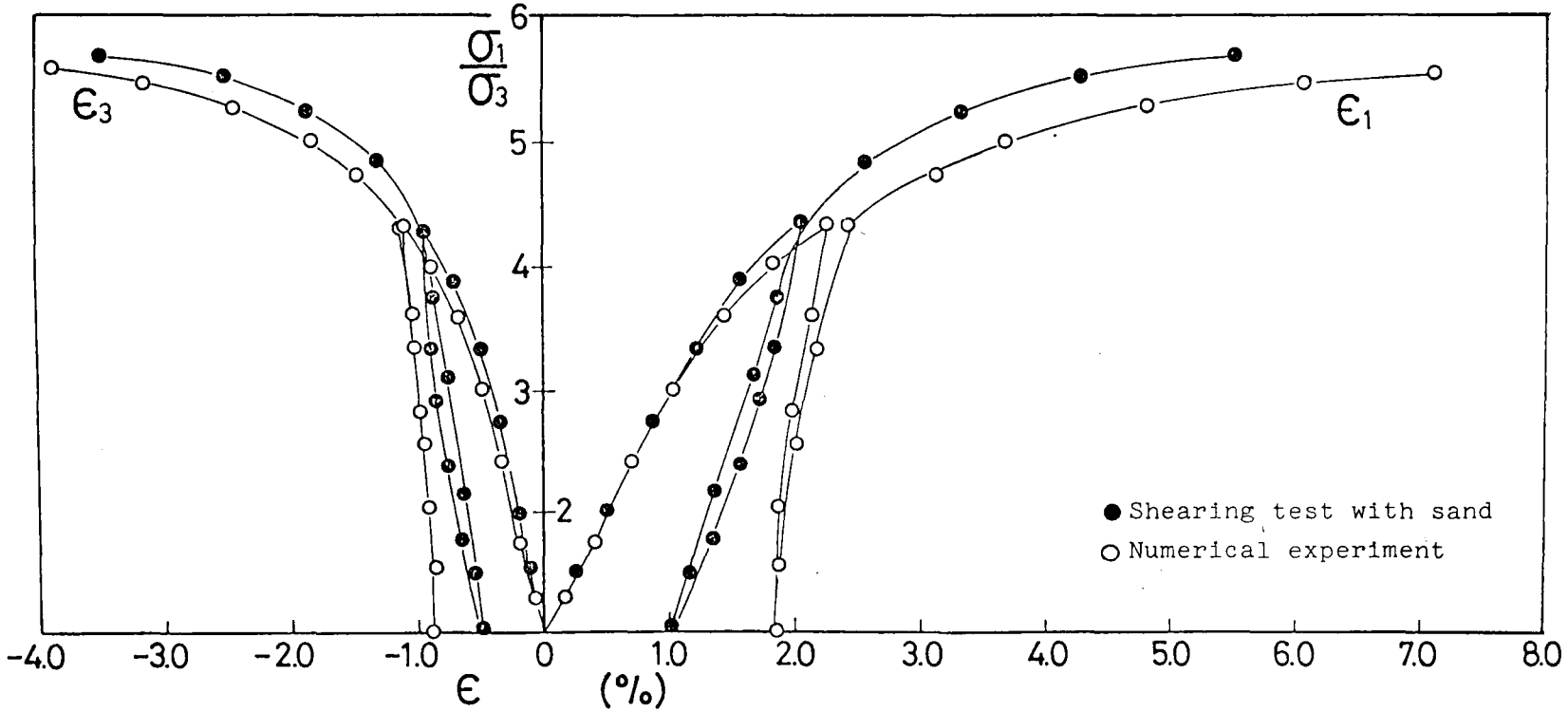

Fig.5.10(d) Stress-strain relations obtained by shearing test and numerical experiment under constant confining pressure, $\bar{\sigma}_3 = 3 kg/cm^2$

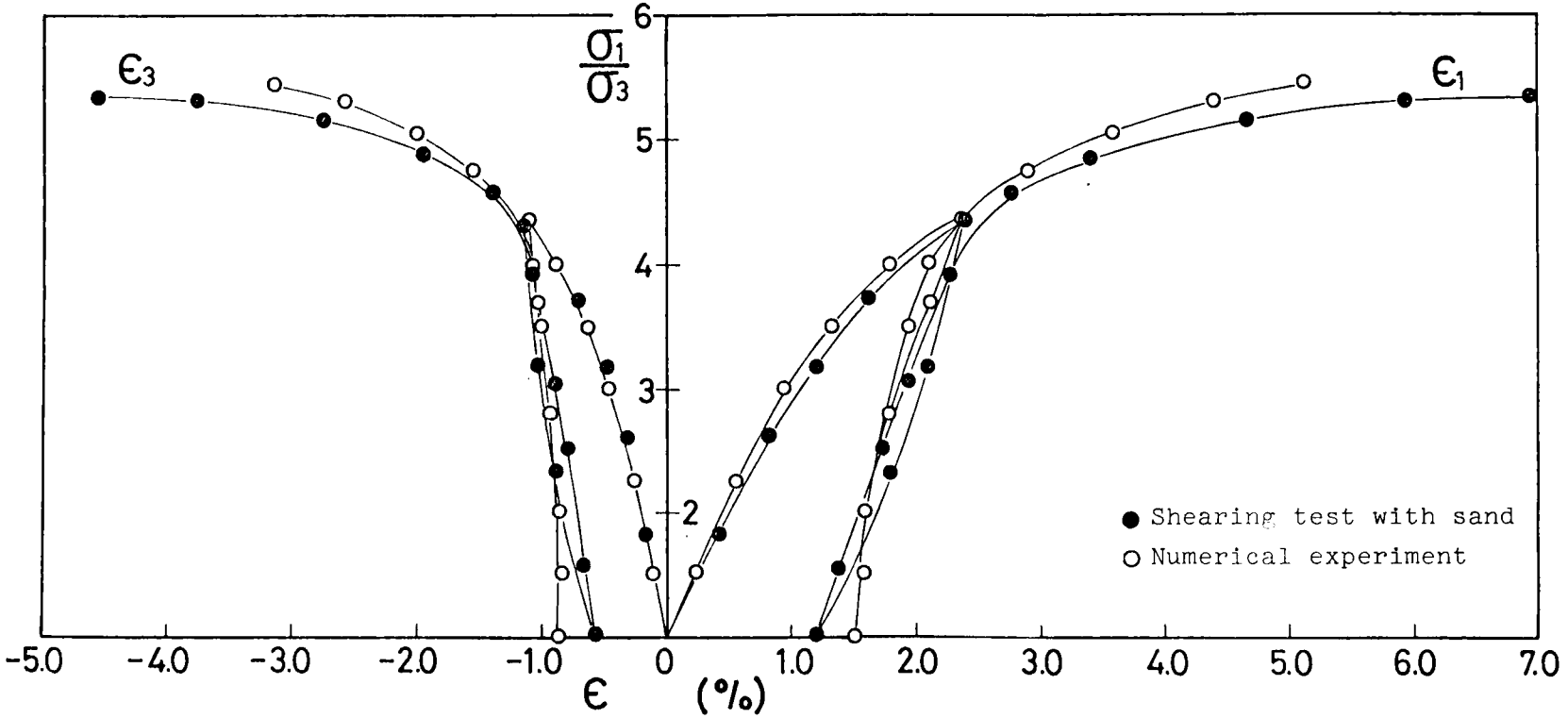

Fig.5.10(e) Stress-strain relations obtained by shearing test and numerical experiment under constant confining pressure, σ_3=4kg/cm^2 .

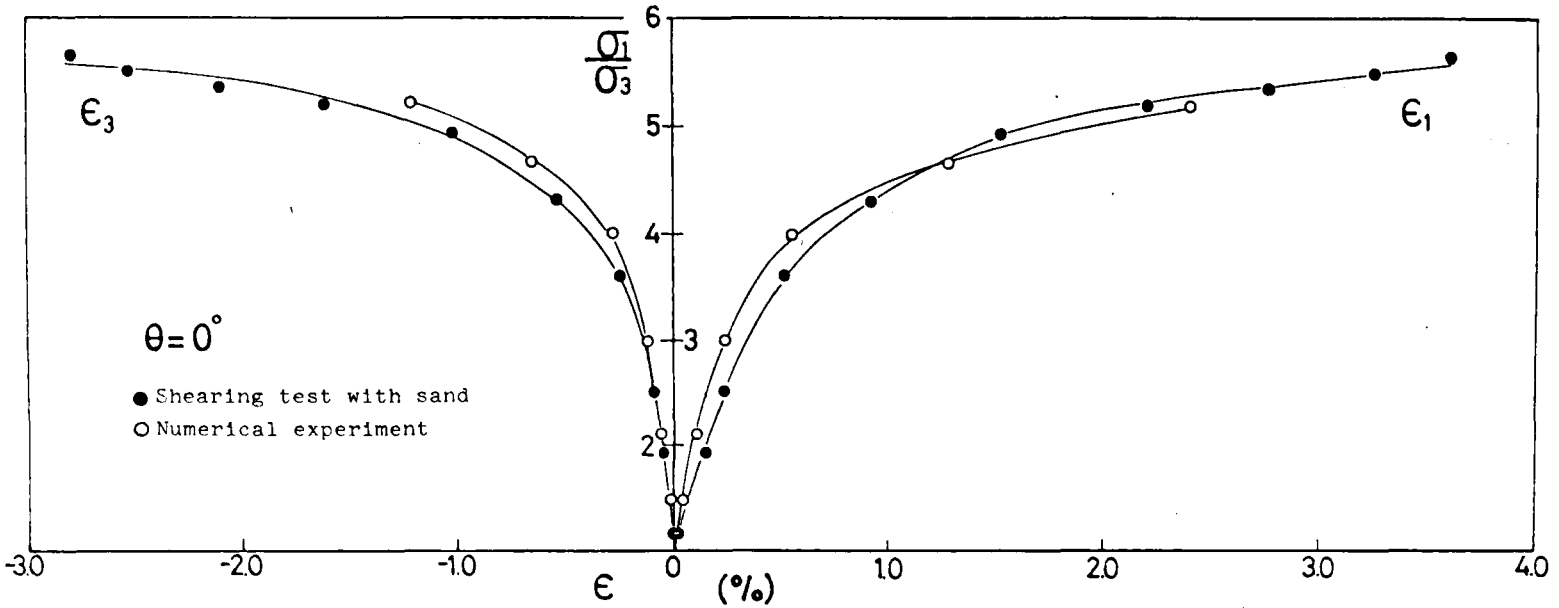

Fig.5.11(a) Stress-strain relations obtained by shearing test and numerical experiment under constant mean effective principal stress

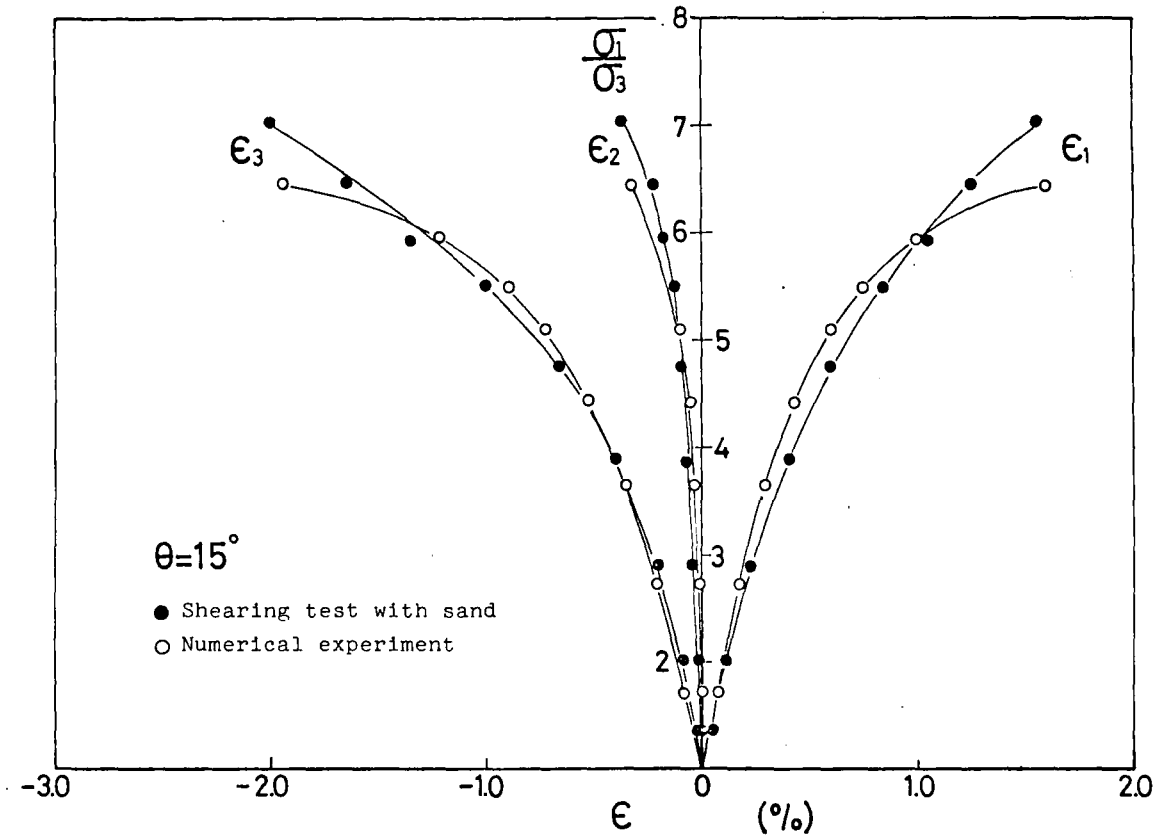

Fig.5.11(b) Stress-strain relations obtained by shearing test and numerical experiment under constant mean effective principal stress

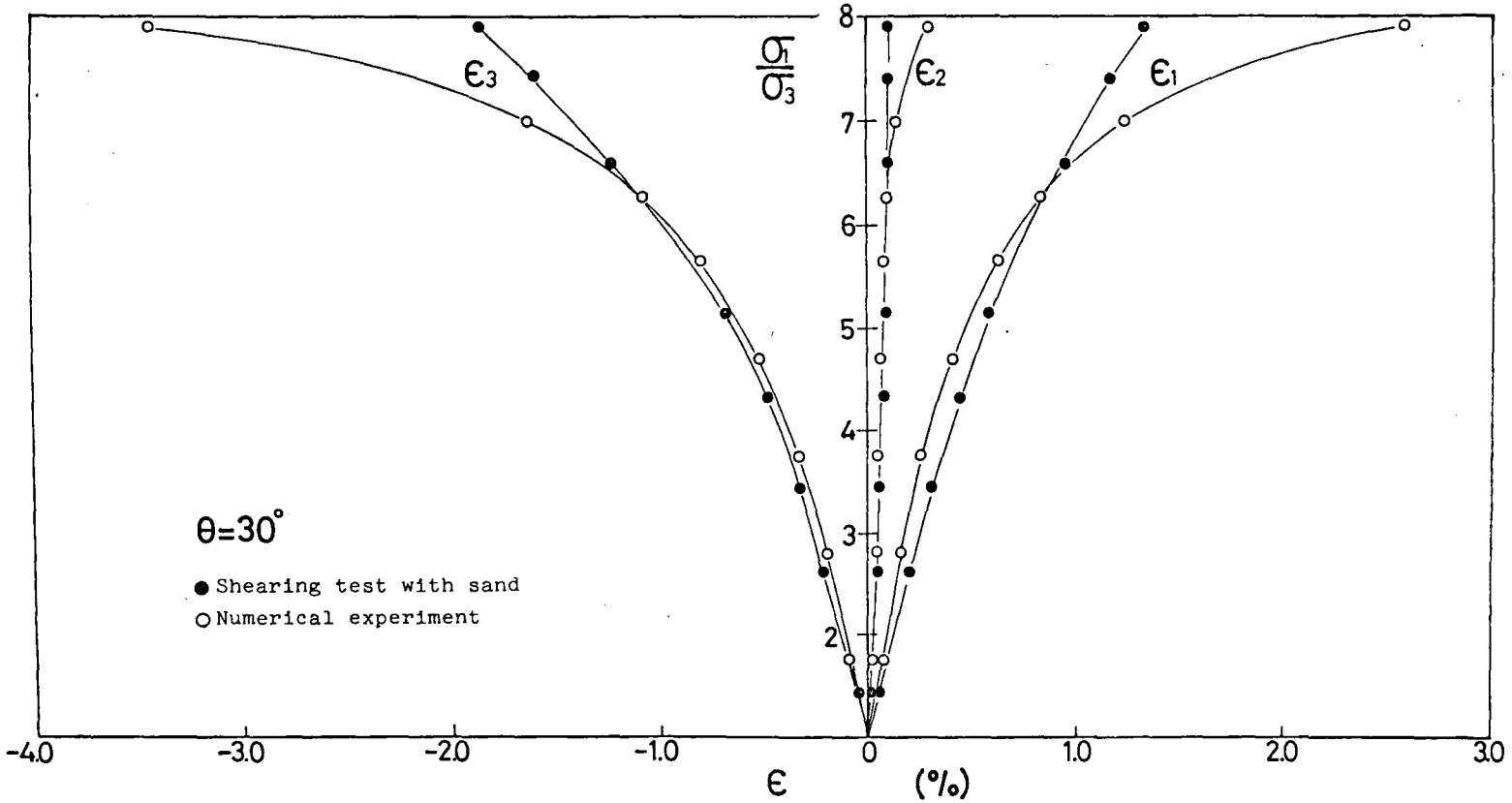

Fig.5.11(c) Stress-strain relations obtained by shearing test and numerical experiment under constant mean effective principal stress

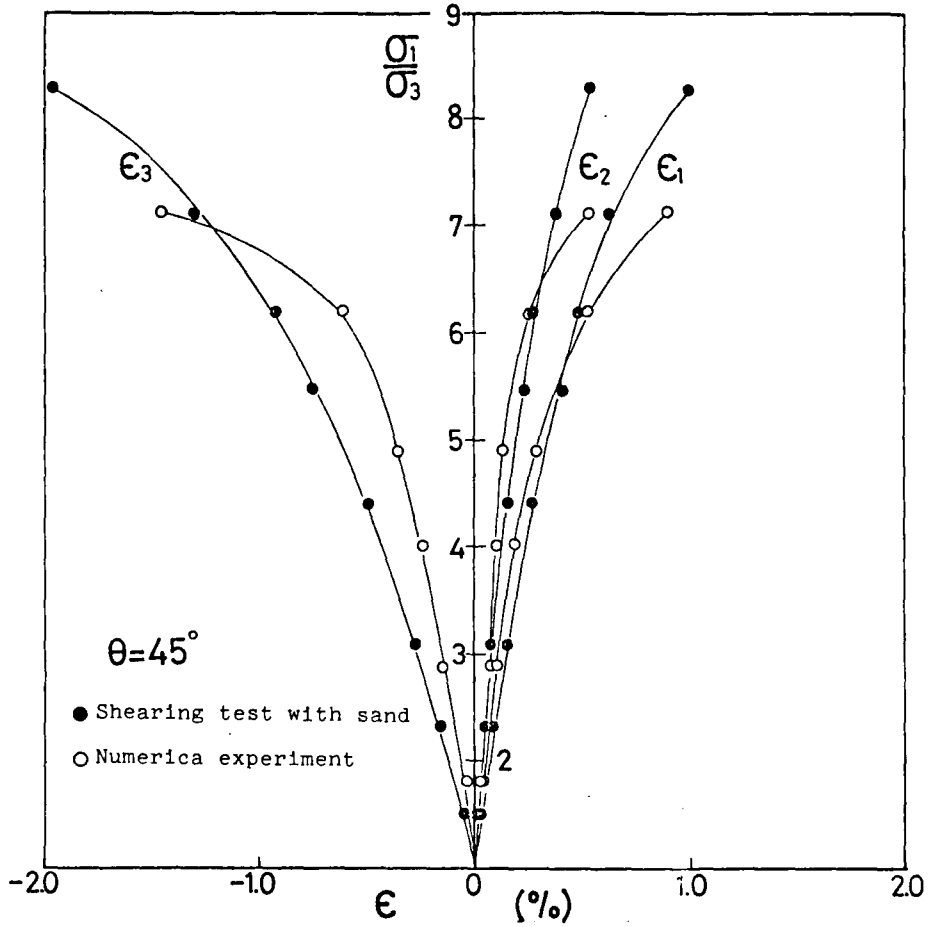

Fig.5.11(d) Stress-strain relations obtained by shearing test and numerical experiment under constant mean effective principal stress

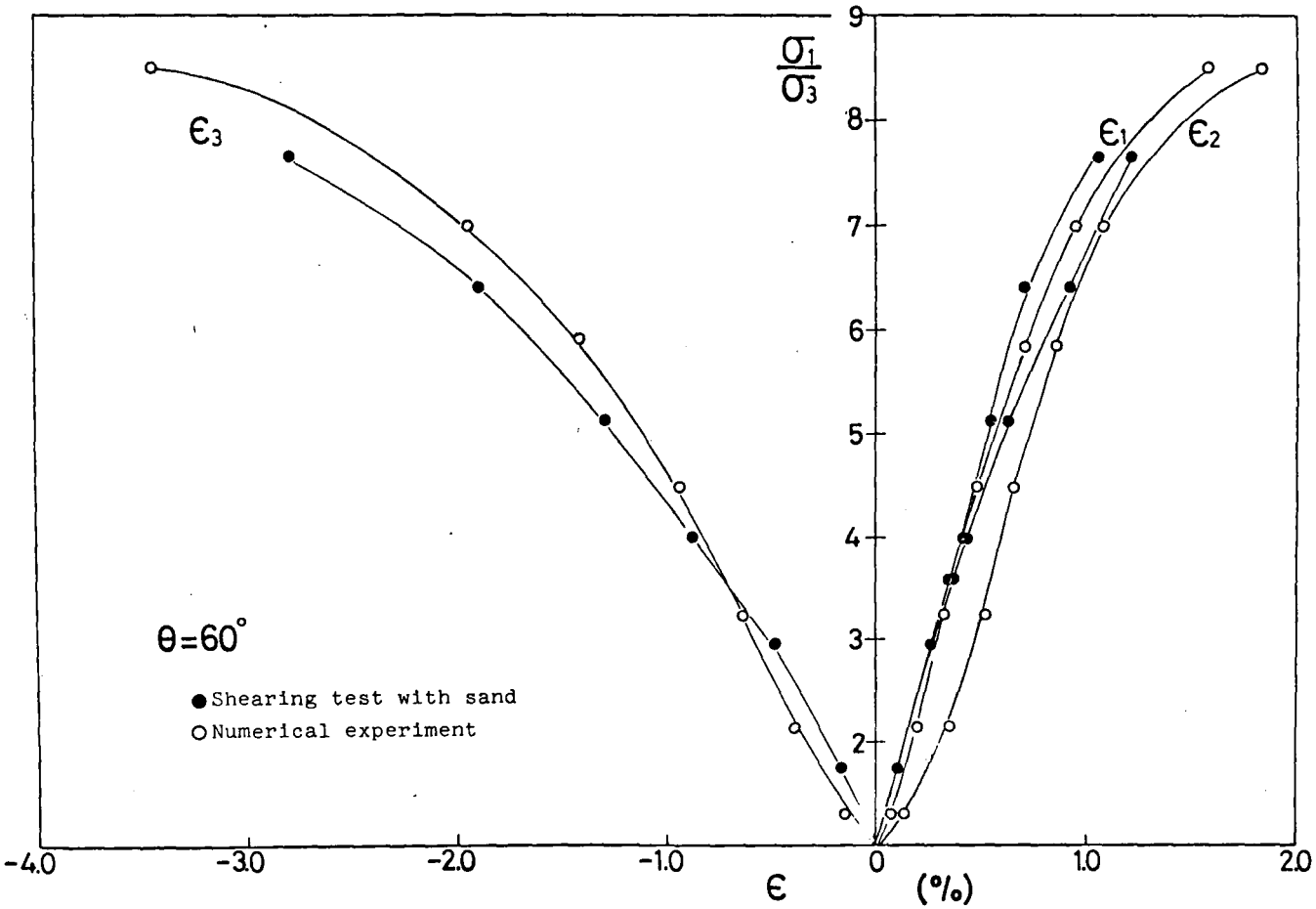

Fig.5.11(e) Stress-strain relations obtained by shearing test and numerical experiment under constant mean effective principal stress

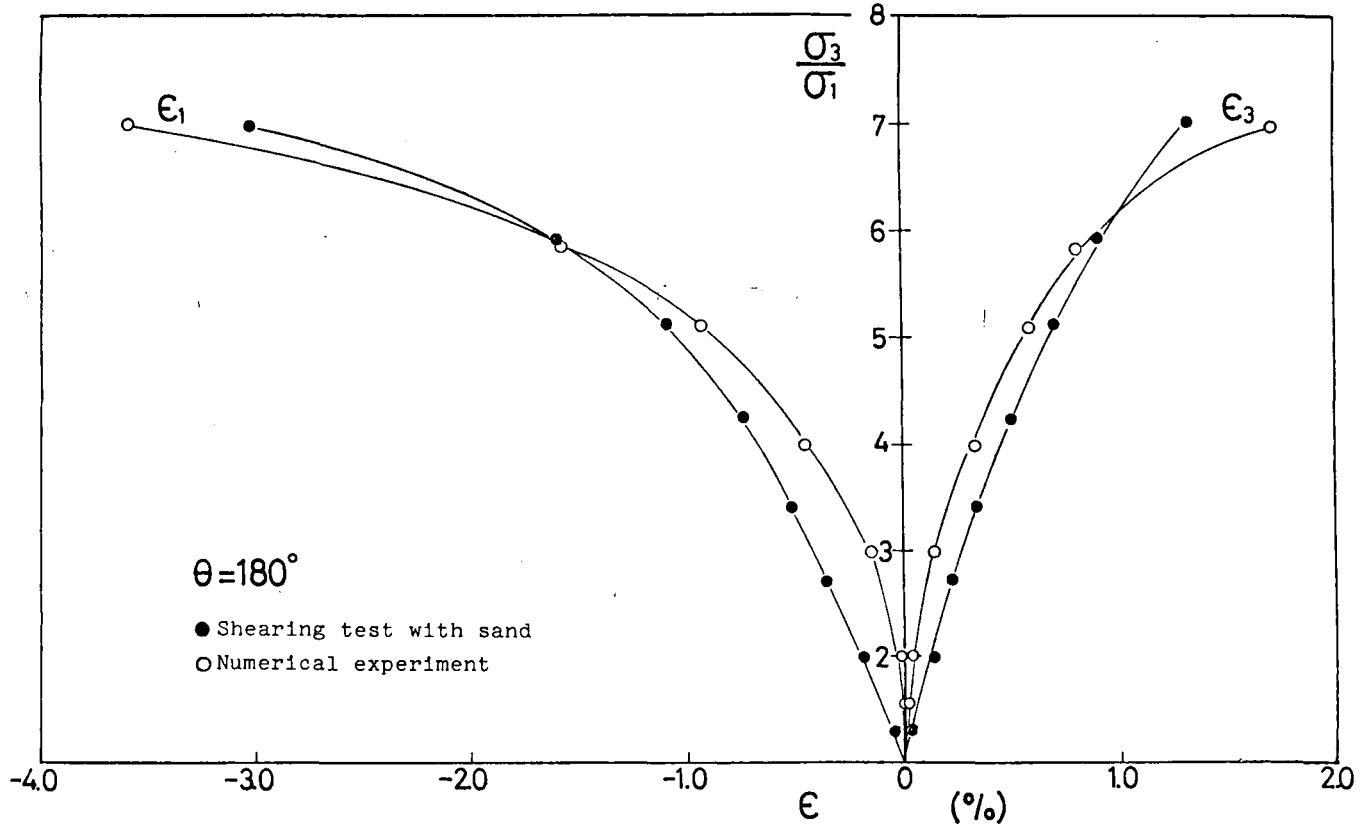

Fig.5.11(f) Stress-strain relations obtained by shearing test and numerical experiment under constant mean effective principal stress

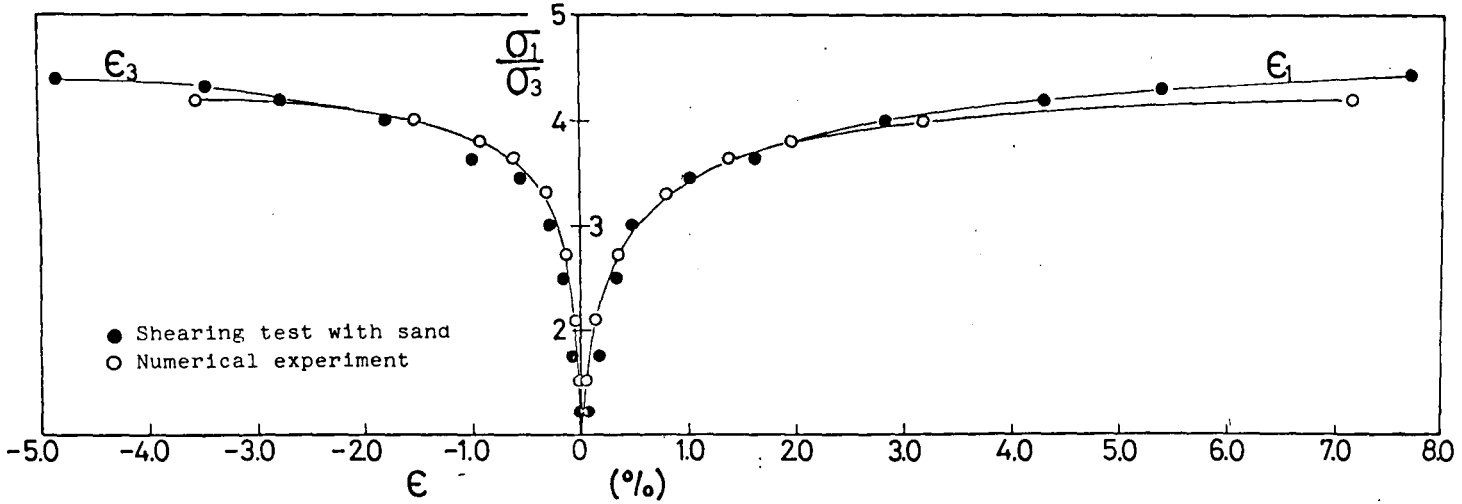

Fig.5.12(a) Stress-strain relations obtained by triaxial compression test for loose specimen and numerical experiment under constant mean effective principal stress

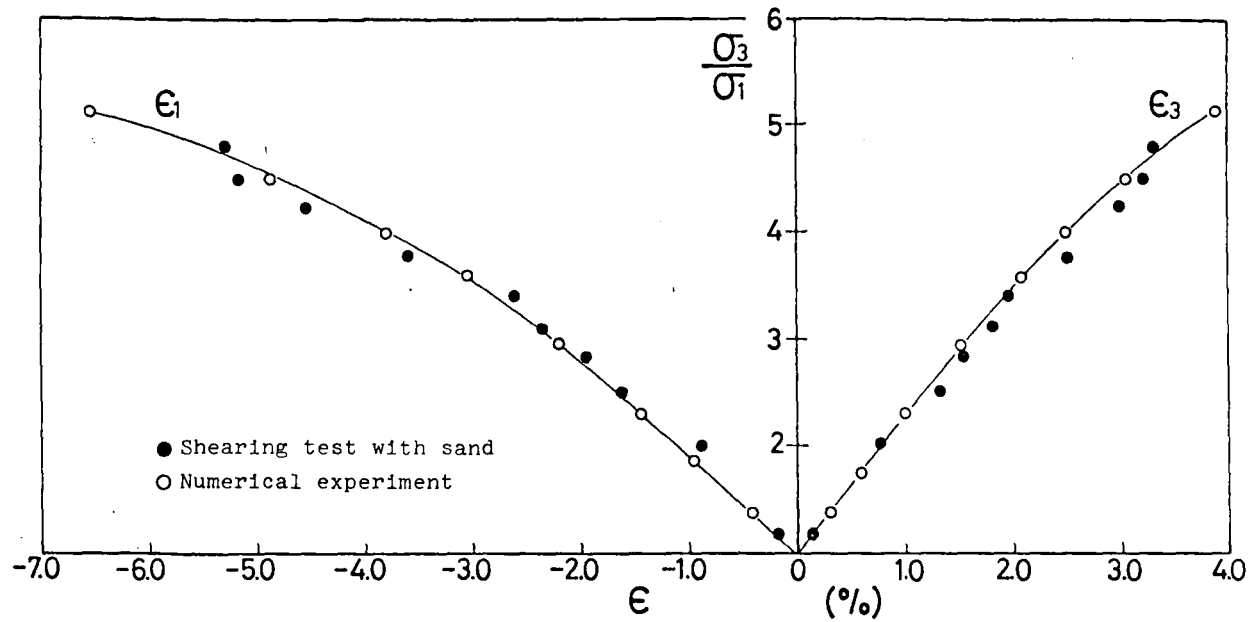

Fig.5.12(b) Stress-strain relations obtained by triaxial extension test for loose specimen and numerical experiment under constant mean effective principal stress

sion ($\theta = 180^\circ$) tests respectively. As the two-way repeated loading test results, Fig.5.13(a)-(b) show the stress-strain relations between the stress ratio τ/σ_m and the shear strain γ . The stresses, τ and σ_m , and the shear strain γ are defined as the following equations.

$$\tau = \sigma_1 - \sigma_3 \tag{5.2}$$

$$\sigma_m = \frac{1}{3}(\sigma_1 + \sigma_2 + \sigma_3) \tag{5.3}$$

$$\gamma = \epsilon_1 - \epsilon_3 \tag{5.4}$$

The specimen for these tests are subjected to the cyclic deviatoric stresses in both triaxial compression and extension sides. The positive sign of τ and γ in Eqs.(5.2) and (5.4) means the triaxial compression side.

Let's consider the observed slip plane at failure in order to verify the validity of the concept of the potential slip plane which is introduced in section 3.4. The slip planes can be generally observed after failures take place. The clear slip planes, however, cannot be observed from the out side of triaxial chamber for the tests under general three dimensional stress conditions because of using cubic specimens and the horizontal loading system. Thus, the angles of slip planes are measured after finishing tests. The angles between the normals to slip planes and the vertical axis are observed as approximately 65°-70° for the tests where the stress σ_1 in the direction of X_1-axis is the maximum principal stress, and as approximately 30° for the tests where the stresses σ_2 and σ_3 in the horizontal direction are the maximum principal stress. In section 3.4 it is introduced the concept of the potential slip plane and assumed that the potential slip plane finally

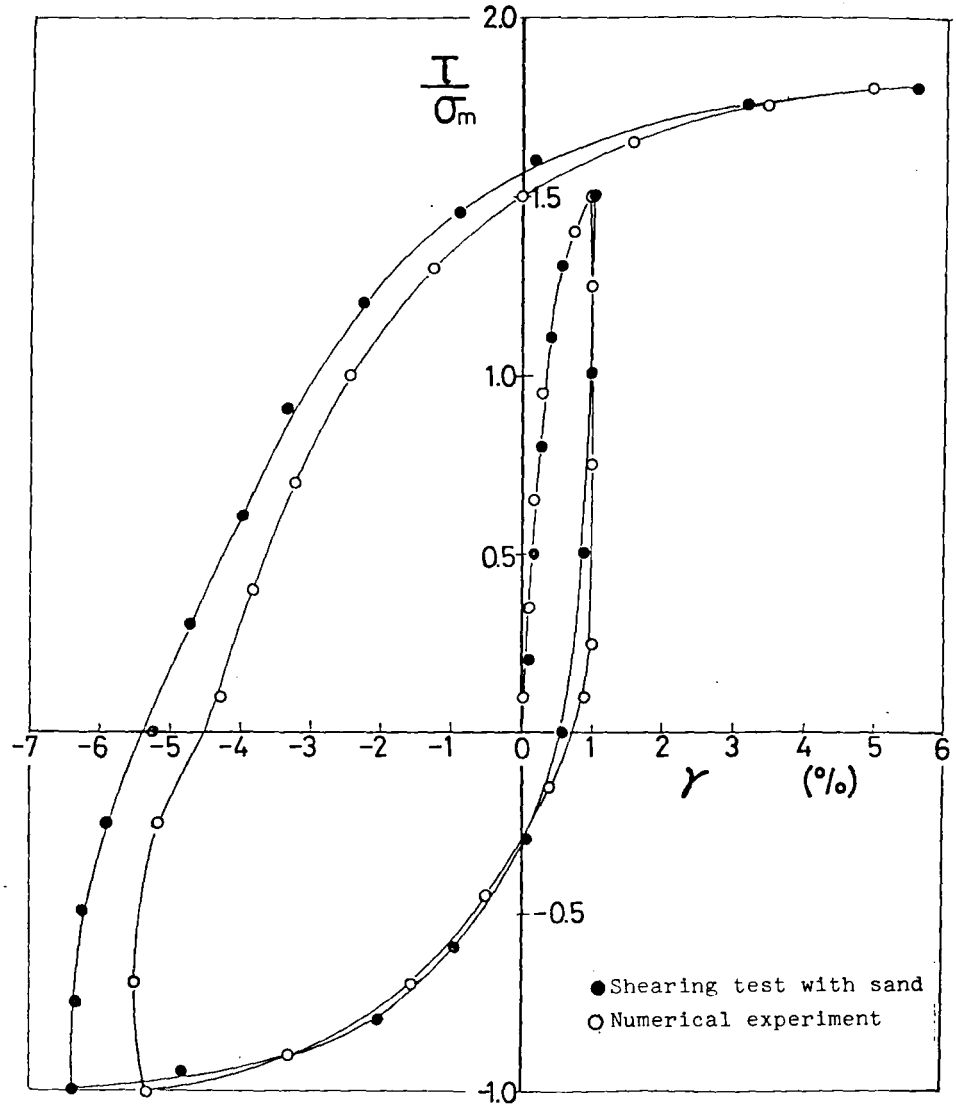

Fig.5.13(a) Stress-strain relations obtained by repeated loading test and numerical experiment under constant mean effective principal stress

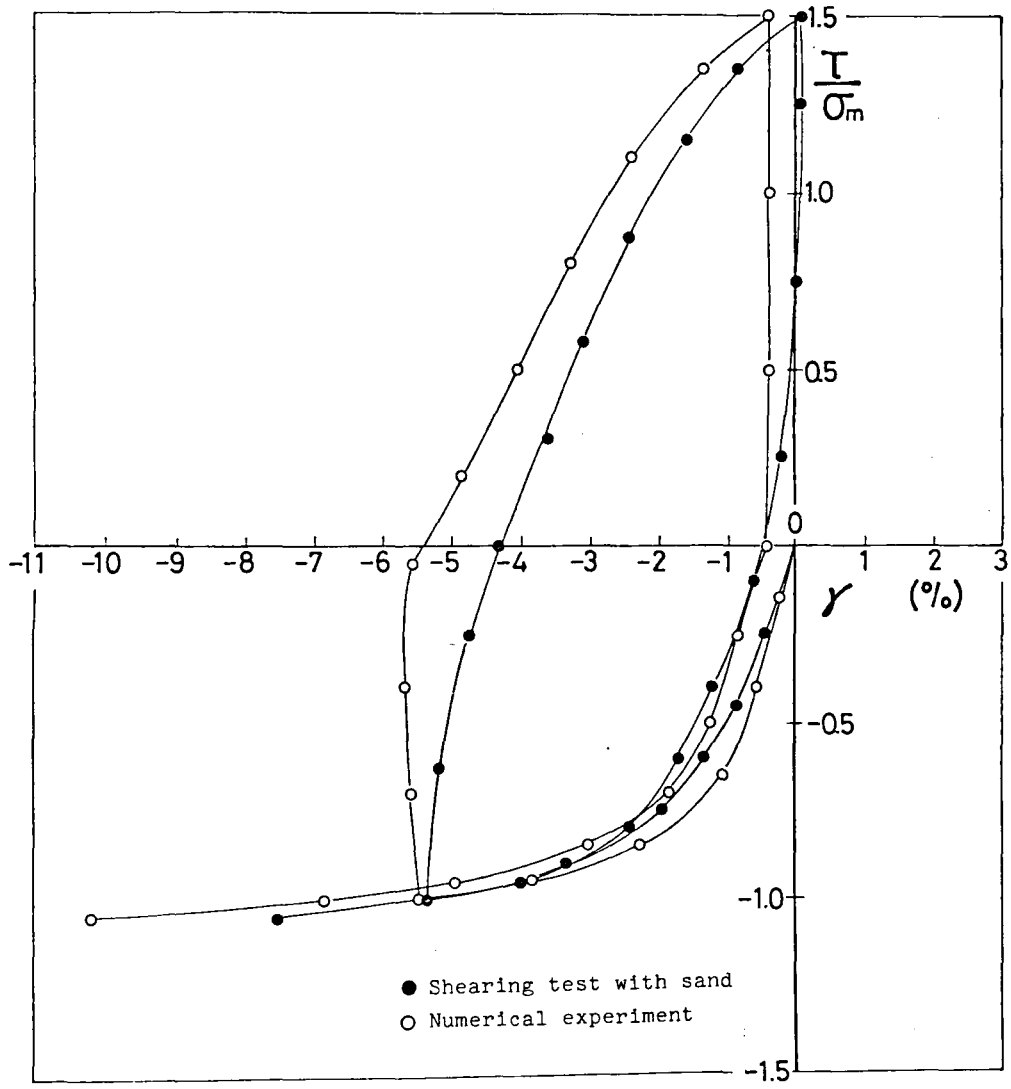

Fig.5.13(b) Stress-strain relations obtained by repeated loading test and numerical experiment under constant mean effective principal stress

coincides with the observed slip plane at failure. In order to verify this assumption, Table 5.3 is prepared for comparing the calculated angles of the potential slip planes at failure with the test results, although the accuracy of measured slip angles is less than those for the conventional axi-symmetric specimens and the slip planes for $\theta = 15°$ and $45°$ cannot be measured from the specimens. From Table 5.3 it is found that the angle β_1 formed between the normals to the potential slip plane and the vertical slip plane and the vertical axis are calculated as $71.2° - 73.5°$ for the tests where the stress σ_1 is the maximum principal stress and $28.1°$ for the conventional triaxial extension test. Comparing these results with the measured values, it is apparent that the concept of the potential slip plane is appropriate, while the measured slip planes are almost parallel to the direction of intermediate principal stress. This means that the failure is independent of the intermediate principal stress. Fig.5.14 illustrates the stress states at failurs given in Table 5.3 on the octahedral plane in the three principal stress space as well as the Mohr-Coulomb failure criterion. The exact stress states at failure cannot be determined in the experiments under general three dimensional stress conditions because the stress-controlled tests are adopted. It may be concluded, however, from Fig.5.14 that the failure criterion for Toyoura sand under three different principal stresses are a little apart from the Mohr-Coulomb criterion as already pointed out by previous researches[19),20),21)]. In investipating the failure criterion of particulate material, strain-controlled tests should be carried out under general three dimensional stress conditions.

In the next chapter, it will be discussed the deformation

Table 5.3 Angles of calculated potential slip planes and observed slip planes at failures of Toyoura sand

θ°	$\frac{\sigma_{max}}{\sigma_{min}}$	calculated value		observed value	
		β_1°	β_2°	β_1°	β_2°
0	5.66	73.5	47.3	68	90
15	7.04	72.2	60.0	—	—
30	7.89	72.2	65.9	70	90
45	8.31	73.4	70.8	—	—
60	7.68	71.2	71.2	70	90
180	7.00	28.1	70.5	30	90

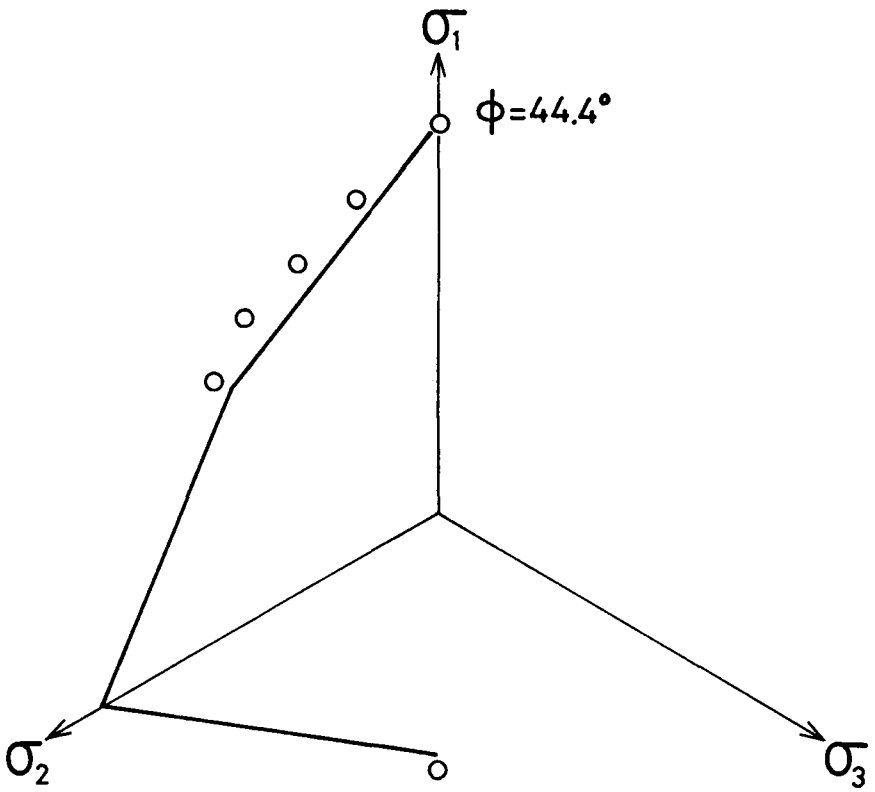

Fig.5.14 Stress states of Toyoura sand at failures on π-plane

mechanisms of particulate materials at the particle scale based on the obtained experimental results.

5.6 Conclusions

In this chapter the newly modified triaxial apparatus is introduced which can generate three different principal stresses. The considerations are conducted for errors caused by this apparatus and correction methods. Finally, the discussions are given for the shearing test results with Toyoura sand.

The main results obtained in this chapter may be summarized as follows.

(1) The true triaxial apparatus are largely divided into three types by means of loading systems, i.e., the hollow cylindrical apparatus, the modified triaxial apparatus and the box type triaxial apparatus. Furthermore, the latter two types are divided into two subgroups whether rigid plates or rubber bags are used as loading device. The true triaxial apparatus used in this study belongs to the group of modified triaxial apparatus. In this modified triaxial apparatus, the horizontal loading system with the rigid plates is installed in the conventional triaxial apparatus.

(2) The saturated Toyoura sand is used in these experiments. The void ratios are adjusted in order to obtain medium dense specimens (e=0.645-0.720) and loose specimens (e=0.801-0.810). All the tests are carried out under the drained condition. The strain-controlled method is adopted in the tests under constant confining pressures and the stress-controlled method is used in the tests under constant mean effective principal stress. The stresses, σ_1 and σ_3, and the strains, ϵ_1 and ϵ_v, are measured in the similar way to the conventional

triaxial tests. The horizontal stress, σ_2 , is loaded by the bellofram cylinder contained in the cell and the horizontal strain, ϵ_2 , are measured by slide calipers.

(3) In the experiments by the newly modified triaxial apparatus the following errors are considered and corrected, i.e., the non-uniformity of stress and strain distribution in the specimen due to the end restraint effects between specimen and cap or pedestal, the errors of vertical force due to the friction between rod and its guide, the errors due to membrane misfits, and the errors due to the horizontal loading system. The validity of these corrections is shown by the conventional triaxial compression test results with the horizontal loading system in the newly modified triaxial apparatus.

(4) The shearing tests with Toyoura sand are carried out under the following stress conditions, i.e., the constant confining pressures and the constant mean effective stress with the radial stress paths on π-plane. One-way and two-way repeated loading tests are also performed under these stress conditions. From the test results it is shown that the stress-strain relations for the particulate materials such as sands depend on void ratios and stress paths. The validity of the concept of the potential slip plane is discussed by using the angles of slip planes observed at failures.

References for Chapter 5

1) Adachi, T. and Kitamura, R.: Modified Triaxial Apparatus, Proc. 24th Symposium of JSSMFE, 1979, pp.137-142,(in Japanese).

2) Akai, K., Adachi, T. and Tabusi, N.: Air Pressure Controlled Triaxial Testing Systems and their Applications, Part 1, Tsuchi-to-Kiso, JSSMFE, Vol.23, No.3, 1975, pp.39-45, (in Japanese).

3) Lade, P.V. and Duncan, J.M.: Cubical Triaxial Tests on Cohesionless Soil, Proc. ASCE, Vol.99, No.SM10, 1973, pp.793-812.

4) Rowe, P.W. and Barden, L.: Importance of Free Ends in Triaxial Testing, Proc. ASCE, Vol.90, No.SM1, 1964, pp.1-27.

5) Barden, L. and McDermott, J.W.: Use of Free Ends in Triaxial Testing of Clays, Proc. ASCE, Vol.91, No.SM6, 1965, pp.1-23

6) Bishop, A.W. and Green, G.E.: The Influence of End Restraint on the Compression Strength of a Cohesionless Soil, Géotechnique, Vol.15, No.3, 1965, pp.243-266.

7) Lee,K.L.: End Restraint Effects on Undrained Static Triaxial Strength of Sand, Proc. ASCE, Vol.104, No.GT6, 1978, pp.687-704.

8) Lee, K.L. and Vernese, F.J.: End Restraint Effects on Cyclic Triaxial Strength of Sand, Proc. ASCE, Vol.104, No.GT6, 1978, pp.705-719.

9) Arthur, J.R.F. and Dalili, A.: On the Lubrication of Rubber Surface, Géotechnique, Vol.29, No.1, 1979, pp.96-98.

10) Moroto, Y.: Recoverable Behaviour of Sand, Soils and Foundations, Vol.12, No.3, 1972, pp.65-74, (in Japanese).

11) Raju, V.S. and Sadasivan, S.K.: Membrane Penetration in Triaxial Tests on Sands, Proc. ASCE, Vol.100, No.GT4, 1974, pp.482-489.

12) Kiekbusch, M. and Schuppener, B.: Membrane Penetration and its Effect on Pore Pressures, Proc. ASCE, Vol.103, No.GT11, 1977, pp.1267-1279.

13) Lade, P.V. and Hernandez, S.B.: Membrane Penetration Effects in Undrained Tests, Proc. ASCE, Vol.103, No.GT2, 1977, pp.109-125.

14) 'Soil Testing Methods' editted by JSSMFE, 1969, p.417.

15) Henkel, D.J. and Gilbert, G.D.: The Effect of the Rubber Membrane on the Measured Triaxial Compression Strength of Clay Samples, Géotechnique, Vol.3, No.1, 1952, pp.20-29.

16) Chandler, R.J.: The Measurement of Residual Strength in Triaxial Compression, Géotechnique, Vol.16, No.3, 1966, pp.181-186.

17) La Rochelle, P.: Membrane, Drain and Area Correction in Triaxial Test on Soil Sample Failing along a Singler Shear Plane, Proc. 3rd Panam. Conf. Soil Mech., Vol.1, 1967, pp.273-292.

18) Pachakis, M.D.: The Influence of the Membrane Restraint on the Measured Strength of a Soil Sample Failing along a Single Shear Plane in the Triaxial Test, Géotechnique, Vol.26, No.1, 1976, pp.226-230.

19) Shibata, T. and Karube, D.: Influence of the Variation of the Intermediate Principal Stress on the Mechanical Properties of Normally Consolidated Clays, Proc. 6th Int.Conf. SMFE, Vol.1, 1965, pp.359-363.

20) Sutherland, H.B. and Mesdary, M.S.: The Influence of the Intermediate Principal Stress on the Strength of Sand, Proc. 7th Int. Conf. SMFE, Vol.1, 1969, pp.391-399.

21) Ramamurthy, T. and Rawat, P.C.: Shear Strength of Sand under General Stress System, Proc. 8th Int.Conf. SMFE, Vol.1.2, 1973, pp.339-342.

CHAPTER 6 NUMERICAL EXPERIMENTS[1)]

6.1 Introduction

In chapters 3 and 4 a mechanical model for particulate material has been theoretically derived by assuming that the motions of particles are the Markov precess. In the derivation the following concepts have been used such as the potential barrier, the potential slip plane, and the ratios of the disappearance and the appearance.

Fig.6.1 shows the flow chart how to obtain the stress-strain relation by using the proposed model. According to Fig.6.1, if the energy transferred into the particulate material due to the change in stress state is known ((1) in Fig.6.1), the coefficients A_i and B_{ci} in the basic equation of Markov process are determined by using the concepts of the potential barrier and the potential slip plane ((2) and (3) in Fig.6.1). Furthermore, the change in the probability density function of contact angles due to the change in stress state is obtained by numerically analysing the basic equation of Markov process ((4) in Fig.6.1). On the other hand, the ratios of the disappearance and the appearance of contact points due to the discontinuous motions of particles are also estimated by using the concepts of the potential barrier and the potential slip plane ((2) and (5) in Fig.6.1). Finally, the strains of particulate material are derived by using the probability density function of contact angles and the ratios of the disappearance and the appearance ((6) in Fig.6.1).

In this chapter the numerical experiments are carried out for the proposed model in accordance with the flow chart in Fig.6.1 in order to verify the validity of proposed model. In the numerical

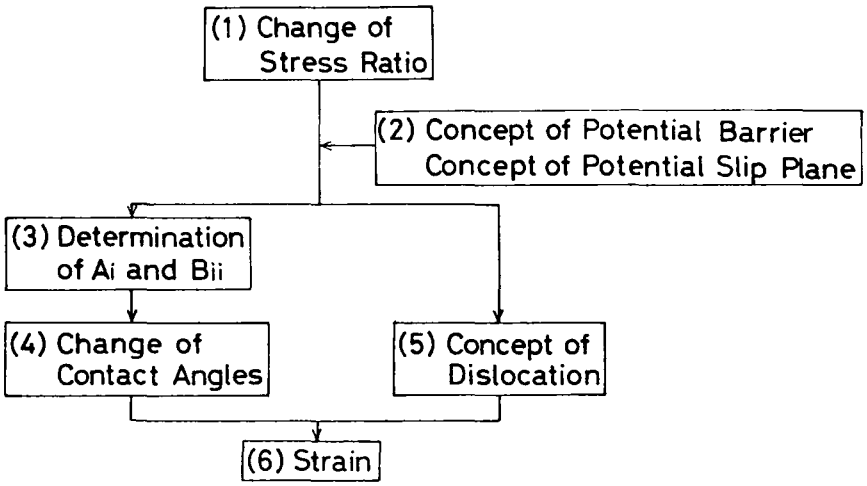

Fig.6.1 Flow chart of proposed mechanical model

experiments the basic equation of Markov process is numerically solved by using the finite difference method (see Appendix 6.1). Before the performance of numerical experiments, the values of model parameters are determined based on the results obtained by the experiments with Toyoura sand given in chapter 5. The deformation mechanisms of particulate material are investigated at the particle scale by comparing the stress-strain relations obtained by numerical experiments with those obtained by the shearing tests under general three dimensional stress conditions.

6.2 Model Parameters used in the Proposed Model

6.2.1 Energy transferred into the specimen

In this subsection we discuss the determination of work done in the particulate material ((1) in Fig.6.1). In the deformation process of particulate material the energy is transferred into or out the specimen due to the change in external actions. The amount of transferred mechanical energy is calculated by the following equation.

$$\Delta W = \sigma_1 \cdot d\epsilon_1 + \sigma_2 \cdot d\epsilon_2 + \sigma_3 \cdot d\epsilon_3 \qquad (6.1)$$

where ΔW ; increment of mechanical energy transferred due external actions per unit volume,

σ_1 , σ_2 and σ_3 ; principal stresses,

$d\epsilon_1$, $d\epsilon_2$ and $d\epsilon_3$; principal strain encrements.

The total energy W during the deformation process is obtained by summing up each energy increment calculated by Eq.(6.1)

The relations between the total energy for dense or loose specimens, W , and the stress ratio, τ/σ_N , defined in Eq.(3.18) are schematically shown in Fig.6.2 for the monotonous loading

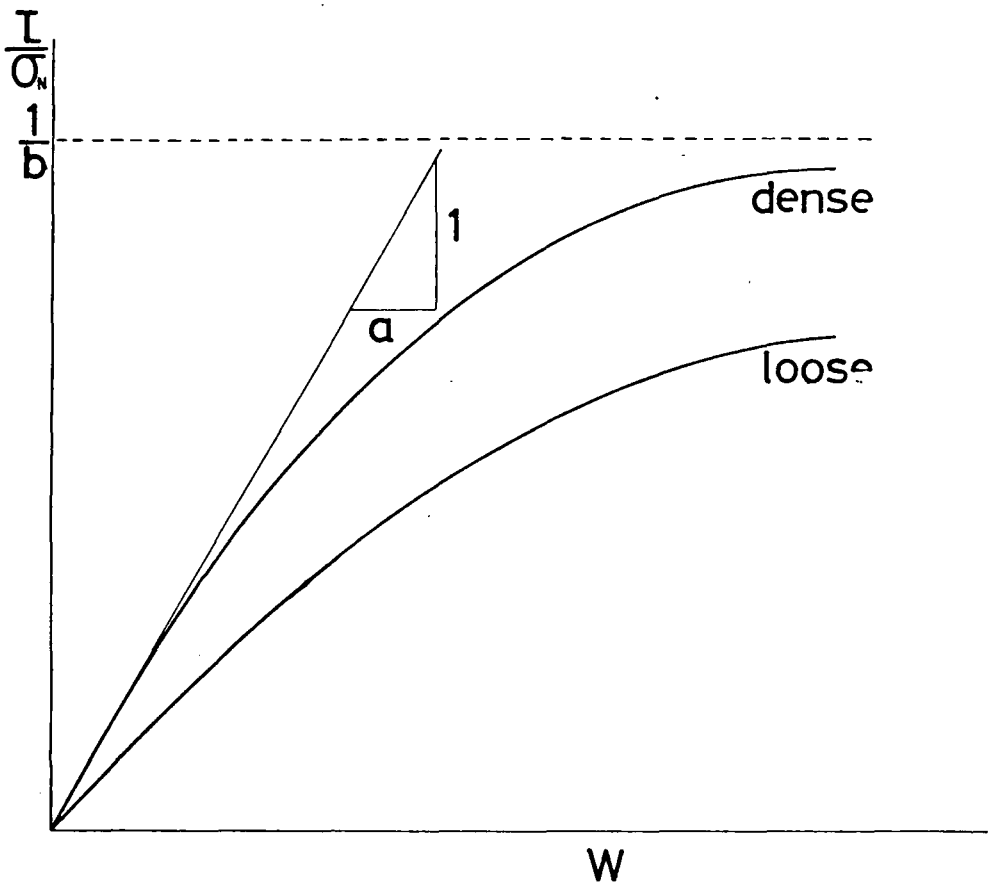

Fig.6.2 Schematical relations between τ/σ_N and W for dense and loose specimens

processes of shearing tests. It has been found that these relations can be approximately represented by hyperbolic curves in each of which the initial slope and the asymptote are $1/a$ and $1/b$ respectively[2]. $W/(\tau/\sigma_N) \sim W$ relations obtained from the experimental results are shown in Figs.6.3, 6.4, 6.5, 6.6 and 6.7. Figs.6.3 and 6.4 show the relations obtained by the monotonous loading test results with medium dense specimens under the constant confining pressures and under the constant mean effective principal stress respectively. Fig.6.5 shows the results obtained by the first and the third loading processes for the one-way repeated loading tests under the constant confining pressures (see Fig.5.6(a)). Fig.6.6 shows the relations obtained by the first, second and third loading processes for the two-way repeated loading tests under the constant mean effective principal stress (see Fig.5.6(b)). Fig.6.7 is the results of compression and extension tests for the loose and the dense specimens. It is found that the parameters a and b for the loose specimen are larger than those for the dense specimen which corresponds to the difference of the relations for the dense and the loose specimens shown in Fig.6.2. In Figs.6.3-6.7 it is found that $W/(\tau/\sigma_N)$ is linearly related to W, i.e., the following hyperbolic equation is empirically derived between the total energy W and the stress ratio τ/σ_N for such tests.

$$\tau/\sigma_N = \frac{W}{a + b \cdot W} \tag{6.2}$$

where a ; reciprocal number of initial tangential slope for $\tau/\sigma_N \sim W$ relation as shown in Fig.6.2 and intercept value of the vertical axis for $W/(\tau/\sigma_N) \sim W$ relation in Figs. 6.3-6.7.

b ; reciprocal number of asymptotic value for $\tau/\sigma_N \sim W$ relation as shown in Fig.6.2 and slope for $W/(\tau/\sigma_N) \sim W$ relation in Figs.6.3-6.7.

It is found that the parameters a and b in Eq.(6.2) may be independent of the stress paths from Fig.6.4 as far as the loading force monotonously increases in the shearing test. It is also found from Fig.6.5 that the relation between τ/σ_N and W is uniquely determined by the hyperbolic equation in the virgin loading processes of one-way repeated loading test. It may be apparent from Fig.6.6 that the hyperbolic relation between τ/σ_N and W is applicable not only to the first loading but also the second and third loadings in the two-way repeated loading test, in which the parameter b is almost same for all the loading process though the parameter a varies a little. Furthermore, it may be concluded from Figs.6.3-6.7 that the parameters a and b in Eq.(6.2) generally depend on the initial void ratio, confining pressure, fabric of particulate material and physico-chemical properties at the particle surface, but are independent of the shearing stress paths as far as the loading process is monotonous.

The relations between τ/σ_N and W during the unloading and reloading processes of repeated loading tests are plotted by the logarithmic scale in Figs.6.8 and 6.9. Fig.6.8 shows the relation between τ/σ_N and W in the first unloading and second loading processes for the one-way repeated loading tests under the constant confining pressures (see Fig.5.6(a)). Fig.6.9 shows the relation in the first and second unloading processes for the two-way repeated loading tests under the constant mean effective principal stress (see Fig.5.6(b)). From Figs.6.8 and 6.9 the relation between τ/σ_N and W is approximated by the following equation.

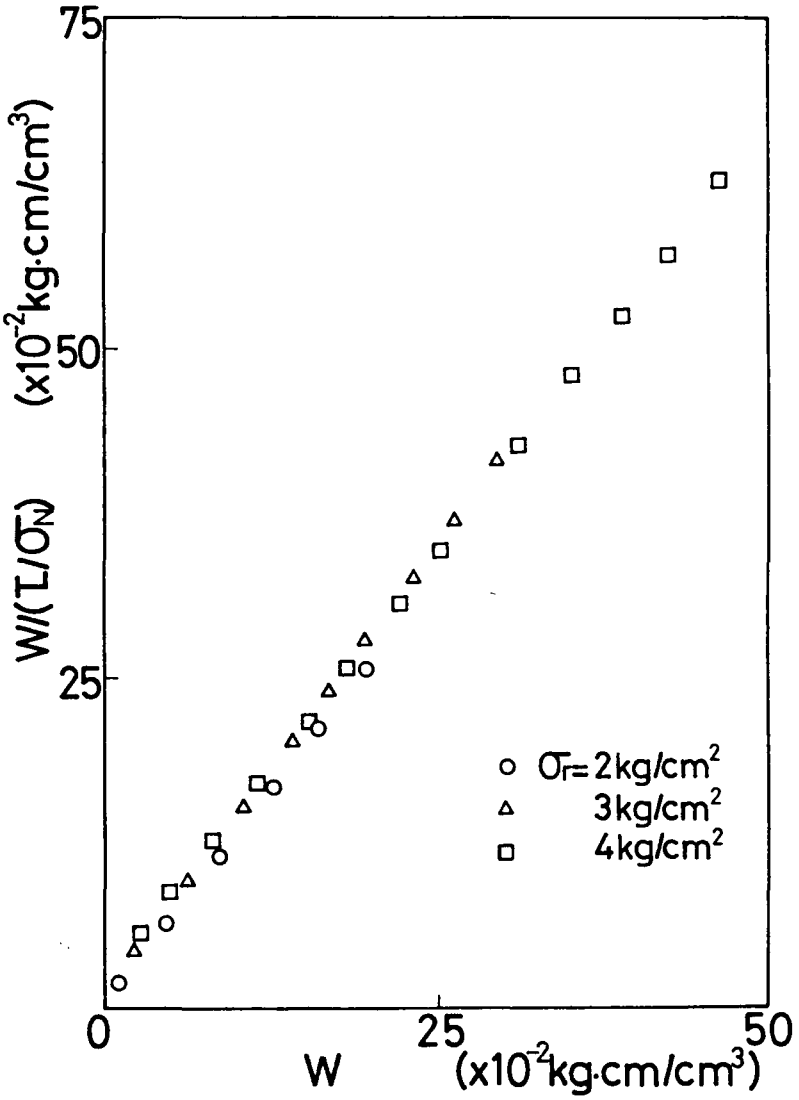

Fig.6.3 Relations between $W/(\tau/\sigma_N)$ and W under constant confining pressures

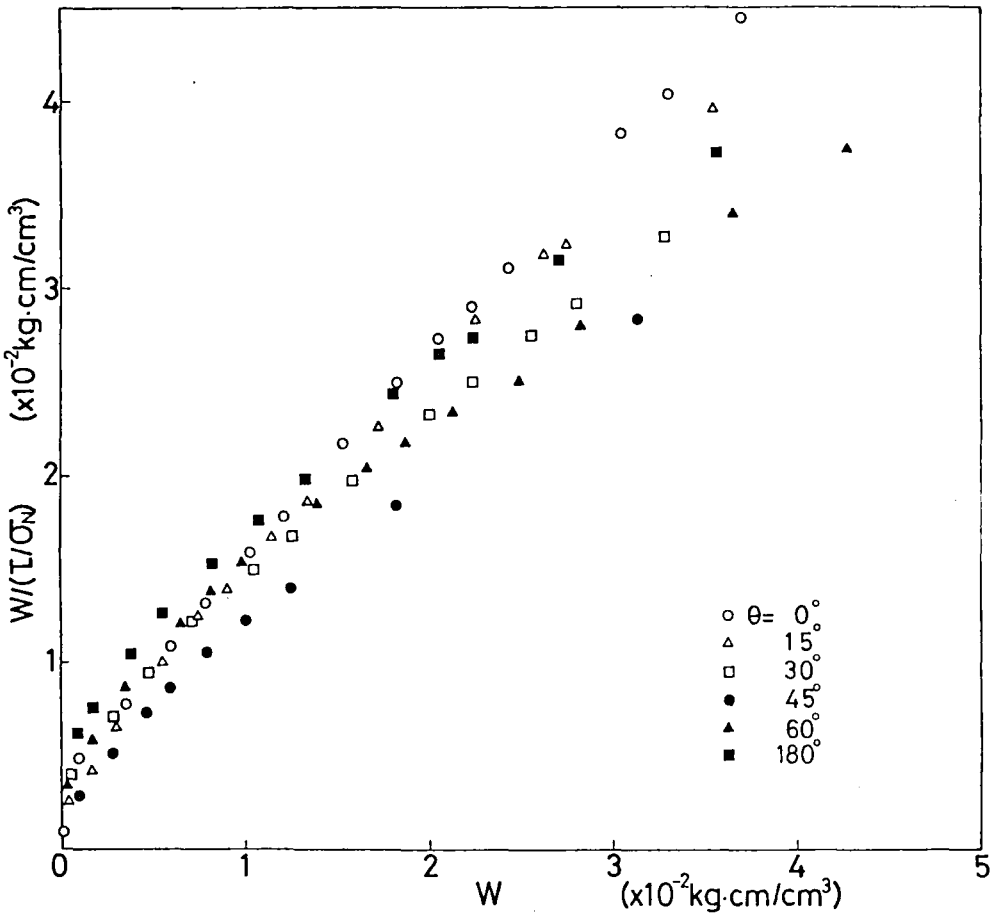

Fig.6.4 Relations between $W/(\tau/\sigma_N)$ and W under constant mean effective principal stress

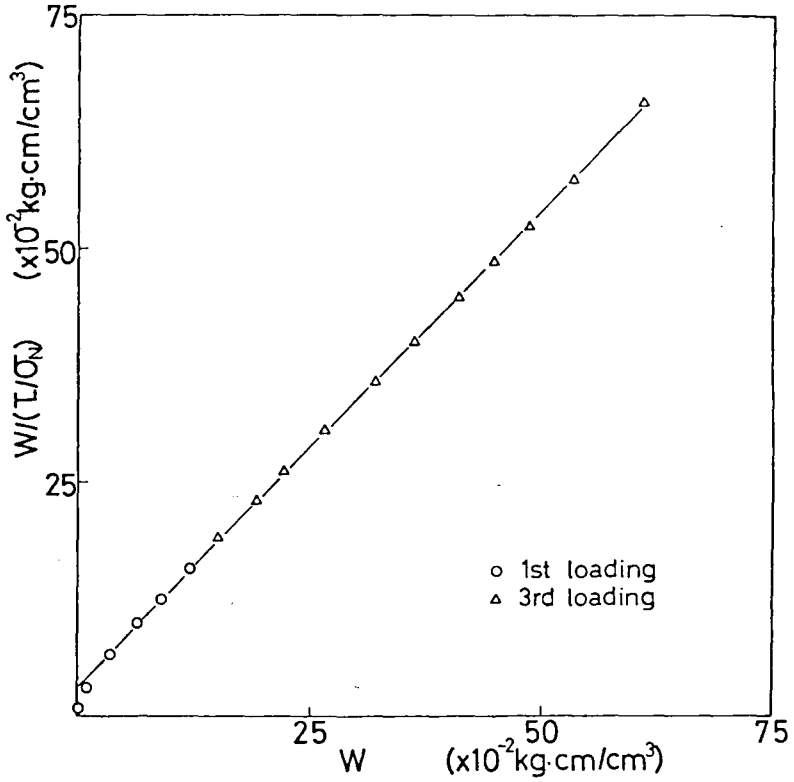

Fig.6.5(a) Relations between $W/(\tau/\sigma_N)$ and W in one-way repeated loading test under confining pressure, $\sigma_r = 3$ kg/cm^2

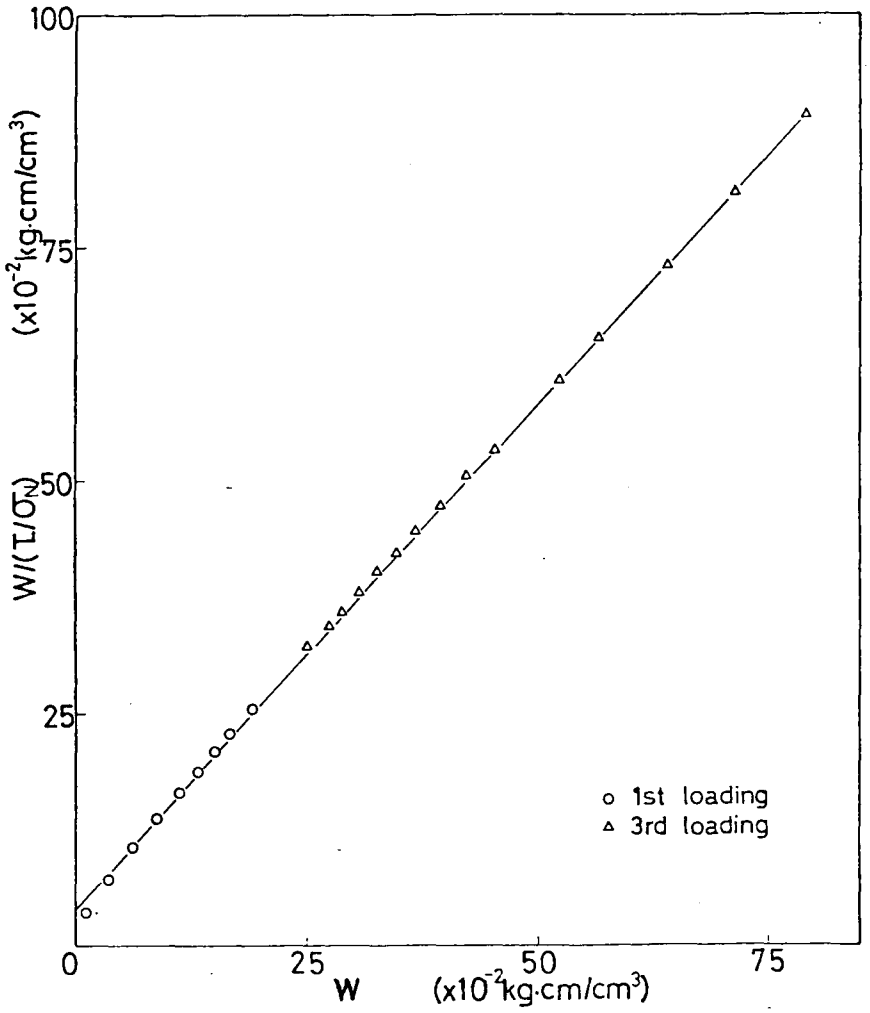

Fig.6.5(b) Relations between $W/(\tau/\sigma_N)$ and W in one-way repeated loading test under confining pressure, $\sigma_r = 4$ kg/cm^2

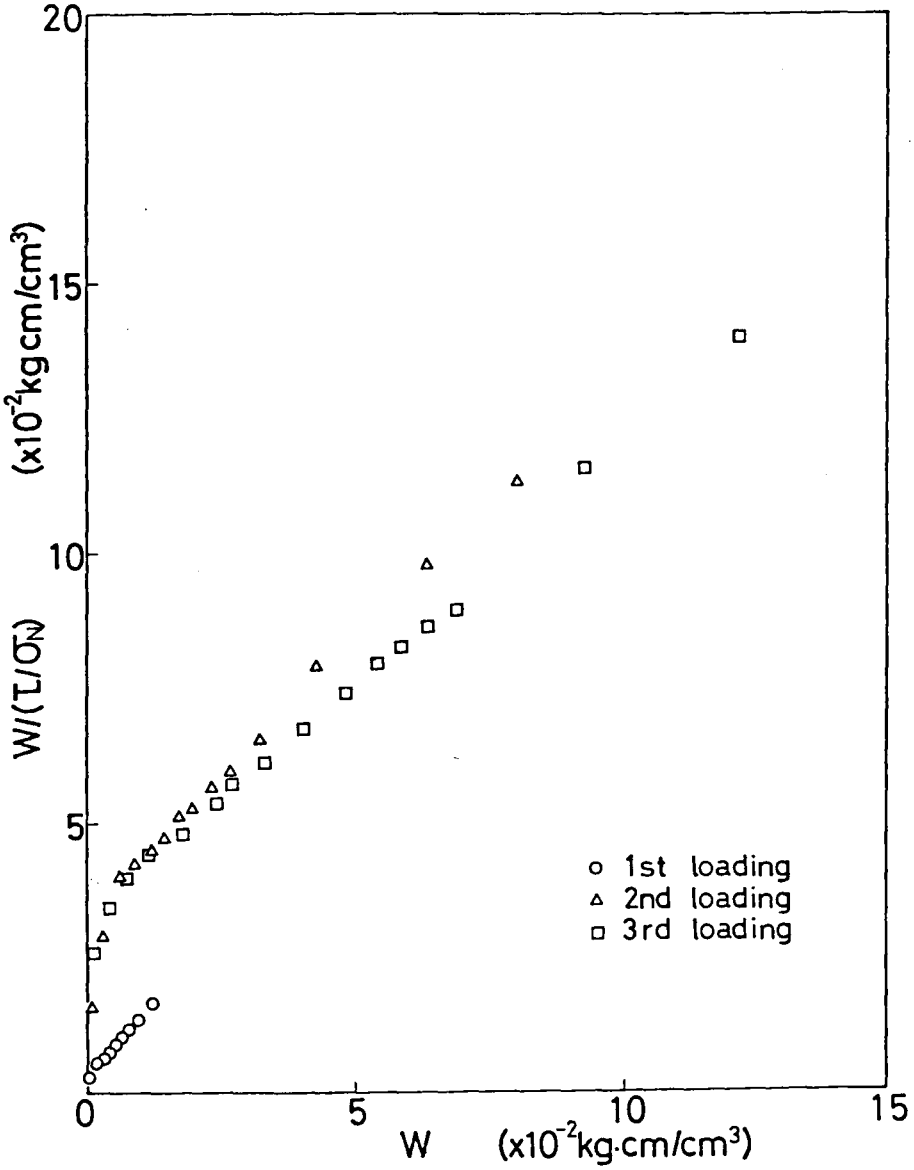

Fig.6.6(a) Relations between $W/(\tau/\sigma_N)$ and W in two-way repeated loading test along the stress path, $\theta = 0^\circ \rightarrow 180^\circ \rightarrow 0^\circ$

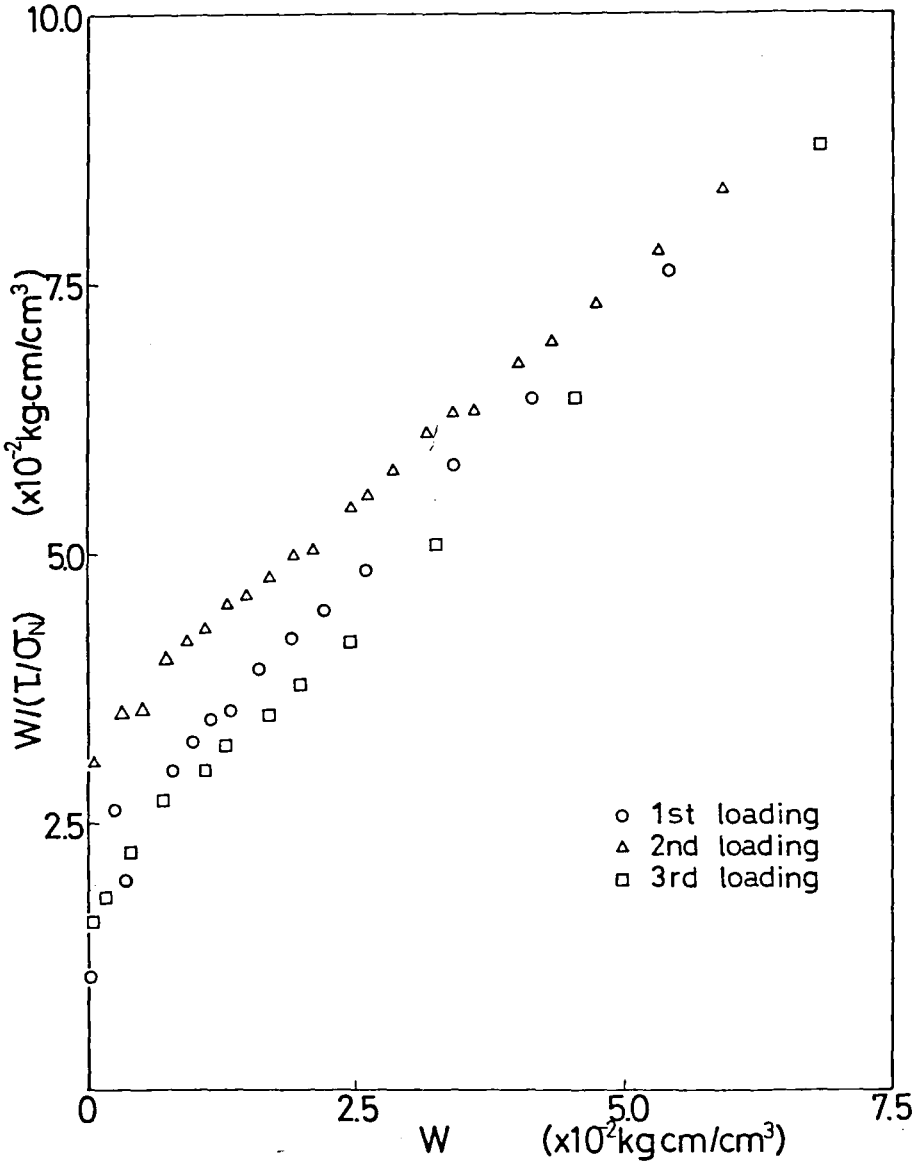

Fig.6.6(b) Relations between $\overline{W}/(\tau/\sigma_N)$ and $\overline{W}$ in two-way repeated loading test along the stress path, $\theta = 180° \rightarrow 0° \rightarrow 180°$

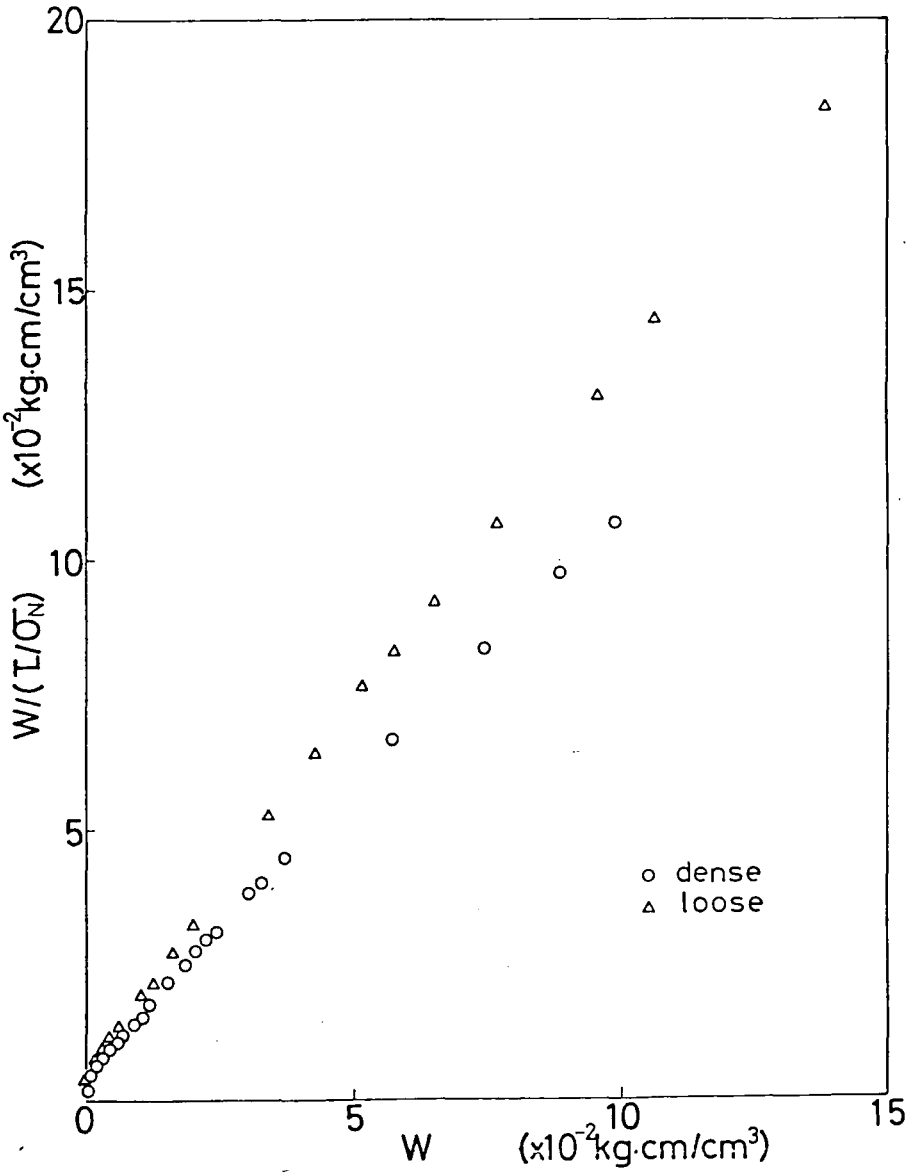

Fig.6.7(a) Relations between $\overline{W}/(\tau/\sigma_N)$ and $\overline{W}$ for triaxial compression tests with dense and loose specimen

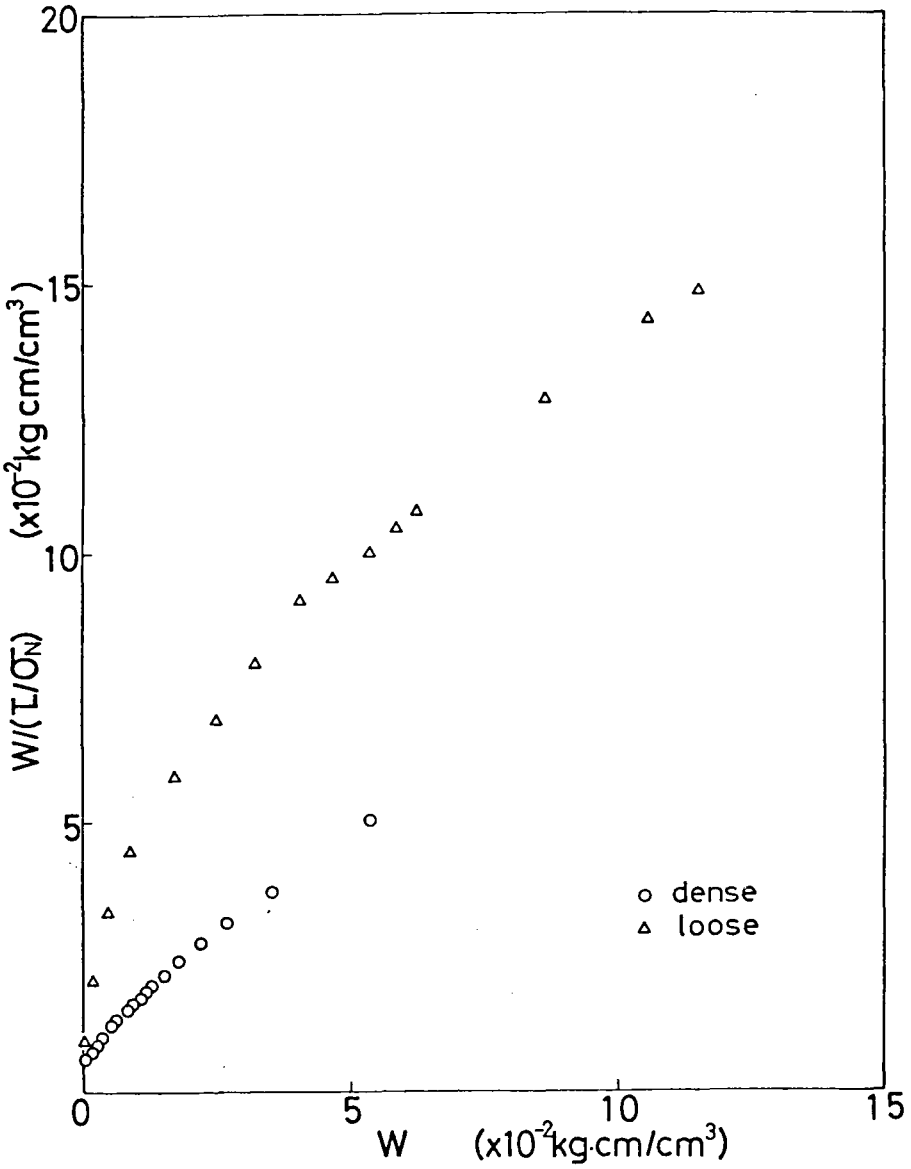

Fig.6.7(b) Relations between $\overline{W}/(\tau/\sigma_N)$ and $\overline{W}$ for tri-axial extension tests with dense and loose specimen

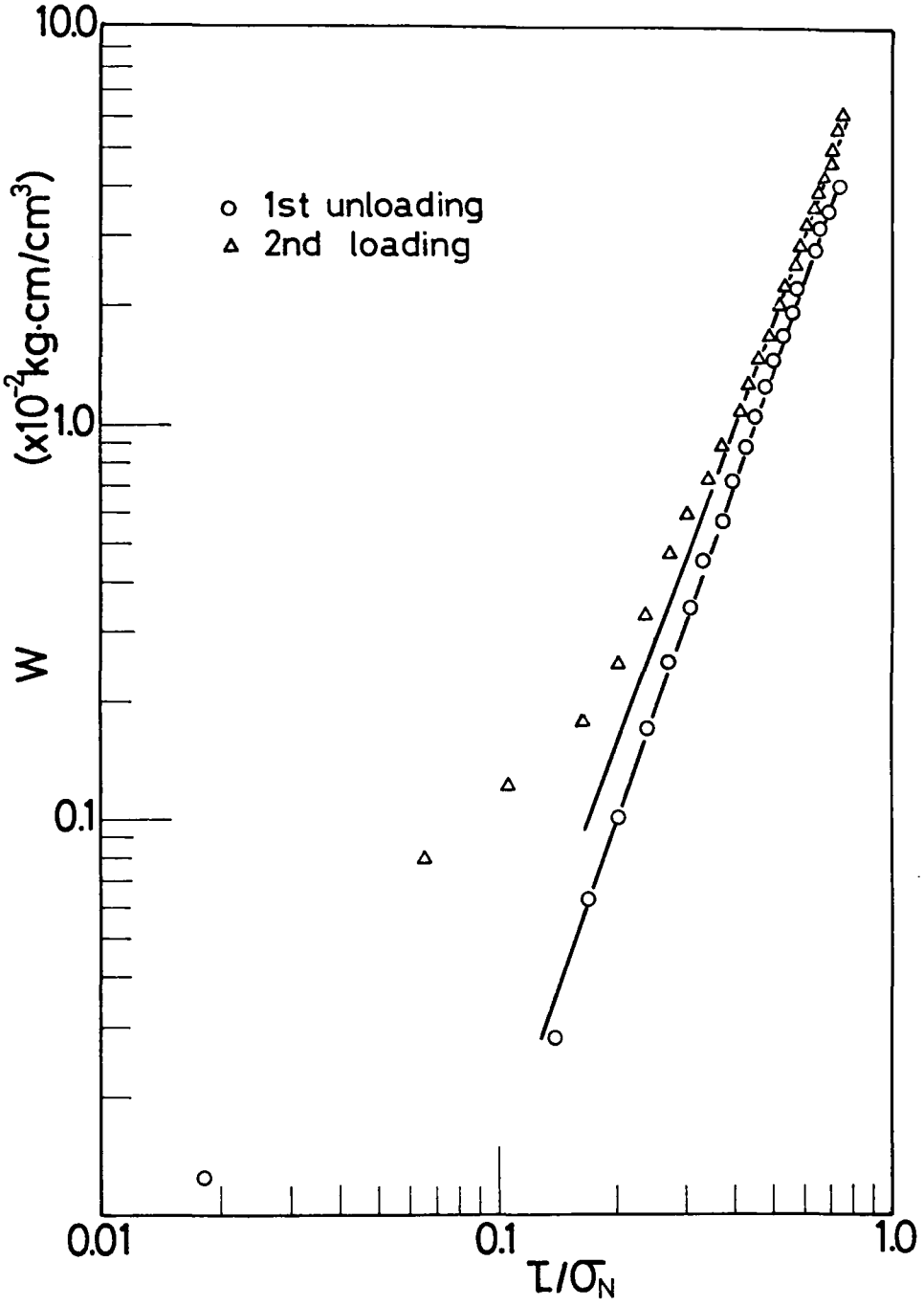

Fig.6.8(a) Relations between W and τ/σ_N for constant confining pressure test, $\sigma_r = 3\,kg/cm^2$

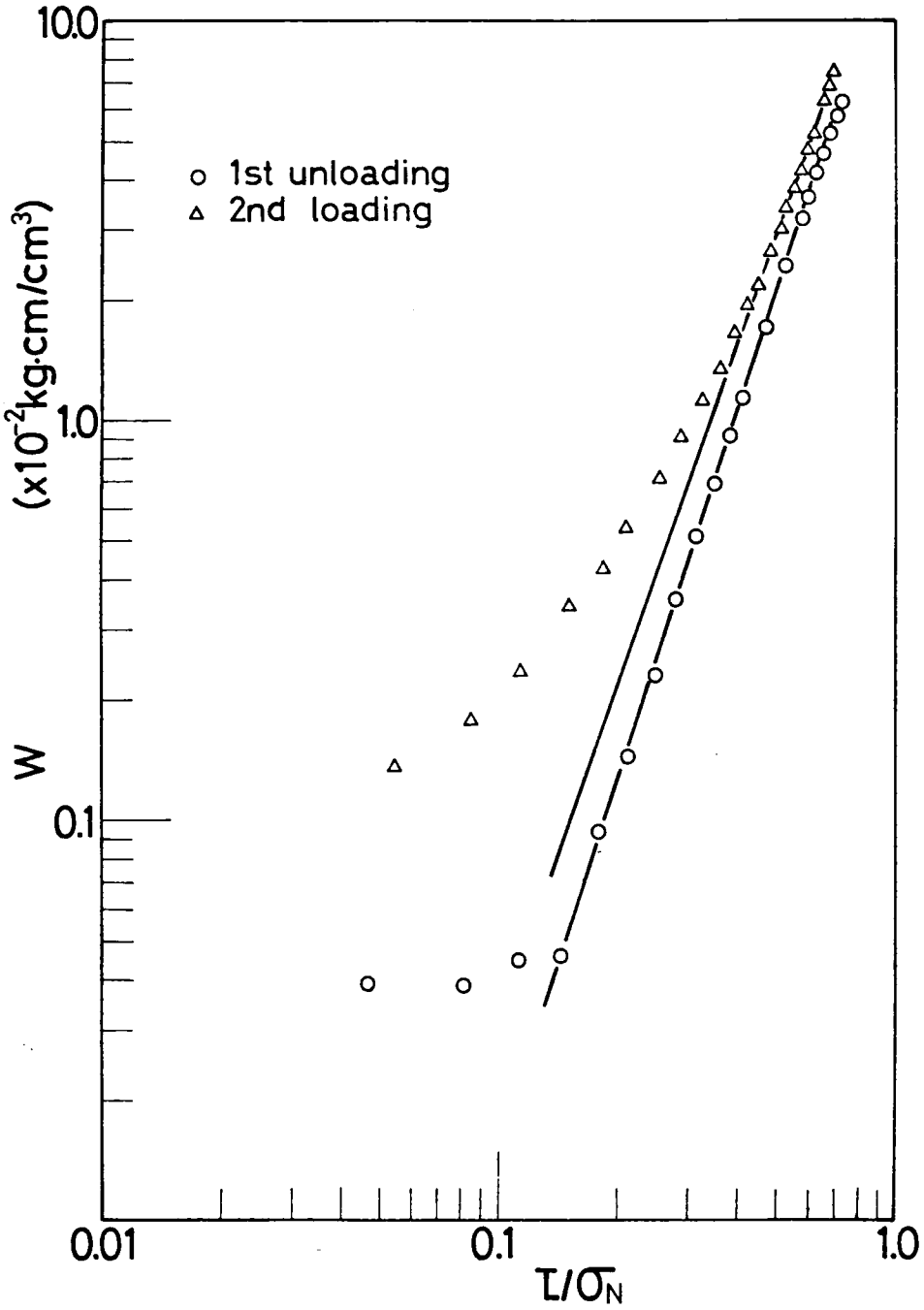

Fig.6.8(b) Relations between W and τ/σ_N for constant confining pressure test, $\sigma_T = 4\ kg/cm^2$

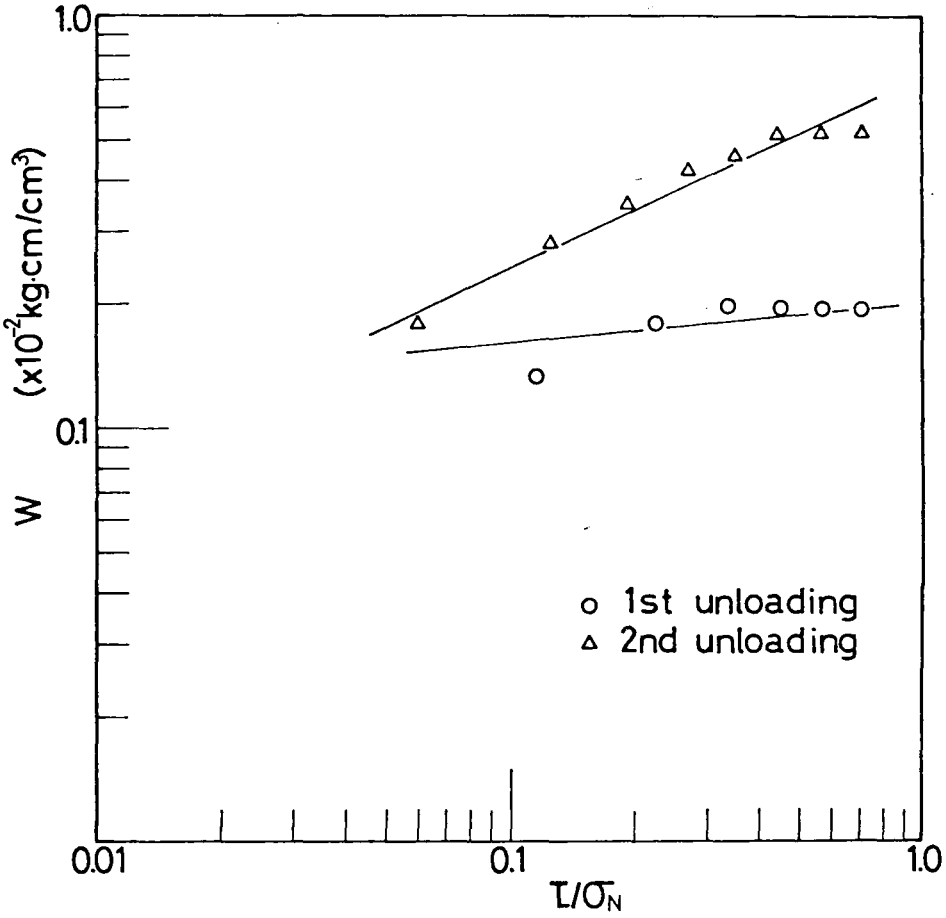

Fig.6.9(a) Relations between W and τ/σ_N for constant mean effective principal stress test along stress path, $\theta = 0° \rightarrow 180° \rightarrow 0°$

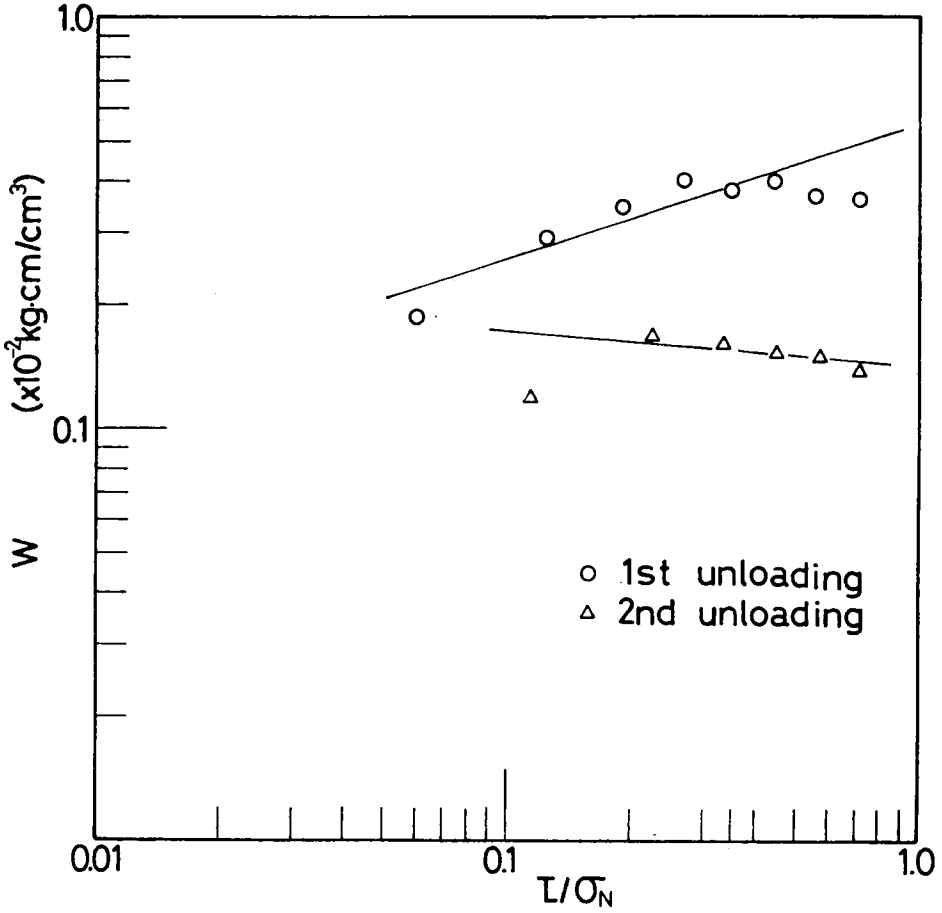

Fig.6.9(b) Relations between W and τ/σ_N for constant mean effective principal stress test along stress path, $\theta = 180° \rightarrow 0° \rightarrow 180°$

$$W = m \left(\tau / \sigma_N \right)^r \qquad (6.3)$$

where m and r ; parameters depending on the void ratio, fabric of particulate material and so on.

In Figs.6.8 and 6.9 data seem to be a little apart from the linear relation expressed by Eq.(6.3) at small stress ratios, but differences between the measured and the calculated energy increments, ΔW, are almost negligible in numerical experiments because the absolute values of ΔW are very small at small stress ratio. In calculation of ΔW in Eq.(3.12), Eq.(6.2) or Eq.(6.3) is used for the loading or unloading processes shown in Figs.6.3-6.9. The values of these model parameters a , b , m and r which are used in the numerical experiments are summarized in Table 6.1.

It is necessary to obtain the elastic component of energy increment ΔW_e in order to determine the parameter R_η in Eq. (3.39). But it is impossible to measure ΔW_e directly at each contact point. As the first approximate values, ΔW_e is assumed to be determined by using the initial tangential slops E_i ($i = 1, 2, 3$) in the stress ratio-strain relation, $\tau / \sigma_N \sim \epsilon_i$ ($i = 1, 2, 3$). These experimentally determined values E_i ($i = 1, 2, 3$) are also listed up in Table 6.1. It is necessary to investigate the elastic state of particulate material which may be the inherent state as finally arrived under the repeated loading tests in future study.

6.2.2 Coefficient of inter-particle friction, μ

Here, we discuss on the determination of the potential barriers for the purpose we have to give the coefficient of inter-particle friction μ in Eq.(3.34). It is clear that the frictional resistance at contact points of particles plays an important role in the non-linear stress-strain relation of particulate material.

As already mentioned, it is, however, really difficult task to determine the coefficient of inter-particle friction μ between two particles. In this study we take the way to deduce the inter-particle coefficient μ from the global friction of particulate material. Matsuoka and Nakai[3] proposed the SMP to explain the global friction of particulate material and derived Eq.(3.36) as a stress-dilatancy equation based on the concept of SMP. They regarded the value of τ/σ_N at the vertical strain increment $d\varepsilon_N = 0$ as the frictional coefficient of particulate material. Furthermore, they experimentally found that this value is independent of void ratio and stress path as far as the material is same.

The relations between τ/σ_N and $-d\varepsilon_N/d\gamma$ for the test results are given in Fig.6.10. Fig.6.10(a) illustrates the results of monotonous loading tests under the constant confining pressures. It is found from this figure that the relation between τ/σ_N and $-d\varepsilon_N/d\gamma$ on the SMP is also independent of the confining pressures. Fig.6.10(b) shows the results of monotonous loading tests with the stress paths shown in Fig.5.5 under the constant mean effective principal stress. It is found from Fig.6.10(b) that the relation of τ/σ_N and $-d\varepsilon_N/d\gamma$ is not influenced by the stress paths and uniquely determined. By comparing the results obtained from the conventional triaxial compression and extension tests for the dense samples with those for the loose samples in Fig.6.10(c), it can be also said that the relation between τ/σ_N and $-d\varepsilon_N/d\gamma$ on the SMP does not depend on the initial void ratio of specimen. It is experimentally concluded from Fig.6.12 that the stress-dilatancy relation on the SMP satisfies Eq.(3.36) and μ in Eq.(3.36) is found to be almost constant. Thus, it is reasonable to regard μ in Eq.(3.36) as the global friction for particulate material.

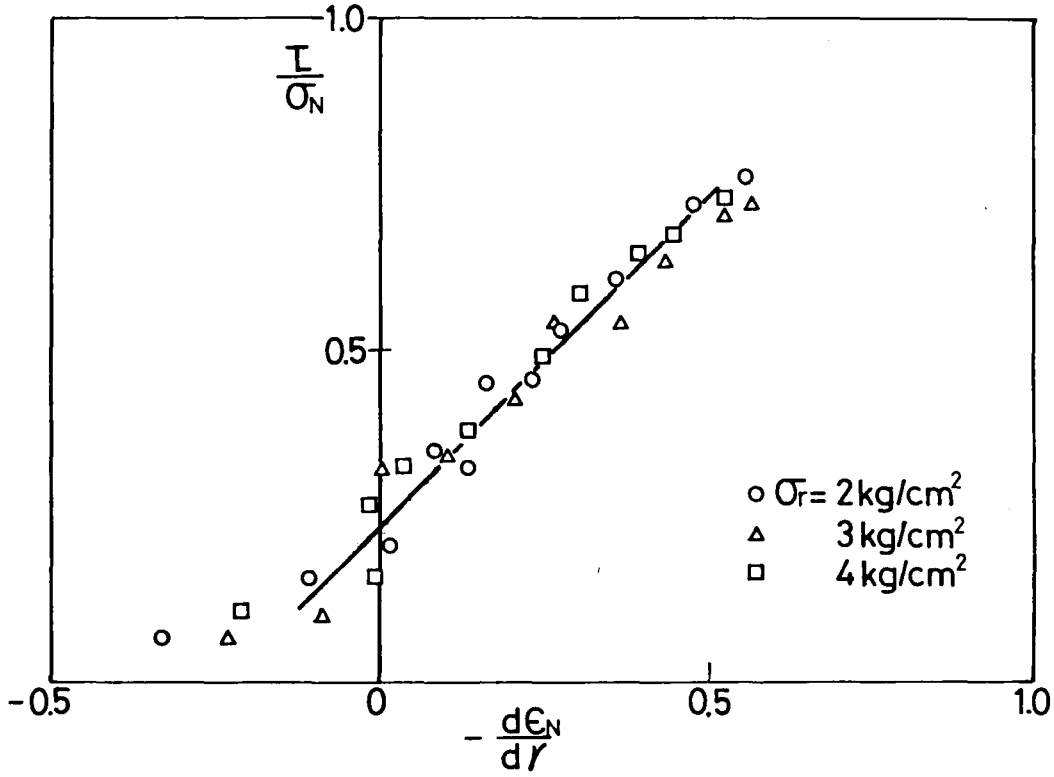

Fig.6.10(a) Relations between τ/σ_N and $-d\epsilon_N/d\gamma$ for constant confining pressure tests

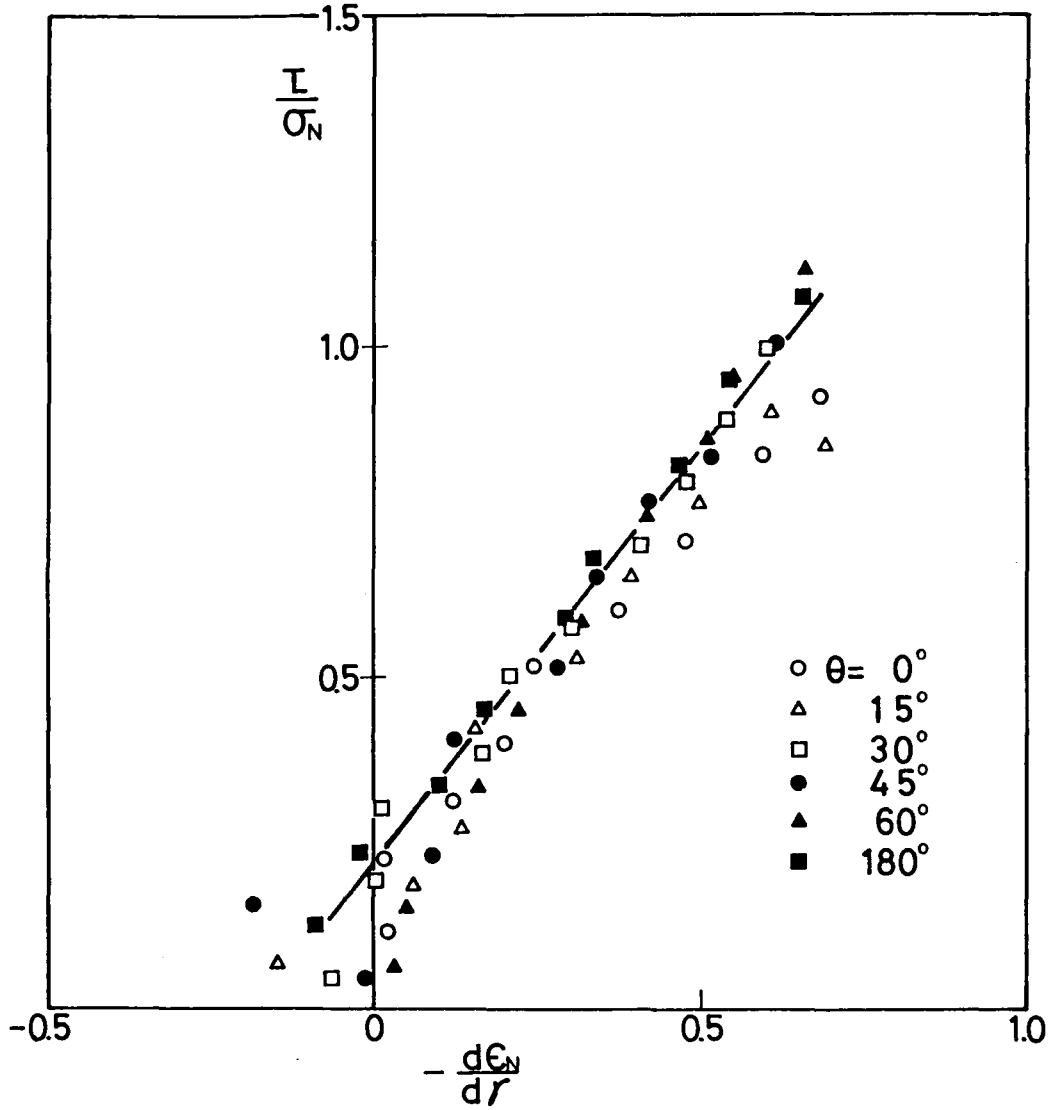

Fig.6.10(b) Relations between τ/σ_N and $-d\epsilon_N/d\gamma$ for constant mean effective principal stress tests

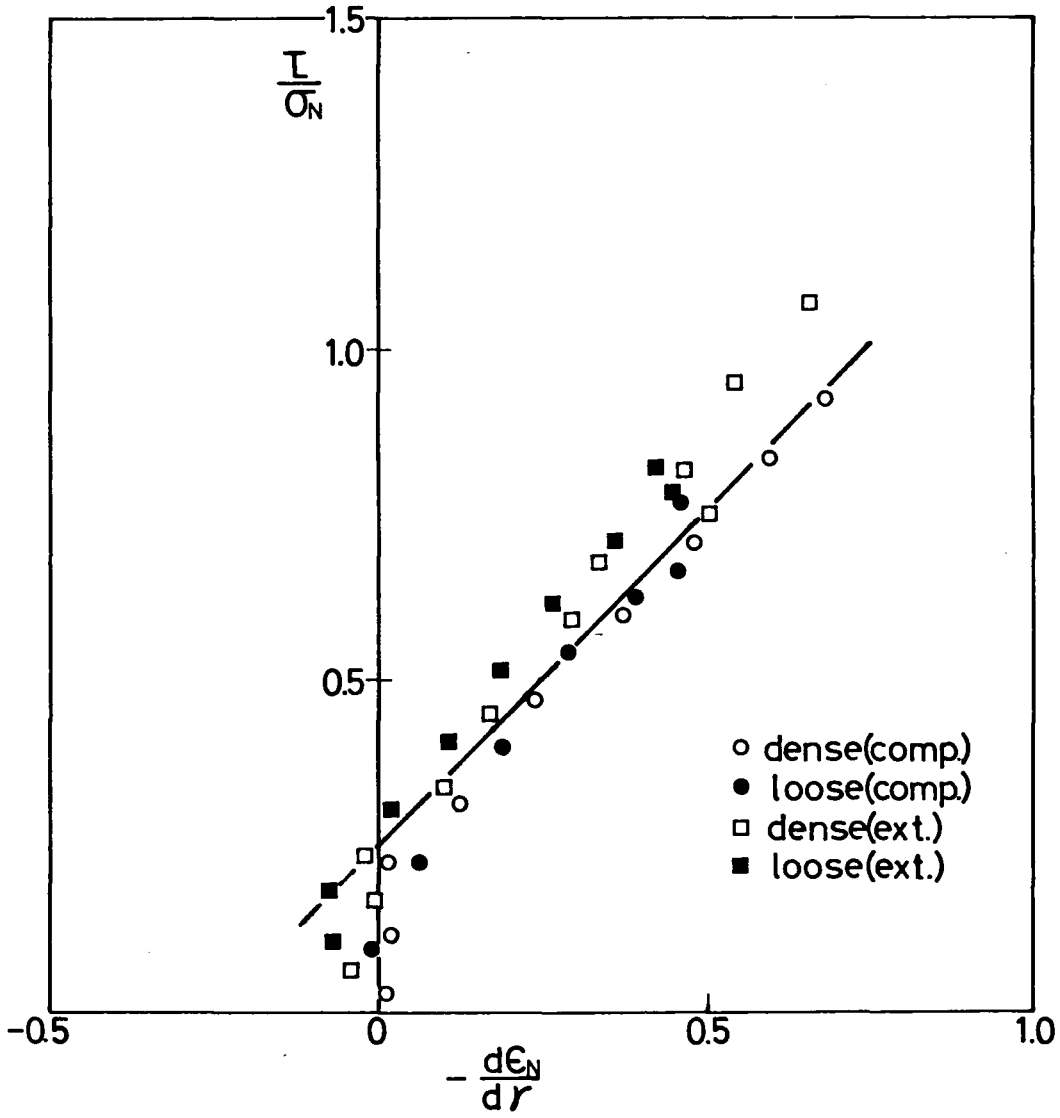

Fig.6.10(c) Relations between τ/σ_N and $-d\varepsilon_N/d\gamma$ for triaxial compression and extension tests with dense and loose specimens

From Fig.6.10 the mean value of μ in these tests is found to be approximately 0.25.

This obtained value of $\mu = 0.25$ for Toyoura sand is used in numerical experiments.

6.2.3 Initial distribution of contact angles

The initial distribution of contact angles at contact points should be given as an initial condition of particulate material in order to solve the basic equation of Markov process. Concerning the initial distribution of contact angles, experimental researches have been carried out by Oda[4] and Matsuoka[5]. According to the results obtained by them who directly measured the contact angles of rods or sands by microscope or photographs, it is found that the initial distribution of contact angles is approximated by triangle or trapezium in form in the two dimensional space if β_1 is adopted to measure the angle of contact plane. This shows that under the gravity field the probability that the normals to contact planes are in the vertical direction is the largest. In the proposed model the initial distribution of contact angles is assumed to be cone shape in form in the three dimensional space.

6.2.4 Ratios of disappearance and appearance of contact points

It has been pointed out in section 4.2 that the discontinuous motions of particles at contact points play very important roles in the deformation process of particulate material. These motions are similar to the dislocation of crystal solid under plastic deformation process. By introducing the concepts of the disappearance and the appearance of contact points, the discontinuous motions have been prescribed. Based on these concepts, it is required to determine the values of λ and K in Eqs.(4.9), (4.10) and (4.11) in order to derive the strains of particulate material.

In the proposed model these parameters are assumed to be simply the linear function of deviatoric stress $(\bar{\sigma}_{max}-\bar{\sigma}_{min})$ as the first approximation. Then, the following equation for λ is given.

$$\lambda = \lambda_1 + \lambda_2 (\bar{\sigma}_{max} - \bar{\sigma}_{min}) \qquad (6.4)$$

where λ_1 and λ_2 ; parameters depending on the mechanical properties of particulate material and its shearing stress path,

$\bar{\sigma}_{max}$ and $\bar{\sigma}_{min}$; maximum and minimum principal stresses.

Fig.6.11 schematically shows how λ effects on the function $P_a(\beta_1)$ defined in Eqs.(4.9) and (4.10). Fig.6.11(a) is for the case when the vertical principal stress $\bar{\sigma}_1$ is maximum and Fig.6.11(b) for the case when the horizontal stress $\bar{\sigma}_2$ or $\bar{\sigma}_3$ is maximum. From these figures it is found that the probability of the disappearance of contact points decrease when the parameter λ is larger.

In the following discussions, let's denote the appearance ratios of new contact points by κ_1 , κ_2 and κ_3 in the directions of X_1- , X_2- and X_3-axes respectively. The values of λ_1 , λ_2 , κ_1 , κ_2 and κ_3 used in numerical experiments are chosen to fit the stress-strain relations obtained by numerical experiments to those obtained by experiments described in chapter 5. These values are summarized in Table 6.1.

Let's consider the discontinuous motions of particles under shearing process based on the parameters λ and κ . As shown in Table 6.1 the parameter λ_2 is found to be positive in all experiments. Thus, λ in Eq.(6.4) increases when the deviatoric stress $(\bar{\sigma}_{max} - \bar{\sigma}_{min})$ increases. This means that the probability of disappea-

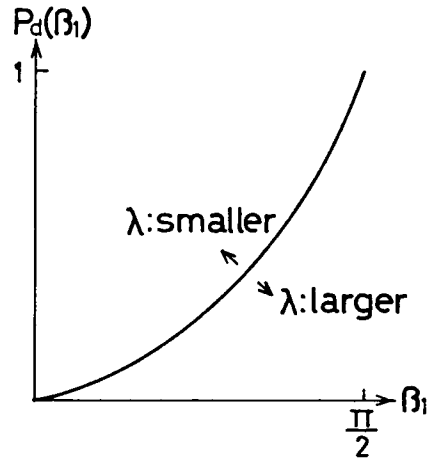

(a)

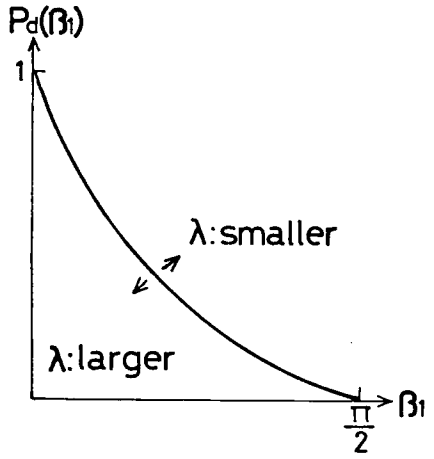

(b)

Fig.6.11 Schematic change of $P_d(\beta_1)$ depending on λ

Table 6.1(a) Values of model parameters for constant confinig pressure tests

σ_3 (kg/cm²)	E_1	E_2, E_3	a	b	m	r	λ_1	λ_2	k_2 , k_3	Remarks
2.0	250.0	833.3	0.700	1.260			7.5	4.0	0.5	monotonous
3.0	133.0	357.5	1.550	1.340			10.0	2.0	0.5	
4.0	175.0	416.7	2.714	1.286			15.0	2.5	0.35	
3.0	94.0	209.4	3.214	1.014			10.0	2.5	0.5	1st load
					9.810	2.850	0.5	6.0	2.5	1st unload
					11.460	2.630	0.5	6.0	2.5	2nd load
			3.214	1.014			10.0	3.0	0.5	3rd load
4.0	88.4	244.9	5.273	0.973			15.0	2.0	0.5	1st load
					17.141	3.029	0.5	6.0	3.0	1st unload
					18.027	2.698	0.5	6.0	3.0	2nd load
			5.273	0.973			15.0	3.0	0.5	3rd load

where a , m ; $[kg.cm/cm3]$

λ_1 , λ_2 , k_2 , k_3 ; $[cm^2/kg]$

Table 6.1(b) Values of model parameters for constant mean effective principal stress tests

θ°	E_1	E_2	E_3	a	b	m	r	λ_1	λ_2	k_1	k_2	k_3	Remaks
0	635.0	2530.0	2530.0	0.358	1.153			10.0	5.0		0.5	0.5	
15	400.0	4000.0	1360.0	0.330	1.100			3.0	4.5		0.2	1.2	
30	420.0	1600.0	410.0	0.375	0.935			10.0	0.5		-0.2	1.3	medium dense,
45	730.0	1400.0	700.0	0.215	0.895			5.0	2.0		-1.0	1.3	monotonous
60	420.0	560.0	300.0	0.775	0.725			10.0	1.5		-2.0	2.0	
180	310.0	310.0	590.0	0.787	0.863			15.0	4.0	2.0			
0	197.7	482.4	482.4	0.600	1.310			15.0	1.5		0.38	0.38	loose,
180	42.3	191.1	191.1	5.000	0.920			15.0	2.0	1.5			monotonous
0→180	325.0	635.0	635.0	0.343	1.088			8.0	3.0		0.5	0.5	1st load
						-0.196	0.064	5.0	1.0		4.0	4.0	1st unload
				3.295	1.025			15.0	0.75	1.75			2nd load
						-0.716	0.460	5.0	1.0	4.0			2nd unload
				2.948	0.932			12.0	3.0		0.5	0.5	3rd load
180→0	53.5	81.0	81.0	2.255	0.995			8.0	0.04	2.0			1st load
						-0.564	0.327	4.0	2.0	0.5			1st unload
				3.325	0.845			10.0	3.0		0.5	0.5	2nd load
						-0.133	-0.046	4.0	2.0		0.5	0.5	2nd unload
				1.908	0.996			8.0	0.3	2.5			3rd load

where a , m ; $\{kg \cdot cm/cm^3\}$

λ_1 , λ_2 , k_1 , k_2 , k_3 ; $\{cm^2/kg\}$

rance at contact points always decreases for shear loading process. It may be considered that the fabric of particulate material is transformed so as to mobilize and stabilize against the shearing stress at the particle scale.

Let's discuss what the parameter K means in the case of the tests under the constant confining pressure, 2 kg/cm^2, for which $K_2 = K_3 = 0.5$. $K_2 = K_3 = 0.5$ means that the number of contact points increase in the horizontal paths by 50% of the number of disappeared contact points in the vertical path. Such motions of particles are schematically shown in Fig.4.4. It is reasonable to consider that K_2 is always equal to K_3 for the conventional compression tests because the stress and the fabric in the specimen are both axi-symmetric. In the case of the test with $\theta = 15°$, $K_2 = 0.2$ and $K_3 = 1.2$ mean that the numbers of contact points increase in the X_2- and X_3-directions by 20% and 120% of the number of disappeared contact points in the vertical path. $K_2 < 0$ for the test of $\theta = 30°$, $45°$ and $60°$ means that the disappearance of contact points occurs in the direction of X_2-axis. For example, $K_2 = -0.2$ for the test of $\theta = 30°$ represents that the number of contact points disappearing along the horizontal path in the direction of X_2-axis is 20% of the number of contact points disappearing along the vertical path. And $K_2 = -2.0$ for the test of $\theta = 60°$ means that the number of contact points disappearing along the horizontal path in the direction of X_2-axis is twice as large as the number of contact points disappearing in the vertical path. The test of $\theta = 60°$ is the extension test where the stresses in the directions of X_1- and X_2-axes are both the maximum principal stresses. Thus, $K_2 = -1.0$ should be theoretically given if the fabric of material is isotropic. Therefore, this discrepancy for K_2 reflects the fabric anisotropy of particulate material. As shown in

Table 6.1 the sign of κ_2 changes from positive to negative between the stress paths of $\theta = 15^\circ$ and 30° . This means that the discontinuous motion of disappearance changes to the discontinuous motion of appearance in the direction of χ_2-axis and corresponds to the fact described in chapter 5 that the stress path under plane strain condition is one between $\theta = 15^\circ$ and 30° .

Next let's investigate the parameters λ and κ for the dense and loose samples. $((\lambda_2)_{dense} = 5.0) > ((\lambda_2)_{loose} = 1.5)$ for the test of $\theta = 0^\circ$ means that the disappearance of contact points for the loose sample tends to occur along the vertical path more than for the dense sample. $((\kappa_2 = \kappa_3)_{dense} = 0.5) > ((\kappa_2 = \kappa_3)_{loose} = 0.38)$ shows that the appearance of contact points for the dense sample tends to occur along the horizontal paths more than that for the loose sample. $((\lambda_2)_{dense} = 4.0) > ((\lambda_2)_{loose} = 2.0)$ for the test of $\theta = 180^\circ$ also means that the disappearance of contact points for the loose sample tends to occur along the horizontal paths more than that for the dense sample. Comparing λ_2 for loose sample with λ_2 for the dense sample, it is found that the discontinuous motions of disappearence tend to occur more in the loose sample. κ_1 has non-zero value only for the case of the triaxial conventional extension tests. $((\kappa_1)_{dense} = 2.0) > ((\kappa_1)_{loose} = 1.5)$ for the test of $\theta = 180^\circ$ also means that the appearance of contact points for the dense sample tends to occur more than that for the loose sample. These facts mean that the larger number of particles for loose samples does not contribute to the deformation process than that for the dense sample.

In the repeated loading tests, $(\lambda_2)_{1st}$ which is the value of λ_2 in the first loading process is smaller than $(\lambda_2)_{3rd}$ which is the values in the third loading process. κ , however, is almost constant under each loading process. For example, in the test

under the constant confining pressure $\sigma_3 = 3$ kg/cm^2, $((\lambda_2)_{1st} = 2.5) < ((\lambda_2)_{3rd} = 3.0)$ and $(\kappa)_{1st} = (\kappa)_{3rd} = 0.5$. This means that as the particulate material experiences the repeated loading, its fabric is transformed so as to resist more against the shearing stress and the discontinuous motion of particles decreases gradually in the repeated loading. According to the parameters λ and κ in Table 6.1 for the unloading process of repeated loading tests, it is supposed that the discontinuous motions of particles become more active than those for the loading process. Especially, this phenomena become remarkable near zero deviatoric stress state.

6.3 Stress-Strain Relations in the Numerical Experiments

The stress-strain relations which are obtained by the numerical experiments are shown in Fig.5.9. These relations are obtained by using the model parameters which are explained in the previous section and summarized in Table 6.1. That is to say, the parameters a and b in Eq.(6.2) are necessary to calculate the energy transferred into the sample for the monotonous or the repeated virgin loading process. The parameters m and r in Eq.(6.3) are used for the unloading and the reloading processes. The elastic component of energy is calculated by the parameters E_1, E_2 and E_3. The parameters λ and κ are chosen in order that the calculated stress-strain curves fit those obtained by the experiments with Toyoura sand.

In the numerical experiments the strain increments suddenly become very large values near the stress conditions at the failures with Toyoura sand. Therefore, it can be considered that the failures in the proposed model also occur at these stress states. The more detailed investigations for the failure mechanisms in the proposed model should be carried out in future study.

Finally, it is concluded from Figs.5.9-5.12 that the proposed mechanical model can versatilely represent the mechanical behaviours of particulate material by taking account of the inherent anisotropy due to the fabric of particulate material, the extrinsic anisotropy due to the stress history and the non-linearity of stress-strain relationships.

6.7 Conclusions

In this chapter the numerical experiments are carried out by using the mechanical model which has been established for particulate materials in chapters 3 and 4. The basic equation of Markov process is solved by the finite difference method. The model parameters used in the numerical experiments are discussed. The obtained stress-strain relations are compared with those obtained by the modified triaxial apparatus.

The results obtained in this chapter may be summarized as follows.

(1) The relations between the work, W , done in the particulate material and the stress ratio, τ/σ_N , are represented by the hyperbolic equations for the monotonous loading processes, the virgin loading processes in the one-way repeated loading tests and the loading processes in the two-way repeated loading tests. For the unloading and reloading processes the relation between W and τ/σ_N are approximated by the linear equations on the logarithmic scale. The parameters in the hyperbolic equation may be supposed to depend on materials, initial void ratios and confining pressures, but to be independent of the stress paths on the π- plane.

(2) The stress-dilatancy relations on the SMP are shown by using the test results obtained by the modified triaxial apparatus.

It is found from these relations that the stress-strain at $d\epsilon_N = 0$ are almost same and independent of void ratios, stress path and confining pressures. Thus. these values are adopted as the coefficient of inter-particle friction in order to obtain the heights of the potential barriers in the numerical experiments.

(3) As the initial distribution of contact angles, the cone shape in the three dimensional space is adopted based on the experimental results of previous researches under gravity field.

(4) The values of the ratios of the disappearance and the appearance are chosen so that the stress-strain relations obtained by numerical experiments are fit to those obtained by shearing tests with Toyoura sand. The deformation mechanisms of particulate material are discussed based on these values which estimate the discontinuous motions of particles. It is shown how the discontinuous motions of particles depend on void ratios, stress paths and confining pressures under deformation process.

(5) The stress-strain relations obtained by the numerical experiments are compared with those by the shearing tests with Toyoura sand. From these comparisons it is apparent that the proposed mechanical model can versatilely represent the various mechanical behaviours of particulate materials such as sands under the general stress conditions including the stress reverse. Thus, it is found that this model is a unified and simple one that takes account of the inherent anisotropy due to the fabric of particulate material, the extrinsic anisotropy due to the stress history and the non-linearity of stress-strain relationships.

Reference for Chapter 6

1) Kitamura, R.: Application of a Markov Process to a Mechanical Model of Particulate Material(2), Annuals, Disaster Prevention Research Institute, Kyoto Univ., No.22B, 1979, pp.107-125, (in Japanese).

2) Kitamura, R.and Adachi, T.: Energetic Consideration for the Mechanical Behaviours of Particulate Material(3), Proc. Annual Meeting of JSCE, Part 3, 1979, (in Japanese).

3) see ref. 31) in Chapter 1.

4) see ref. 12) in Chapter 3.

5) see ref. 3) in Chapter 4.

Appendix 6.1

The basic equation of Markov process, Eq.(3.8), is nonlinear parabolic partial differential equation. It is impossible to analytically solve this equation. Thus, in this study Eq.(3.8) is numerically solved by using the finite difference method which gives the approximate solutions.

There are various finite difference equations. In this study the advancing ty e as the calculus of finite difference is applied numerically to solve.

Eq.(3.8) is rewritten as follows.

$$\frac{\partial}{\partial s} w(\eta, s) = -\frac{\partial}{\partial \beta_1}\left[A_1(\eta, s)\, w(\eta, s)\right] - \frac{\partial}{\partial \beta_2}\left[A_2(\eta, s) w(\eta, s)\right]$$

$$+\frac{\partial^2}{\partial \beta_1^2}\left[B_{11}(\eta, s) w(\eta, s)\right] + \frac{\partial^2}{\partial \beta_2^2}\left[B_{22}(\eta, s)\, w(\eta, s)\right]$$

Transforming the above equation, we get the following equation.

$$\frac{\partial}{\partial s} w(\eta, s) = -A_1(\eta, s)\frac{\partial}{\partial \beta_1} w(\eta, s) - w(\eta, s)\frac{\partial}{\partial \beta_1} A_1(\eta, s)$$

$$-A_2(\eta, s)\frac{\partial}{\partial \beta_2} w(\eta, s) - w(\eta, s)\frac{\partial}{\partial \beta_2} A_2(\eta, s)$$

$$+B_{11}(\eta, s)\frac{\partial^2}{\partial \beta_1^2} w(\eta, s) + 2\frac{\partial}{\partial \beta_1} B_{11}(\eta, s)\frac{\partial}{\partial \beta_1} w(\eta, s) + w(\eta, s)\frac{\partial^2}{\partial \beta_1^2} B_{11}(\eta, s)$$

$$+B_{22}(\eta, s)\frac{\partial^2}{\partial \beta_2^2} w(\eta, s) + 2\frac{\partial}{\partial \beta_2} B_{22}(\eta, s)\frac{\partial}{\partial \beta_2} w(\eta, s) + w(\eta, s)\frac{\partial^2}{\partial \beta_2^2} B_{22}(\eta, s)$$

Each term of this equation is approximated by the advancing type difference equation as follows.

$$\frac{\partial}{\partial s} w(\eta, s) \longrightarrow \frac{w(\eta, s+\Delta s) - w(\eta, s)}{\Delta s}$$

$$\frac{\partial}{\partial \beta_1} w(\eta, s) \longrightarrow \frac{w(\beta_1+\Delta\beta_1, \beta_2 : s) - w(\beta_1, \beta_2 : s)}{\Delta \beta_1}$$

$$\frac{\partial^2}{\partial \beta_1^2} w(\eta, s) \longrightarrow \frac{w(\beta_1+\Delta\beta_1, \beta_2 : s) - 2w(\beta_1, \beta_2 : s) + w(\beta_1 - \Delta\beta_1, \beta_2 : s)}{(\Delta\beta_1)^2}$$

$$\frac{\partial}{\partial \beta_1} A_1(\eta, s) \longrightarrow \frac{A_1(\beta_1+\Delta\beta_1, \beta_2 : s) - A_1(\beta_1, \beta_2 : s)}{\Delta\beta_1}$$

$$\frac{\partial^2}{\partial \beta_1^2} B_{11}(\eta, s) \longrightarrow \frac{B_{11}(\beta_1+\Delta\beta_1, \beta_2 : s) - 2B_{11}(\beta_1, \beta_2 : s) + B_{11}(\beta_1 - \Delta\beta_1, \beta_2 : s)}{(\Delta\beta_1)^2}$$

CHAPTER 7 CONCLUSIONS

The main purpose of this thesis are as follows.

(1) To apply the probability theory to analyse the mechanical behaviours of particulate materials such as sands at the particle scale.

(2) To establish a mechanical model of particulate material by applying the Morkov process to the motions of particles with irregular shapes and sizes under deformation process.

(3) To carry out the shearing tests with Toyoura sand by using a newly modified triaxial apparatus which can generate three different principal stresses and to show the stress-strain relationships of Toyoura sand under the various stress conditions.

(4) To carry out the numerical experiments by using the proposed mechanical model based on the considerations for the shearing test results and to verify the validity of proposed mechanical model by comparing the stress-strain relationships with those obtained by the shearing tests.

In the present chapter the important conclusions obtained in the previous chapters are summarized and a prospect of continued future work is given.

In chapter 1, previous researches on the constitutive equations of soil are reviewed and divided into two categories by means of their approaches. One approach is called macroscopic approach and based on the theory of elasticity and/or plasticity. The main yield function and/or the plastic potential functions used in the works are shown since these functions play important parts of theoretical considerations in this approach. Another approach is

called microscopic approach. In this approach the constitutive equations are derived by analysing the motions of particles and summing up these motions in the whole particulate material. Finally, the general scope of this thesis is given.

In chapter 2, the mathematical explanations are given for the Markov process which is one of the well-known stochastic processes. The basic equation of one-dimensional Markov process is derived based on three mathematical assumptions. Furthermore, this equation is extended to the n-dimensional Markov process.

In chapter 3, the Markov process is applied to the deformation process of particulate material and the basic equation of Markov process is derived for the particulate material. In this equation the contact angle at a contact point is adopted as a random variable which represents the inner state of particulate material. The coefficients A_i and B_{ii} in the basic equation represent the mechanical properties of particulate material at the particle scale. The concepts of the potential barrier and the potential slip plane are introduced in order to determine these coefficients. Finally, the method is described to obtain the coefficients A_i and B_{ii} by giving the probabilistic considerations to the motions of particles.

In chapter 4, the strains of particulate material are defined by considering the relative motions of particles. It is found that the strains can be represented by the probability density function of contact angles and the ratios of disappearance and appearance. These ratios estimate the discontinuous motions of particles at contact points which correspond to the dislocation of crystal solid under plastic deformation. These discontinuous motions contribute the deformation of particulate material as well as the continuous changes in contact angles. The method to esti-

mate the discontinuous motions should be developed in future study.

In chapter 5, the shearing tests are carried out by a modified triaxial apparatus which can be generate three different principal stresses by means of the horizontal loading system in the conventional triaxial cell. The system of this apparatus is explained. The true triaxial apparatus in previous researches are also reviewed and divided into three groups in terms of loading systems. The used material is Toyoura sand and tests are performed for relatively dense and loose specimens. The drained condition is adopted in all tests. The shearing tests are conducted under the constant confining pressures and the constant mean effective principal stress. The used stress paths include the monotonous loadings, one-way and two-way repeated loadings. The considerations are added to the errors caused by the modified triaxial apparatus. The validity of correction methods is shown by the results of a conventional triaxial compression test with the horizontal loading system. The obtained stress-strain relationships are illustrated and it is shown that the mechanical behaviours of particulate materials depend on the initial void ratios and stress conditions. Finally, the validity of the concept of the potential slip plane is considered based on the observed slip planes at failures. The improvements of correction methods should be done to obtaine the more accurate data for the mechanical behaviours of particulate material in future study.

In chapter 6, the numerical experiments are carried out by using the mechanical model which has been established in chapters 3 and 4. The basic equation of Markov process is solved by finite difference mehtod. The used model parameters are discussed, i.e., the work done into particulate material under shearing process, the initial distribution function of contact angles, the coeffici-

ent of inter-particle friction, and the ratios of the disappearance and the appearance. These parameters are obtained by the shearing tests with Toyoura sand. Finally, by comparing the obtained stress-strain relationships with those obtained by the shearing tests with Toyoura sand, it is shown that the proposed mechanical model can versatilely represents the various mechanical behaviours of particulate materials.